APPLYING A MODEL-BASED OBSERVER TO QUANTITATIVELY

ASSESS SPATIAL DISORIENTATION AND LOSS OF ENERGY

STATE AWARENESS

A Thesis
Presented to
The Academic Faculty

by

Anil E. Bozan

In Partial Fulfillment
of the Requirements for the Degree
Aerospace Engineering in the
School of Aerospace Engineering

Georgia Institute of Technology
May 2015

APPLYING A MODEL-BASED OBSERVER TO QUANTITATIVELY ASSESS SPATIAL DISORIENTATION AND LOSS OF ENERGY STATE AWARENESS

Approved by:

Dr. Amy Pritchett, Advisor
School of Aerospace Engineering
Georgia Institute of Technology

Dr. Eric N. Johnson
School of Aerospace Engineering
Georgia Institute of Technology

Dr. Santosh Mathan
Human Centered Systems
Honeywell Laboratories

Date Approved: April 24, 2015

www.manaraa.com

ACKNOWLEDGEMENTS

First and foremost, I would like to thank Dr. Pritchett for giving me the opportunity to join the Cognitive Engineering Center (CEC). Working in the CEC has taught me what it means to be a *helluva* engineer, as I have learned more about engineering during my years in the CEC than any former training has taught me. I also want to acknowledge those who have served on my committee: Dr. Santosh Mathan, Dr. Karen Feigh, and Dr. Eric N. Johnson. I would like to thank them for serving on my committee and devoting their time to help me with the thesis.

I would also like to thank my colleagues and friends in the CEC. It was a pleasure to work side-by-side with an inspiring and intelligent group of people; I only hope that in my future endeavors I can be pushed intellectually as I was in the CEC. I would like to extend a special thanks to my project colleague, Can Onur. Without his contribution, my thesis would have taken a very different direction.

Finally, I would like to thank my family and friends. Without their support, none of this could have happened.

TABLE OF CONTENTS

LIST OF TABLES

LIST OF FIGURES

viii

SUMMARY

This thesis demonstrates how a model-based observer can be applied to estimate the reference pilot expectation that can be achieved with any instrument scanning behavior and established models of vestibular inputs. The MBO, developed by the Georgia Tech Cognitive Engineering Center, is applied here in both simple maneuvers examining spatial disorientation and full Air Traffic Control concepts of operations examining loss of energy state awareness. The computational experiments presented in this thesis examine how different effects (i.e., instrument scan pattern, accuracy of pilot perception of flight display information, and awareness of control surface deflections) can prevent or mitigate the susceptibility to spatial disorientation and loss of energy state awareness, thus setting requirements for intervention and countermeasure designs in terms of the scanning behavior they must foster.

CHAPTER 1

INTRODUCTION

Motivation

Loss of control is currently the leading contributor of fatal aircraft accidents worldwide (Boeing, 2013) and is prevalent among all vehicle classes, operational categories, and phases of flight (Belcastro, 2010). There are many contributing factors to loss of control, but spatial disorientation and loss of energy state awareness account for roughly 70% of all loss of control accidents (Bailey, 2013; Bateman, 2010). Thus, these two highly fatal phenomena have been and continue to be a hazard in aviation.

Several underlying mechanisms of spatial disorientation and loss of energy state awareness cause a pilot's expectation of the aircraft's state to deviate from the actual state of the aircraft. However, the majority of spatial disorientation and loss of energy state awareness related mishaps are caused by failure to monitor some or all of the primary flight instruments and/or incorrect or conflicting input from vestibular and instrument visual sensing.

Research, development, and regulations have sought to mitigate spatial disorientation and loss of energy state awareness. For example, countermeasures to spatial disorientation include synthetic vision, aural alerts, instrument scan training, spatial disorientation training, tactile situation awareness system, etc. (Bateman, 2010; Belcastro, 2010; Rupert, 2000; Previc, 2004). Likewise, Crew State Monitoring technologies may further prevent loss of energy state awareness beyond current-day low speed/stall warnings (kinetic energy) and ground proximity warning (potential energy) systems (Bailey, 2010). However, designers do not have sufficient tools to examine the efficacy of their designs or technologies in the early development stages or guide them

1

towards the aspect of visual scans of flight displays that may best mitigate spatial disorientation and loss of energy awareness.

This thesis will demonstrate how a model-based observer (MBO) can be applied to estimate the reference pilot expectation (RPE) that can be achieved with any instrument-scanning behavior and established models of vestibular inputs. The MBO, developed by the Cognitive Engineering Center (CEC), is applied here in spatial disorientation and loss of energy state awareness related scenarios to predict the RPE of the aircraft's state. These predictions will be used to determine what aspects of visual instrument scans can prevent or mitigate the susceptibility to spatial disorientation (and associated illusions) and loss of energy state awareness.

Objectives

The goal of this thesis work is to determine what aspects of visual scans of flight displays can prevent or mitigate the susceptibility to spatial disorientation (and associated illusions) and loss of energy state awareness. This goal corresponds to three specific objectives:

1) Apply an established MBO to quantitatively assess the RPE that can be achieved with any given instrument scan and established models of vestibular sensing.

2) Identify aspects of visual scans of primary flight data that can reduce error in the RPE of the aircraft state.

3) Relate this analysis into requirements for intervention and countermeasure designs.

2

Overview of Thesis

This thesis applies an established MBO to identify aspects of visual scans of primary flight data that can reduce error in the RPE. The goal is to relate this analysis to requirements for intervention and countermeasure designs. Chapter 2 provides a background on spatial disorientation and loss of energy state awareness with respective causal factors and countermeasures, pertinent display information for spatial orientation, the role of the vestibular system in spatial orientation, and modeling pilot perception of aircraft state. A review of the model-based observer is also provided in this chapter.

Chapter 3 provides a review of common vestibular illusions and the MBO's ability to capture these illusions. Chapter 4 examines spatial disorientation in the context of several case studies examining the impact of scan pattern, accuracy of pilot perception, and awareness of control surfaces in maneuvers conducive to spatial disorientation due to vestibular illusions. Chapter 5 presents the results of case studies examining the impact of scan pattern on loss of energy state awareness in Next Generation Air Transportation System (NextGen) arrival routes.

Finally, Chapter 6 summarizes the thesis, notes its contributions to the field, and discusses potential future research and further application of the MBO and these results towards reducing spatial disorientation and loss of energy state awareness.

CHAPTER 2

BACKGROUND: SPATIAL DISORIENTATION AND LOSS OF ENERGY STATE AWARENESS

Spatial disorientation in aviation is widely defined as the pilot's "[failure] to sense correctly the position, motion, and attitude of his/her aircraft or of him/herself within the fixed coordinate system provided by the surface of the earth and gravitational vertical" (Benson, 1999). This definition has been widely used and supported by the spatial disorientation research community. Other proposed definitions include "the erroneous perception of any of the parameters displayed by the aircraft control and performance instruments … regardless of a pilot's experience or proficiency, sensory illusion can lead to differences between instrument indications and what the pilot 'feels' the aircraft is doing" (USAF, 2005), and "the failure of a pilot to correctly sense the attitude or motion of the aircraft or of him or herself, resulting from inadequate or erroneous sensory information (from the receptors)" (Navanthe, 1994). Though these definitions vary in purpose – some focusing on the pilot's sense of spatial orientation and some on perception of instrument readings – one thing is common: there is a mismatch between the pilot's expectation of the aircraft's state and what is actually going on. The first presented definition of spatial disorientation will be used throughout the remainder of this thesis.

There are three types of spatial disorientation: Type I (unrecognized), Type II (recognized), and Type III (incapacitated). When Type I spatial disorientation occurs, the pilot is unaware that he or she is experiencing spatial disorientation. The pilot believes that his or her expectation of orientation and control input is correct, though it may be significantly different from what the aircraft is actually doing. Type II spatial disorientation differs from Type I spatial disorientation; the pilot is aware that he or she may be suffering from spatial disorientation. Though the pilot may be unsure of what is

correct or incorrect, he or she suspects a mismatch between the aircraft dynamics, flight displays, his or her expectation, or the out-of-window view. Something is wrong, and the pilot knows it. Finally, though not as common, Type III spatial disorientation occurs when Type II spatial disorientation transitions to a dangerous level due to stress and causes the pilot to become psychologically incapacitated. The pilot, in many cases, is unable to control the aircraft or read the flight instruments. Incident studies reveal that the majority of spatial disorientation related mishaps occur from Type I SD (Previc, 2004).

Similarly, loss of energy state awareness is characterized as a "failure to monitor or understand energy state indications (e.g., airspeed, altitude, vertical speed, commanded thrust) and a resultant failure to accurately forecast the ability to maintain adequate airspeed and energy for safe flight conditions." Loss of energy state awareness typically leads to aircraft stall, which has resulted in extensive research, development and regulator work to address aircraft stall and upset related to loss of energy state awareness (Bailey, 2013; Bateman 2010).

Studies reveal that there are many contributing factors to spatial disorientation and loss of energy state awareness. For example, failing to monitor primary flight instruments is deemed as a leading contributing factor. Accident reports also suggest that susceptibility to spatial disorientation and loss of energy state awareness heightens in instrument meteorological conditions or poor visual conditions. In these conditions, it is crucial that the pilot examines the instruments as trained, as any deviations may lead to spatial disorientation or loss of energy state awareness. Finally, spatial disorientation and loss of energy state awareness are also associated with high workload environments, such as descent, takeoff, and maneuvering. In these high workload environments, pilots often become distracted due to fixation on tasks, other cockpit information, or external cues (Bailey, 2013; Bateman, 2010; Belcastro, 2010; Previc, 2004).

To combat contributing factors of spatial disorientation and loss of energy state awareness, such as failure to monitor primary flight instruments, engineers and scientists

5

have and are studying potential countermeasures. Some interventions interventions are synthetic vision, aural alerts, instrument scanning training, and tactile situation awareness system (Bailey, 2010; Bateman, 2010; Belcastro, 2010; Rupert, 2000; Previc, 2004). However, despite these efforts, there is still much work to be done to address the contributing factors of spatial disorientation and loss of energy state awareness.

Critical Display Information for Spatial Orientation and Energy State Awareness

The critical, minimum, information necessary to maintain spatial orientation comprises attitude, altitude, airspeed, and heading (Previc, 2004) and to maintain energy state awareness comprises airspeed, altitude, and vertical speed (Bailey, 2013). The critical instruments and the information they provide are presented in Table 1. The altimeter and attitude indicator provide the pilot with an accurate estimate of position and motion, i.e., height above Earth's surface and orientation with respect to the lateral (pitch) and longitudinal (roll) axes. The airspeed indicator is also important, as it provides necessary information about the motion and speed of the aircraft. The heading indicator provides the pilot with some trajectory information. The vertical speed indicator provides climb and descent rate information. Pilots are trained to conduct the T scan of these displays at each display's required frequency, with the attitude indicator scanned most often.

Table 1. *Critical Instruments and Display Information*

State, x	AI	ASI	Altimeter	HI	VSI	T/C	SCC	Otolith
Altitude, h			✔					
Forward Component Airspeed, u		✔						$\frac{d}{dt}$
Side Component Airspeed, v						✔ (β)		$\frac{d}{dt}$
Vertical Component Airspeed, w					✔			$\frac{d}{dt}$
Roll rate, p							✔	
Pitch rate, q							✔	
Yaw rate, r						✔	✔	
Pitch, θ	✔							✔
Roll, ϕ	✔					✔		✔
Yaw, ψ				✔				

Basic-T
Basic-Six
Vestibular

Research on pilot scanning behavior suggests that the majority of visual dwell time is spent on attitude (approximately 50%), with the remaining time spent primarily on altitude, airspeed, and heading (approximately 10% each), and then on other displays such as vertical speed that only need to be scanned during particular maneuvers. These approximations provided are rough estimates as these numbers can change significantly from pilot to pilot and with other factors such as pilot experience, flight conditions, and the aircraft (Previc, 2004, Spady, 1988).

Studies have shown that Type I spatial disorientation will occur when critical information is absent (Bryan, 1954; Previc, 2004). Critical information is typically absent when the pilot does not scan the flight instruments, whether intentionally or unintentionally. Critical display information can also be absent because of factors such as instrument failure.

The Vestibular System

The vestibular system provides a sense of balance. Located in the labyrinthine structure behind the auditory portion of each ear, the vestibular system is responsible for postural control and sensing body motion, particularly self-motion perception.

The vestibular system consists of two organ systems: the semicircular canals (SCC) and the otoliths. The SCC consists of three canals in each ear that together sense rotational motion. The afferent firing rate of the SCC is triggered by endolymph fluid motion in each canal due to angular acceleration. It is important to note that the response of the SCC, i.e., afferent firing rate, is in a head-fixed reference frame and not an inertial or ground-fixed reference frame (Angelaki, 2004; Lone, 2010; MacNeilage, 2008). The otoliths consist of two canals that act as linear accelerometers and provide a sense of tilt or specific force, also in a head-fixed frame reference frame. However, human perception of linear acceleration is limited since the otoliths are unable to distinguish between translational acceleration and a component of gravity resulting from tilt relative to local 'down' (Angelaki, 2004; Lone, 2010). Thus, with no visual reference for attitude, the human has difficulty differentiating between tilt and linear acceleration. Despite each unique function of the SCC and the otoliths, the human does not interpret the response of each separately. Instead, the responses are integrated together and act as an inertial reference system, which provides a sense of balance and orientation.

The vestibular system is often incorrect in the aerospace environment. The vestibular system is capable of correctly sensing orientation and balance, but typically in motions such as walking, running, and jumping. In the aerospace environment, however, the vestibular system is incapable of adapting to the constantly changing accelerations experienced in flight.

8

The vestibular system is limited in its ability to perceive angular motion under certain thresholds. The stimulation of the vestibular system is dependent on the angular acceleration and the duration of time the acceleration is applied. This relationship is known as Mulder's law (Equation 1), which states that the magnitude of the angular acceleration, α, times the duration the acceleration is applied, τ, must equal a specified constant, k. This constant is called Mulder's constant (Previc, 2004).

$$\alpha\tau = k \qquad\qquad (1)$$

To illustrate the meaning of Mulder's law, consider an angular acceleration about the roll axis of 2°/s^2, and assume Mulder's constant (i.e., vestibular threshold) is 2.5°/s. If this angular acceleration is applied for 1 sec in flight, the pilot will not sense the acceleration.and resulting angular velocity of 2.0 °/s. However, if this acceleration is applied for 1.25 sec or longer, then the pilot will sense the motion once an angular velocity reaches 2.5°/s (Small, 2006).

Mulder's constant varies for all humans, but various researchers have determined mean estimates of what it should be. The most commonly accepted are as follows:

- Mulder (Guedry, 1974): k = 2.5 °/s for all three axes.
- Stapleford (1968): k = 3.2 °/s for roll, k = 2.6°/s for pitch, and k = 1.1°/sec for yaw.
- Oman (2005): k = 1.5°/s for all three axes.
- Davis (2008): k = 2.0 °/s for all three axes.

These values of Mulder's constant are based on measures taken from the general population. However, there is evidence that pilots have more stable vestibulo-ocular

9

reflex than non-pilots, resulting in pilots having higher thresholds than the general population (Previc, 2004).

As stated earlier, the otoliths detect specific force. Studies performed by Guedry provide rough estimates of thresholds for the otoliths. These estimates are 0.006g in both the X (roll) and Y (pitch) axes, and 0.01g in the Z (vertical axis) (Previc, 2004; Small, 2006; Davis, 2008). Other studies show that the minimum perceived linear accelerations range from 0.001g to 0.03g (Gillingham, 1986).

Thus, flight regimes can be categorized as above-threshold or sub-threshold. These flight regimes can be conducive to vestibular illusions if the pilot does not scan the instruments or the external environment. Perception of spatial orientation is usually dominated by visual senses but, in the absence of visual sensing, perception of spatial orientation is then driven by the vestibular system, which can cause pilot misperception of orientation (Lessard 2000; Lone 2010; McGrath, 2002; Newman 2012). Two common types of vestibular illusions are somatogyral and somatogravic illusions, which will be discussed in greater detail in Chapter 3.

Relevant Computational Pilot Models

In the late 1960s and early 1970s, researchers began applying control theory to model pilot control and visual sampling behavior. A group of researchers, led by Kleinman and Baron, showed that the optimal control model (OCM) could be used to provide a good description of pilot control performance, and to predict changes in visual scanning. To be fully comprehensive, the OCM is an optimal linear regulator combined with an optimal estimator (i.e., Kalman filter). This optimal estimator provides an estimate of the state variables of the optimal linear regulator, which are produced given noisy measurements or observations of the state variables. The pilot OCM models developed by Kleinman et al. proved to accurately estimate pilot manual control

10

performance, and also proved to be a useful tool for testing flying qualities before development of an aircraft (Kleinman, 1970; Hess, 1996). The OCM predictions of pilot control behavior were validated against pilot behavior in a fixed-base flight simulator in instrument meteorological conditions (IMC) situations and shown to perform well in a vertical take-off and landing experiment. This same team of researchers also showed that the OCM is capable of predicting instrument-monitoring behavior of the human operator (Baron, 1969).

Concurrently during the 1960s, researchers at the MIT Man-Vehicle Lab (MVL) applied the concepts of control theory to the dynamics of the vestibular system. The result was a biocybernetic model, capable of predicting perceived orientation, postural reactions, nystagmus eye movements, and actions based on motion cues (Young, 1969). This model has been used and further developed by the MIT MVL (Nashner, 1970; Ormsby, 1974; Borah, 1979, 1988; Newman, 2009, 2012).

The semicircular canal (SCC) model is based on the works of Steinhausen and Van Egmond et al. In the 1930's, Steinhausen proposed the idea of modeling the vestibular system as a torsion pendulum, but was unable to prove his hypothesis. However, in the 1940's, Van Egmond et al. took up the challenge and presented a simple torsion pendulum model to capture the mechanics of the SCC and satisfy the concepts of Mulder's Law. The original simple torsion pendulum model replicated known behavior of the SCC: accurate estimate of angular velocity for transient movements and response decay to equilibrium for long-duration constant velocity (Van Egmond, 1948).

Despite the accuracy of the model, the MIT MVL argued that the model was limited since it did not provide an explanation for adaptation or habituation. Though they did not describe habituation, the MIT MVL did present a viable extension of the torsion pendulum model to account for adaptation (Young, 1969). In the 1970's, the model was extended to its current form to account for rate sensitivity as well (Nasher, 1970; Ormsby 1974). The SCC model can be seen in its current form in Equation 2 (Borah 1979, 1988),

11

where Y is the SCC model response, or afferent firing rate, and U, the angular velocity, is the stimuli input:

$$\frac{Y}{U} = \frac{0.547s(s + 100)}{(s + 0.1)(s + 0.0333)} \qquad (2)$$

Merfeld, also a student of MIT's MVL, implemented an SCC model which was based upon experimental work of Fernandez & Goldberg (Merfeld, 1990; Fernandez & Goldberg, 1976). Merfeld's model is a second order high-pass filter where angular velocity is the input, U, and the afferent firing rate is the output, Y:

$$\frac{Y}{U} = \frac{(80 * 5.7)s^2}{(80s + 1)(5.7s + 1)} \qquad (3)$$

Until the 1960's, hardly any research was dedicated to modeling the mechanics of the otoliths. Young proposed that the otoliths resemble linear accelerometers based on what little research existed at the time. The MIT MVL originally presented a second order model to account for acceleration and jerk. A further revision of the model allows the model to respond to lateral specific force (gravity minus acceleration). The revised otoliths model proved to agree with perception of tilt and translation (Young, 1969). The otoliths model in its current form was developed by Borah (1979, 1988), where Y is the otolith model response, or afferent firing rate, and U, specific force, is the stimuli input:

$$\frac{Y}{U} = \frac{90(s + 0.1)}{(s + 0.2)} \qquad (4)$$

12

Pommellet, another student of the MIT MVL, implemented a model of the otolith organs based on the work of Grant and Best (Pommellet, 1990). This otolith model uses second order dynamics with two time constants:

$$\frac{Y}{U} = \frac{1}{(s+100)(s+0.1)} \tag{5}$$

By the mid to late 1970s, researchers began combining the vestbiular model and the OCM to predict pilot perception of orientation. In 1976, Curry extended the OCM model developed by Kleinman et al. to account for motion cues (using Young's model) and external visual cues. The primary goal of this model was to incorporate motion cues by altering the state vector, x, to account for vestibular outputs, i.e., pitch and roll. The second goal of Curry's model was to validate the use of such a model for visual meteorological conditions (VMC). Visual and motion cues were captured by a measurement observation parameter, y, in a Kalman filter. Curry was able to "accurately predict the difference between fixed-base and differing motion-base cues in a VTOL hovering task." The model performed well in mid to high frequency ranges, but was unable to predict behavior at low frequencies (Curry, 1976).

In 1979, Borah presented a multisensory input pilot model to "predict pilot dynamic spatial orientation," again using Young's model. This reference frame of this model is the perception of a pilot's perception of his or her orientation, and not that of the aircraft. The model consisted of two parts: an internal model and a time history. The internal model calculated expectations of orientation, represented by the Kalman filter gains. The time history included the visual, vestibular, tactile and proprioceptive models and respective stimuli, integrated via a Kalman filter. The Kalman filter used the gains calculated from the internal model and the responses generated from the multisensory

13

input to estimate pilot's perception of spatial orientation. The model was validated and shown to exhibit "correct, qualitative human response characteristics" (Borah, 1979; Borah 1988).

In recent years, Newman et al. presented a new orientation perceptual tool using data from on-board recorders (e.g., acceleration, control inputs, etc.) as inputs. The model takes in actual data from an aircraft's on-board recorders as input and calculates an estimate of the pilot's perception of his or her own orientation via vestibular cues. The tool was developed to support accident investigators in determining if spatial disorientation is or was a probable cause. This orientation model takes advantage of vestibular model developments by the MIT MVL, as well as other sensory models (i.e., visual, tactile, etc.).

Reviewing these models relative to this thesis' objectives, Merfeld et al. and Newman developed observer models which incorporated the internal models of the SCC and otolith dynamics. However, these models did not include internal models of the aircraft dynamics (Merfeld, 1993; Newman, 2009), but instead modeled any changes in motion as exogenous inputs that could not be predicted. Thus, these models do not account for expert pilot knowledge capable of predicting and projecting the aircraft dynamics between visual scans.

Computational Models

Computational modeling is not an end in and of itself. However, according to researchers in this domain "if the human spatial orientation system could be modeled then (new) maneuvers with proposed aircraft design could be evaluated to determine the likelihood of spatial disorientation problems in advance" (Previc, 2004). Computational modeling may fill the gap between countermeasure design and implementation.

14

Most applications of prediction-type models have analyzed pilot's perception based on limited stimuli alone. Previous models have not modeled the pilot's knowledge of aircraft dynamics. Instead, these models match data streams from aircraft involved in accidents to the vestibular cues they would have provided (Borah, 1988; Newman, 2012).

Computational models can be used to improve the design of countermeasures to spatial disorientation nad loss of energy state awareness by determining what visual scanning behavior or external cues could possibly increase or decrease the likelihood of spatial disorientation or loss of energy state awareness, and by identifying particularly problematic maneuvers or scenarios that should be used in evaluations of designs.

To this end, the model-based observer (MBO) applied in this thesis provides a cogent method of estimating the pilot's expectation of the aicraft state by including an internal aircraft model that represents the pilot's internal expectation of the aircraft state. This internal aircraft model accounts for expert pilot knowledge of the aircraft. Specifically, this thesis applies a MBO originally developed by Onur in the Cognitive Engineering Center at the Georgia Institute of Technology (Onur, 2014). The lower half of Figure 1 represents the model of $\hat{x}$, i.e., the reference expectation the pilot (RPE) could have at any particular time. The RPE is updated through the optimal integration of the pilot's knowledge of the aircraft, with visual and vestibular sensing. The estimated state and input matrices ($\hat{A}$ and $\hat{B}$, respectively) model the pilot's knowledge of the aircraft's dynamics and control inputs.

The upper half of the MBO in Figure 1 simulates reality, or the aircraft state which is labeled as (1). In this thesis work, the state of the aircraft, x, is simulated by the six degree-of-freedom aircraft model in the Work Models that Compute (WMC) simulation framework. In theory, the MBO can be connected with any aircraft model, but this thesis work uses a Boeing 747 type aircraft model. The aircraft state, x, comprises altitude, three components of airspeed in the body frame (u, v, and w), rotational rate in the body frame (p, q, and r), and the quaternion. The overall MBO structure contains

continuous dynamics with continuous and discrete measurements to estimate the RPE due to vestibular sensing and a given visual scan. For more information on the details of the model, including specific properties of the extended Kalman filter used in the model-based observer, please refer to Onur (2014).
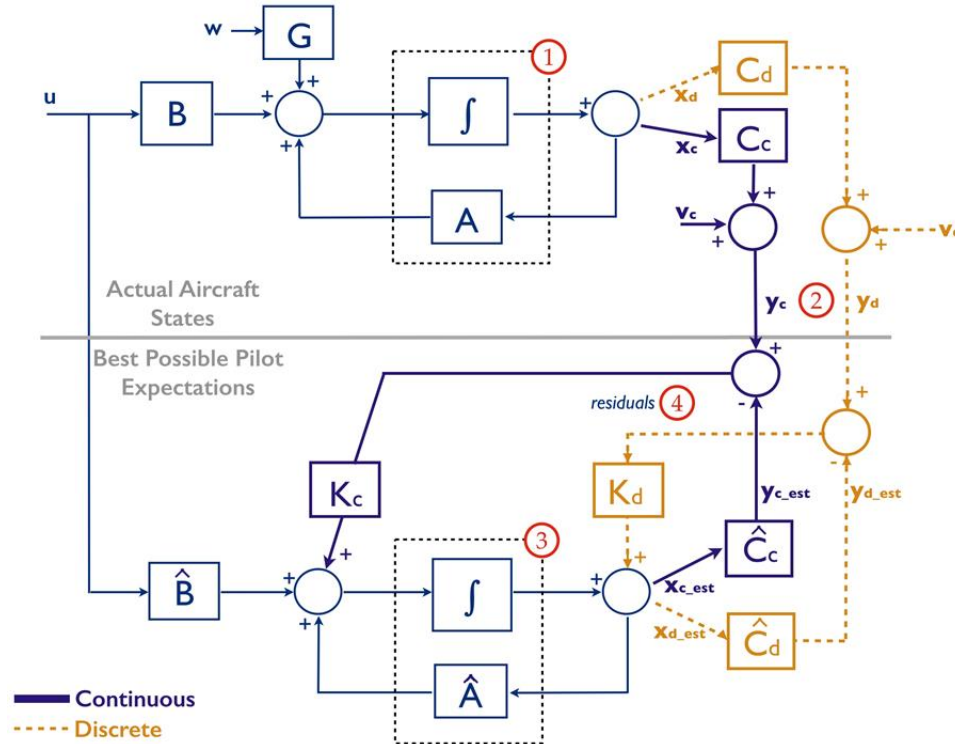
Figure 1. *Model-based Observer with Continuous and Discrete Measurement Updates*

Visual scanning of the flight instruments is simulated using visual-scanning actions. Each visual-scanning action is a discrete measurement, i.e., y_D in the upper half of Figure 1 (see label 2), of the aircraft's state. These visual-scanning actions can be scheduled to occur synchronously or asynchronously, and at high or low frequencies. This is controlled through each instrument-scanning actions' update time, t_{sample}. The work in this thesis is carried out under the assumption that flight occurs in instrument meteorological conditions (IMC), hence no external visual or horizon, and is limited only to simulating pilot scanning of the primary flight instruments (i.e., altimeter, airspeed indicator, attitude indicator, and heading indicator).

The vestibular system model simulates vestibular cues to the MBO. Continuous measurements, y_C (see label 2), will capture the output of this vestibular system model. Both continuous (vestibular) and discrete (visual) measures, y, are compared with the measures the pilot would expect, $\hat{y}$, given his or her internal expectation of the state, $\hat{x}$ (see label 3). This expectation of the state is the optimal estimation calculated via an extended Kalman filter. The difference, i.e., the residual, v (see label 4), is used to correct the pilot's internal expectation. The vestibular model can apply any transfer function and threshold in modeling both the SCC and the otoliths. Here, Merfeld's SCC model and Grant & Best's otolith model are used to model the vestibular system. For the SCC model the threshold is set at 2.5 °/s for all three axes. For the otolith model the threshold is set at 0.006g for the x and y axes and 0.01 for the z-axis.

The MBO computes both the RPE and the error covariance in the RPE. From this, the standard deviation in the error in the pilot's expectation, σ, can be derived for each state. Assuming this error is zero mean and normally distributed, the two-sigma (2σ) value corresponds to a 95% confidence interval (CI) on the error of each state. For example, consider the following scenarios shown in Figure 2, 3, and 4: no distraction, 5-second distraction, and 10-second distraction, all during a subthreshold roll (right wing down) initiated 5 seconds into the simulation. The RPE for each of these durations of distraction is shown in Figure 2; once the distraction ends, the RPE is quickly corrected by the resumed visual scan.

17
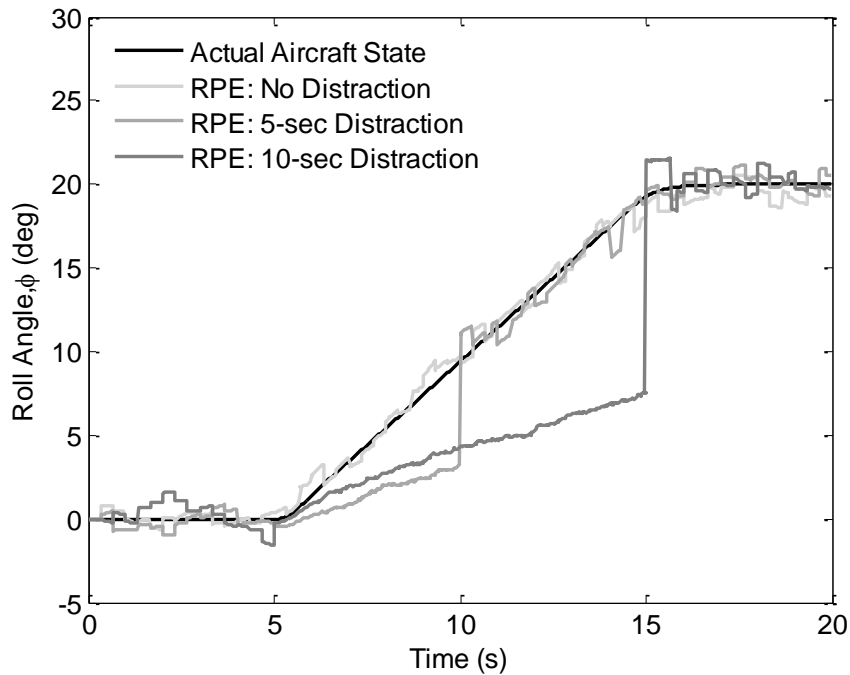
Figure 2: *Reference Pilot Expectation of Roll Angle with No Distraction, a 5-second Distraction, and a 10-second Distraction from the Primary Flight Instruments during a Subthreshold Roll.*

The corresponding error is shown in Figure 3. Figure 4 thus summarizes how the longer distractions increase the value of the 95% CI of the error in RPE.

The aviation community has called for a computational model to evaluate spatial disorientation and loss of energy state awareness countermeasures. The MBO now exists, building on earlier models, to provide the capability to evaluate such countermeasures. The MBO can fully analyze basic properties of visual scan for impact on the RPE, highlighting things important to spatial disorientation and loss of energy state awareness.

18
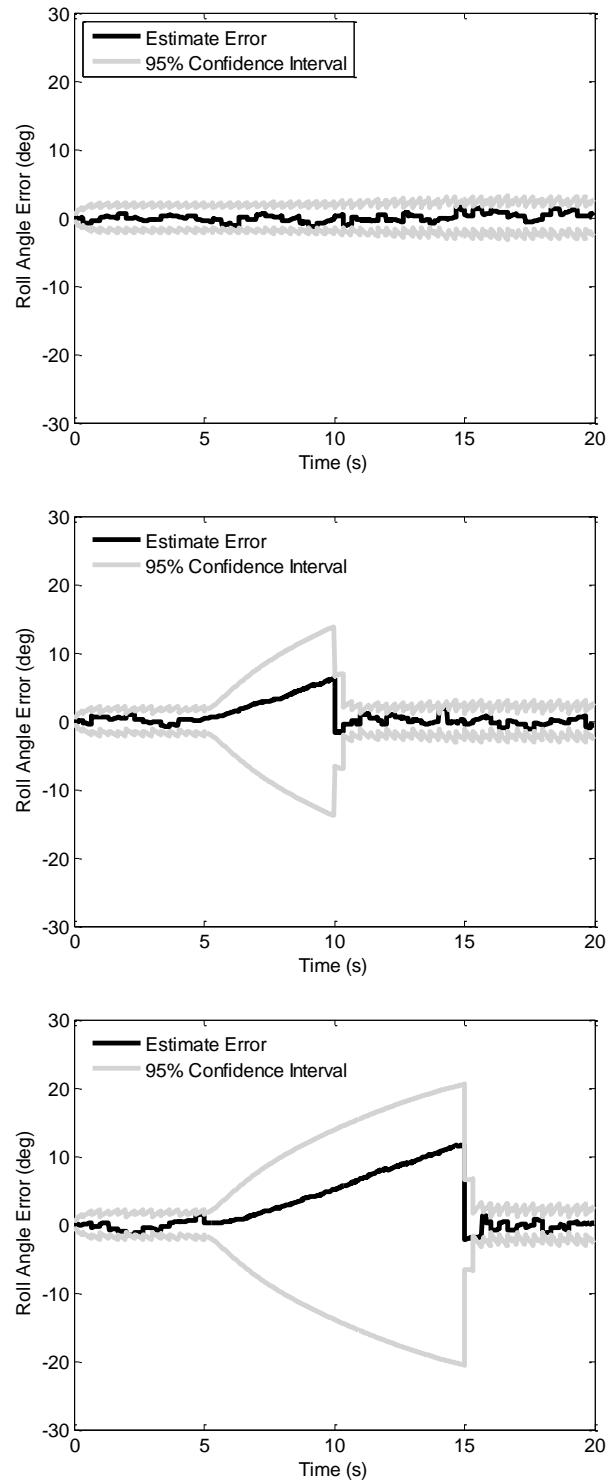
Figure 3: *Comparison of the 95% Confidence Interval of Roll Angle Due to No Distraction, a 5-second Distraction, and a 10-second Distraction During a Sub-Threshold Roll*

19
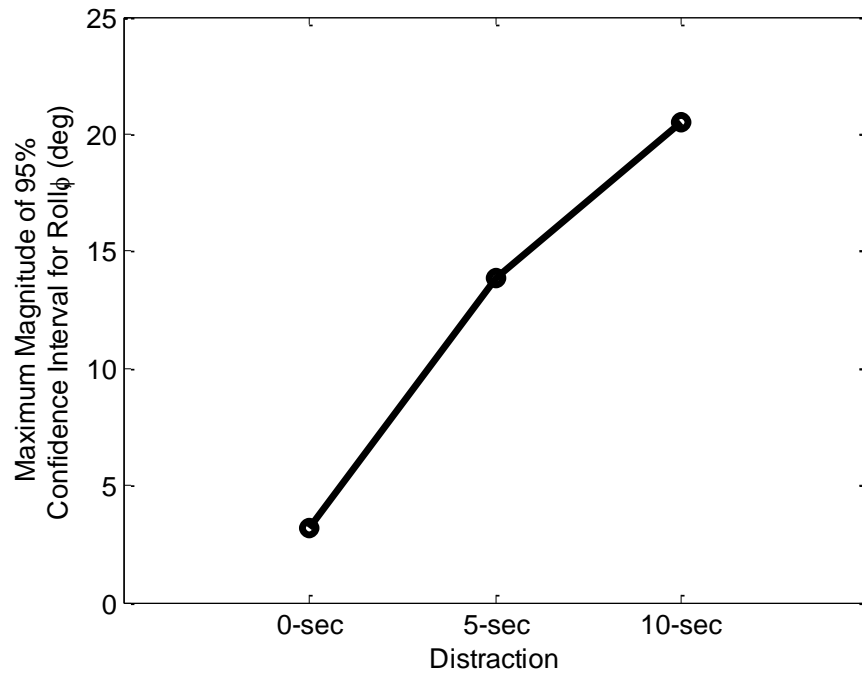
Figure 4. *Maximum Magnitude of the 95% Confidence Interval Bounding the Error in the Reference Pilot Expectation of Roll due to Duration of Distraction during a Sub-threshold Roll*

20

CHAPTER 3

MANEUVERS CONDUCIVE TO SPATIAL DISORIENTATION

As set out by the Commercial Aviation Safety Team (CAST), Safety Enhancement (SE) 207 urges the aviation community to conduct research to "enable the development, implementation, and certification of technologies that enhance flight crew awareness of airplane energy state and conditions likely to produce spatial disorientation." SE 207 also urges the community to conduct research in finding "cost-effective, user-centered flight deck alerting systems to alert flight crews to the two conditions that produced spatial disorientation:" slow subthreshold rolls (conducive to the somatogyral illusion) and the somatogravic illusion (CAST, 2013). Somatogyral illusions arise due to inadequacies of the semicircular canals (SCC), leading to erroneous perception of the aircraft's attitude. Somatogravic illusions arise when the otolith organs interpret a linear acceleration as a tilt. The following sections describe each, and how each can be captured by the MBO.

Somatogyral Illusions: Illusions Arising from Stimulation of the Semicircular Canals

Somatogyral illusions occur due to the SCC's inability to detect angular rotation below a certain threshold (Previc, 2004). For example, a common somatogyral illusion, known as the leans, is caused by an above-threshold return to level flight after a subthreshold roll into a coordinated turn unnoticed by the pilot. In Figure 5, a subthreshold roll (right wing down) begins at 10 seconds. The pilot is distracted from scanning the flight instruments from the start of the maneuver at 10 sec until time 40 sec, i.e., the entire duration of the maneuver. The reference pilot expectation (RPE) of roll and

roll rate estimates the aircraft is at wings level due to the distraction and the SCC's inability to detect rotation during the subthreshold roll. At 30 seconds, the aircraft returns from right wing down to wings level at an above-threshold roll while the pilot is still distracted from scanning the flight instrument, but the SCC detects the motion and causes the RPE to estimate a rotation from wings level to left wing down, instead of the right wing down returning to wings level. This maneuver causes the RPE to incorrectly estimate the aircraft's attitude until visually corrected at time 40 sec.
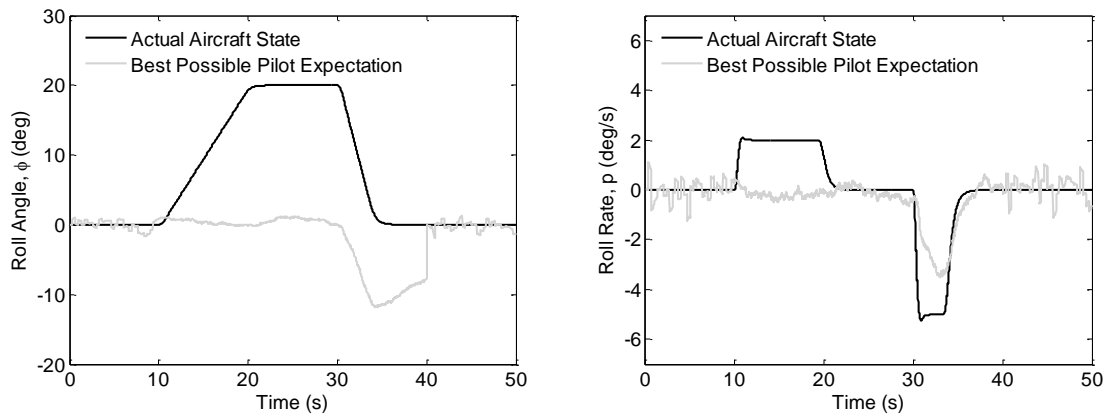
Figure 5. *Depiction of the Leans Illusion in Roll (left) and Roll Rate (right)*

Somatogyral illusions can also occur from angular accelerations about other axes. The left plot in Figure 6 demonstrates an above-threshold pitch up to 15 degrees and an above-threshold level off. The semicircular canals detect the angular velocity of the motion throughout the maneuver. However, the otolith organs also detect the changes in specific forces (most notably seen between 25 seconds and 40 seconds) due to increased tilt and counter-act the illusion. Conversely, the plot on the right shows the reference pilot expectation without the contribution of the otolith organs during the same maneuver. Without the otolith contribution, the RPE would be conducive to somatogyral illusions. The two plots in Figure 6 demonstrate that with the counter-acting otolith organ

22

contribution in a pitching maneuver, the RPE does not demonstrate the same magnitude of a somatogyral illusion as the rolling maneuver in a coordinated turn.
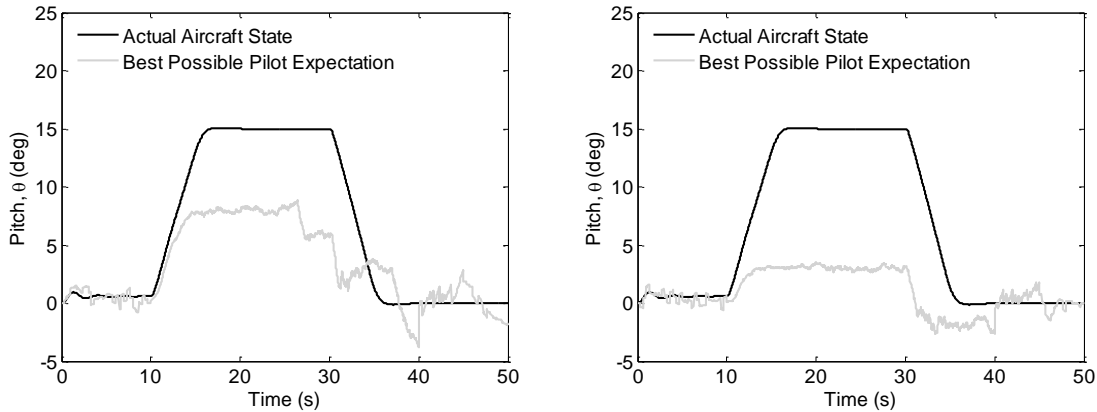
Figure 6. *Somatogyral Illusion During a Pitch Maneuver with Semicircular Canals and Otolith Organs Detection (left) and Only Semicircular Canals Detection (right)*

In Chapter 4, several computational experiments will be conducted to examine the impact of pilot visual scans in these coordinated turns conducive to somatogyral illusions. Specifically, the aircraft will begin at an altitude of 28,000 ft at wings level with an indicated airspeed of 300 knots. The bank maneuver involves the aircraft rolling from wings level to a 20-degree roll angle, holding the roll angle for a few moments, and then returning to steady, level flight. The roll is conducted below the vestibular threshold with a roll rate of 2.0 °/s. (as demonstrated in Figure 7) or above the vestibular threshold with a roll rate of 3.0 °/s (as demonstrated in Figure 8), with the MBO configured to have a threshold of 2.5 °/s. All degradations from a proper T scan (e.g., omission and distraction) will occur at the onset of the roll. These computational experiments assume the pilot is aware of the control surface deflections and that poor external visual conditions exist (e.g., weather, night flight, etc.). (The script used to perform the bank maneuvers is provided in Appendix A.)

23
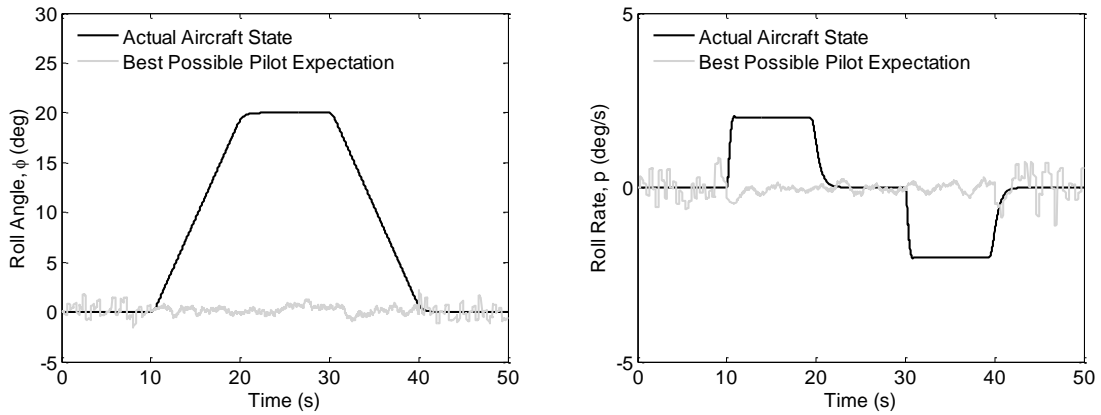
Figure 7. *Reference Pilot Expectation of Roll and Roll Rate During a Sub-threshold Bank Maneuver with No Awareness of Control Surface Deflections*
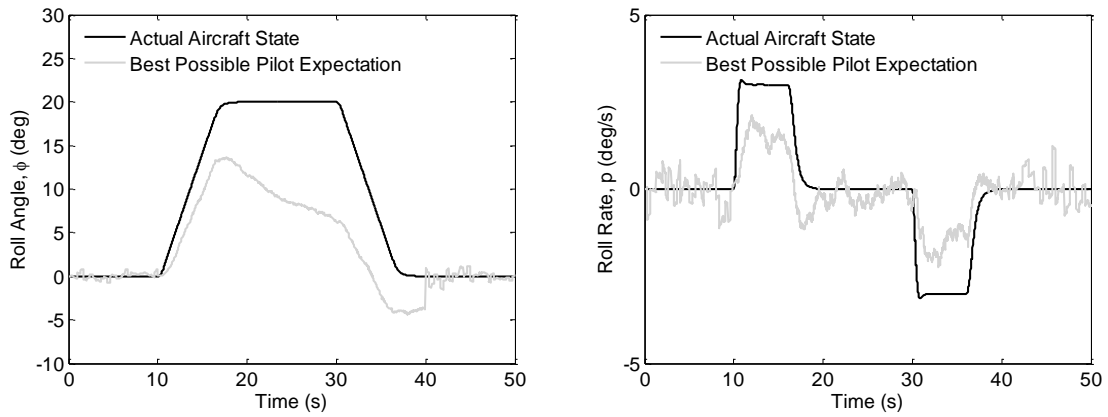
Figure 8. *Reference Pilot Expectation of Roll and Roll Rate During an Above-threshold Bank Maneuver with No Awareness of Control Surface Deflections*

It is also important to note the impact of turbulence levels on the error in RPE of roll angle during maneuvers conducive to somatogyral illusion. The turbulence placed on the aircraft is treated by the MBO as white noise, though in reality turbulence is not Gaussian. Table 2 provides the ranges for the process error used to simulate the different turbulence intensities, i.e., light, moderate, and severe. Onur provides a detail description of how these ranges were identified (2014).

Table 2. The Process Error Ranges for each of the Aircraft States

	Light Turbulence	Moderate Turbulence	Severe Turbulence
Altitude (ft)	100	250	500
Linear Velocities (for x, y, z) (ft/s)	35 5 10	200 60 75	400 10 150
Angular Velocities (for x, y, z) (rad/s)	0.04 0.04 0.04	0.1 0.1 0.1	0.2 0.2 0.2
Quanternion	0.04	0.07	0.13

The maximum 95% confidence interval of error in RPE of roll angle with a 30-second distraction as a function of turbulence level is provided in Figure 9 during subthreshold and above-threshold roll maneuvers to four different target roll angles. These results quantify how the growth of the maximum 95% CI of error in RPE of roll depends on the turbulence intensity. In light turbulence, the maximum 95% CI of error in RPE is relatively constant for each roll maneuver. For moderate turbulence, there is a slight linear growth in the maximum 95% CI of error in RPE. Finally, for severe turbulence, the linear growth is greater than the previous turbulence intensities. Overall, the relationship quantifies how the growth of the maximum 95% CI of error in RPE of

25

roll angle increases with turbulence levels. For the remainder of this thesis work, light turbulence and a target roll angle of 20 degrees will be applied in the simulated maneuvers.
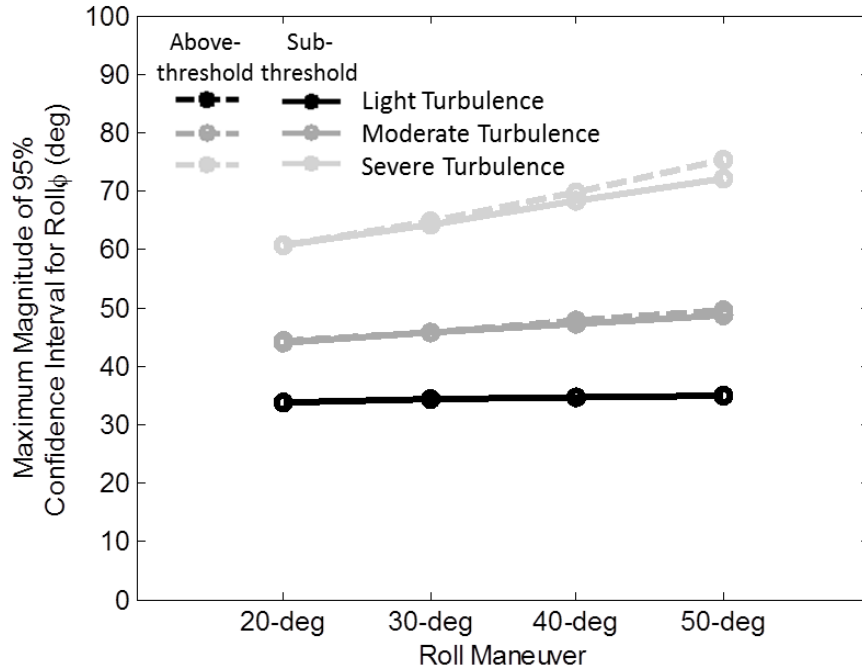
Figure 9. *Maximum 95% Confidence Interval of Error in RPE of Roll Angle with a 30-second Distraction During Roll Maneuvers to Different Roll Angles as a Function of Turbulence Level*

Somatogravic Illusions: Illusions Arising from Stimulation of the Otolith Organs

Pilots are also susceptible to somatogravic illusions which occur due to sudden changes in linear accelerations. These illusions are caused by limitations in the otolith organs' ability to distinguish between linear accelerations and tilt, especially in aviation operations. The most common somatrogravic illusion is the head-up illusion (Figure 10) during sudden forward linear accelerations in steady, level flight without any visual correction (e.g., distracted from the primary flight instruments and no external visual). The otolith organs detect the linear acceleration, but interpret it as pitching up (as seen in the left plot of Figure 10).

26
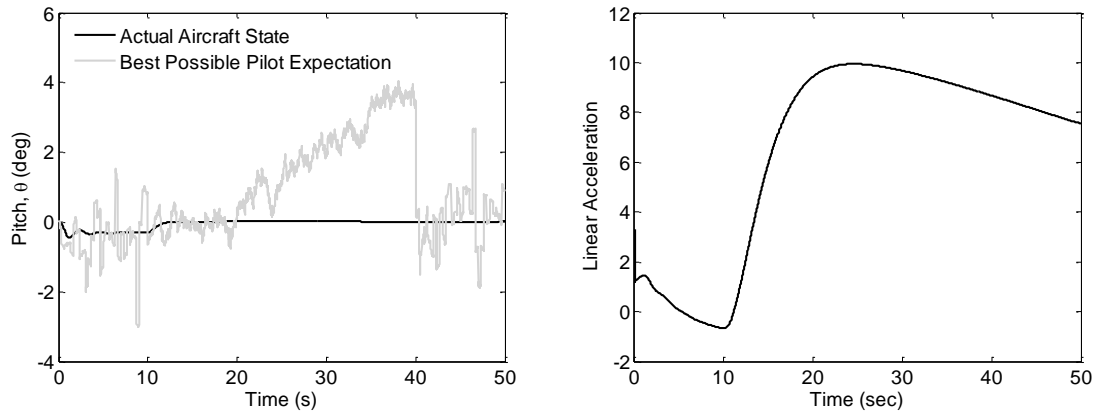
***Figure 10**. Depiction of the Head-up Illusion During a No-pitch, Forward Acceleration Maneuver Conducive to Somatogravic Illusions*

In Chapter 4, several computational experiments will be conducted to examine the impact of pilot visual scans in no-pitch, forward acceleration maneuvers that can cause somatogravic illusions. The aircraft will begin at an altitude of 10,000 ft at wings level with an indicated airspeed of 350 knots. An increase in acceleration, created by commanding maximum thrustis initiated 10 seconds into the simulation (Figure 10). All degradations of a proper T scan (e.g., omission and distraction) will start at the onset of the acceleration. It is also assumed for these cases that the pilot has awareness of control surface deflections and poor external visual conditions exist (e.g., weather, night flight, etc.). (The script used to perform this maneuver is provided in Appendix A.)

27

CHAPTER 4

QUANTITATIVE ASSESSMENT OF SPATIAL DISORIENTATION

This chapter provides a quantitative assessment of the impact of the pilot's visual scan of primary flight information during the maneuvers conducive to vestibular illusions described in Chapter 3. The computational experiments in this chapter begin with analyzing a proper scan pattern (i.e., a T scan), wherein all of the primary flight instruments are scanned with a specified scan period which is varied; then, degradations of this proper scan are examined, i.e., omission of an instrument or distraction from all instruments. Next, the experiments examining the accuracy of pilot perception of flight instruments analyze the extent to which designing displays with finer resolution can improve the reference pilot expectation (RPE). Finally, a comparison between these effects and a brief comparison against the impact of pilot control surface awareness is provided.

These computational experiments will present the relevant aircraft states to the maneuvers being simulated: roll and roll rate for the somatogyral illusion, and pitch, altitude, and true airspeed for the somatogravic illusion. More details about these experiments and how the data can be retrieved are provided in Appendix B.

The Impact of Scan Pattern in Maneuvers Conducive to Vestibular Illusions

This computational experiment examines the impact of proper scanning of the primary flight instruments, i.e., conducting a T scan at different scan periods, followed by the impact of degradations in the scan pattern, i.e., omitting an instrument during a T scan or being completely distracted from all primary flight instruments for some duration of time. These effects are examined in three maneuvers: subthreshold and above-threshold

bank maneuvers (conducive to somatogyral illusions), and a no-pitch, forward acceleration (conducive to somatogravic illusions).

The relationship between the maximum 95% confidence interval (CI) of error in RPE of roll and T scan period during subthreshold and above-threshold bank maneuvers conducive to somatogyral illusions is provided in the left plot of Figure 11a. The same relationship is provided for error in RPE of roll rate in the right plot of Figure 11a. These relationships quantify how the error grows with larger scan periods: with larger scan periods the error in RPE increases linearly until the error plateaus at a constant value. The error in roll rate corresponds to the roll rate at the onset of the roll maneuver (at 10 s in Figure 12), and the plateau starts when the roll rate zeros out at the target roll angle (approximately 3 to 4 seconds after the onset of the maneuver). Note that there is little difference between the error in the subthreshold and above-threshold maneuvers since the pilot is consistently scanning all of the instruments with a proper T scan.
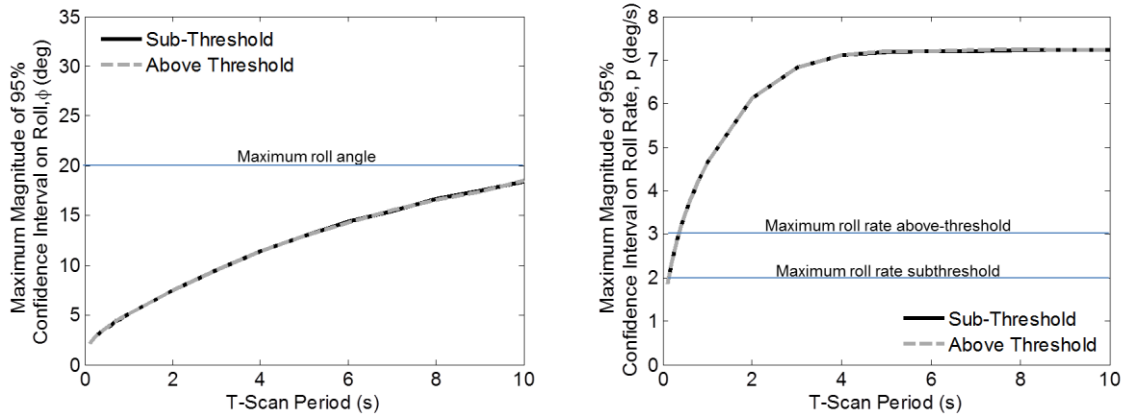
(a) Error in RPE of Roll and Roll Rate with T Scan
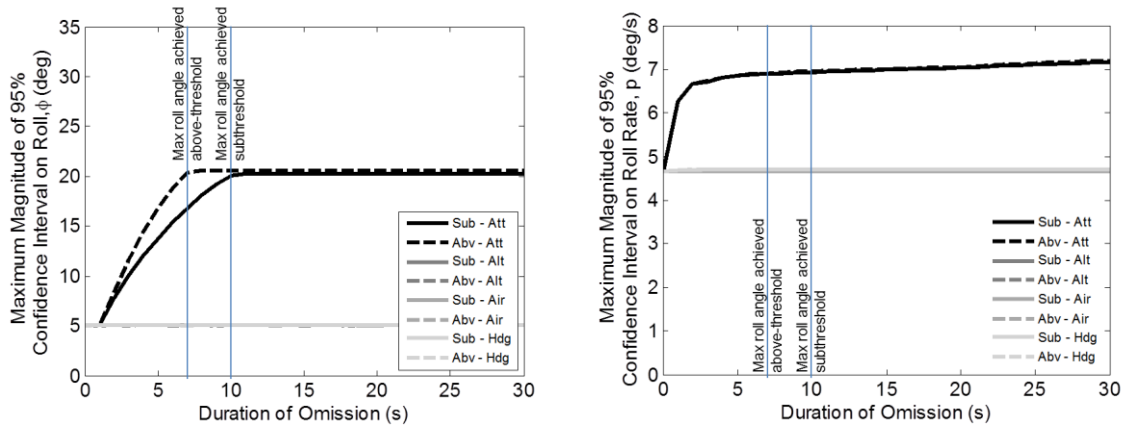
(b) Error in RPE of Roll and Roll Rate with Omission of a Flight Instrument
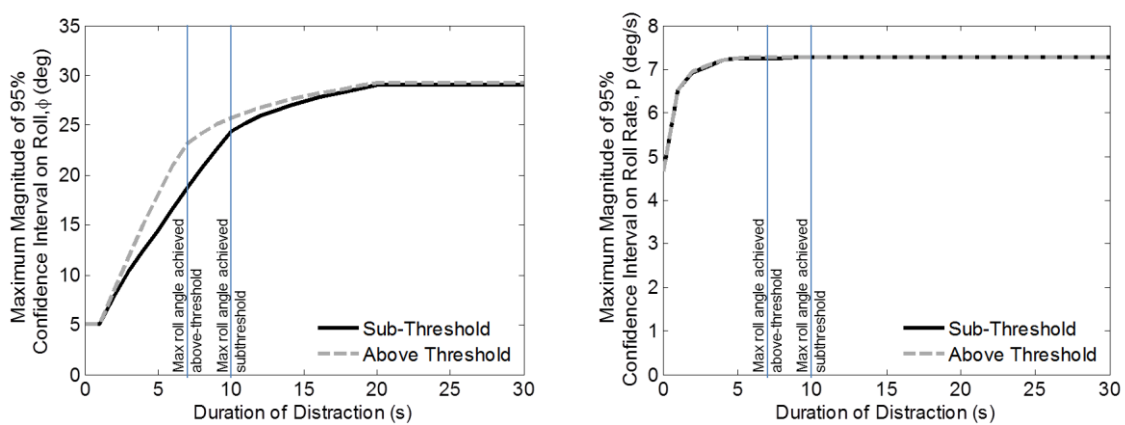
(c) Error in RPE of Roll and Roll Rate with Distraction

Figure 11. *Maximum 95% Confidence Interval of Error in RPE of Roll and Roll Rate Resulting in a Banking Maneuver Conducive to the Somatogyral Illusion*
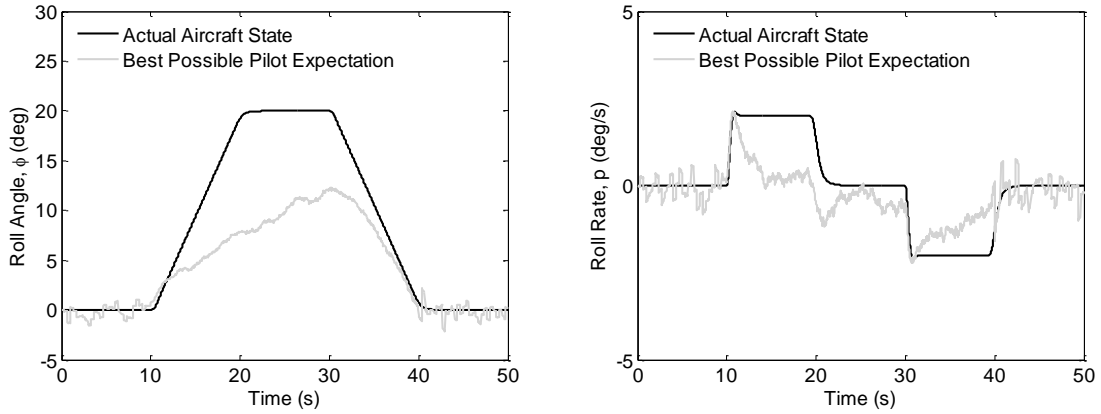
Figure 12. *Reference Pilot Expectation of Roll and Roll Rate During a Sub-threshold Bank Maneuver with a 30-second Distraction from 10 Seconds to 40 Seconds*

In the omission experiments, a T scan is conducted at a 1.0 sec scan period but then omits one of the primary flight instruments from the visual scan at the start of the roll. The relationship between the maximum 95% CI of error in RPE of roll and the duration of omission of an instrument from the visual scan is provided in the left plot of Figure 11b. The same relationship for the error in RPE of roll rate is provided in the right plot of the Figure 11b. These relationships for the error in RPE of roll and roll rate show that the error initially increases linearly with greater duration of omission of the attitude indicator from the visual scan. Once the roll rate zeros out, the error in RPE of roll rate plateaus. Likewise, as the roll angle reaches the target roll angle, the error in RPE of roll plateaus too. The relationship between the maximum 95% CI of error in RPE of roll and duration of omission of the attitude indicator also reveal the impact of subthreshold and above-threshold rolls: despite vestibular sensing, the error in RPE of roll grows faster during the faster above-threshold maneuver than the subthreshold roll. Thus, the disparity in growth of error in RPE of roll during the subthreshold and above-threshold roll is a direct consequence of the slower roll rate during the subthreshold roll. However, despite the disparity in growth of error in RPE of roll, the maximum 95% CI of error in RPE of roll during the subthreshold roll reaches the same value as the above-threshold roll during

31

the omission of the attitude indicator. The slower growth in the error in RPE of roll during the subthreshold roll does correspond to a mitigating factor: there is more time to counter illusions that might arise in maneuvers where there is no vestibular sensing. Note: This is not to say that subthreshold cases are better than above-threshold or vice versa. The results just simply show that the growth of error in RPE of roll in above-threshold rolls is faster than the growth of the error in RPE of roll in a subthreshold roll maneuver.

Similarly in the distraction experiments, a T scan is conducted at a 1.0 sec scan period before and after the distraction, which begins at the start of the roll. The relationship between the maximum 95% CI of error in RPE of roll and duration of distraction from all primary flight instruments is provided in the left plot of Figure 11c. The same relationship for the error in RPE of roll rate is provided in the right plot of Figure 11c. Each of the NextGen arrivals of roll and roll rate has similar growth characteristics as omission of the attitude indicator during a roll: with greater duration the error increases linearly and then plateaus once the aircraft reaches the target roll angle. However, the rate of increase is even greater with distraction than omission since the expectation is not corrected by any of the other primary flight instruments.

Comparatively, the relationships presented in Figure 11 reveal that the maximum 95% CI of error in RPE of roll and roll rate increases with increased degradation of the visual scan (especially for the expectation of roll). The error in RPE due to the omission is larger than with a T scan. This result is even greater for distraction, where the rate of increase of error in RPE is even greater with distraction than with omission or a T scan. These findings highlight the efficacy of a proper T scan in preventing a somatogyral illusion.

Similarly, conducting a proper T scan can reduce the susceptibility to somatogravic illusions due to sudden changes in linear accelerations (Figure 13). Here, the relationship between T scan period and the maximum 95% CI of error in RPE of

32

pitch, altitude, and airspeed is provided in the left plots of Figure 13a, b, and c, respectively, and quantifies that, with larger scan periods, the error in RPE increases.

(a) Maximum 95% CI of Error in RPE of Pitch due to T Scan, Omission, and Distraction
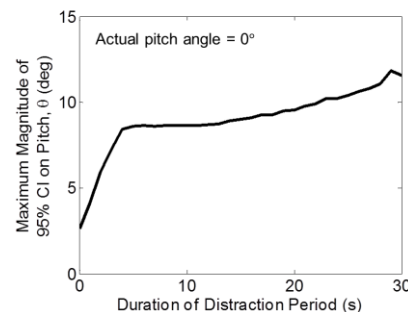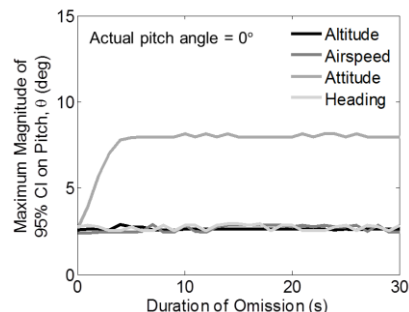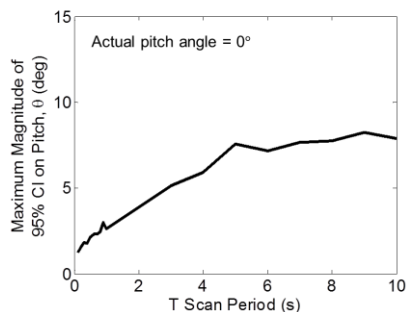
(b) Maximum 95% CI of Error in RPE of Altitude due to T Scan, Omission, and Distraction
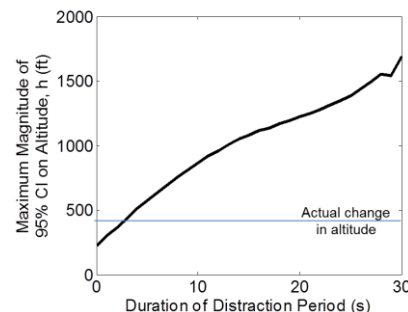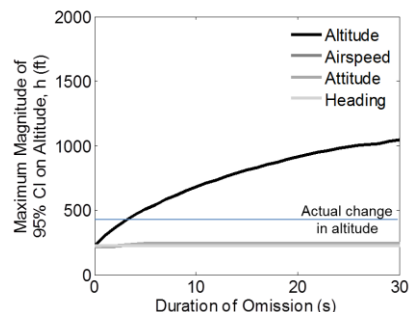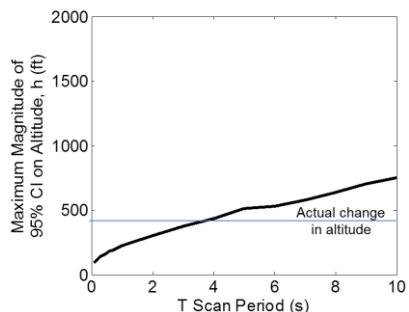
(c) Maximum 95% CI of Error in RPE of True Airspeed due to T Scan, Omission, and Distraction
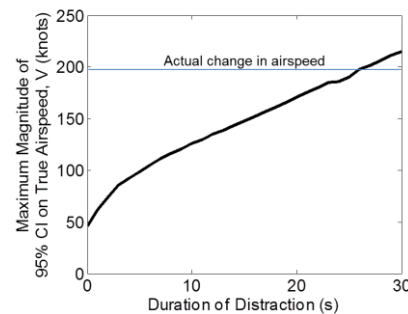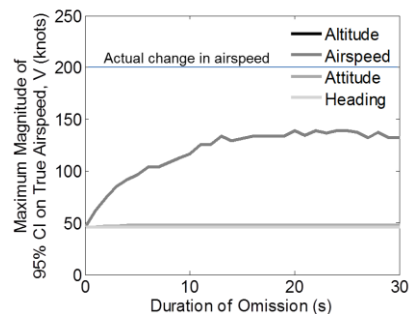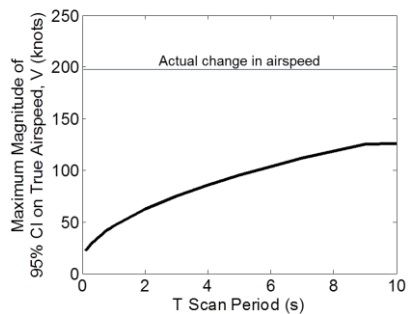
Figure 13. Maximum 95% Confidence Interval of Error in RPE of Pitch, Altitude, and True Airspeed in a No-pitch, Forward Acceleration Maneuver Conducive to the Somatogravic Illusion

34

The relationship between the duration of omission and the maximum 95% CI of error in RPE of pitch, altitude, and airspeed during a no-pitch, forward acceleration is presented in the center plots of Figure 13a, b, and c, respectively. These relationships show similar trends as omission of the attitude indicator during roll: With greater duration of omission of the attitude indicator the error in RPE of pitch increases linearly and then plateaus (Figure 13a). This plateau results from scanning the remaining instruments. With greater duration of omission of the altimeter the error in RPE of altitude increases linearly (Figure 13b) and with greater duration of omission of the airspeed indicator the error in RPE of airspeed increases as well (Figure 13c). While the error in RPE of altitude and airspeed do increase due to omission of the altimeter and the airspeed indicator, respectively, the growth of error in RPE does abate but does not necessarily plateau. This is because the altitude and airspeed continue to change due to the acceleration held throughout the scenario (Figure 14), hence the continued growth of the error in RPE of altitude and airspeed.
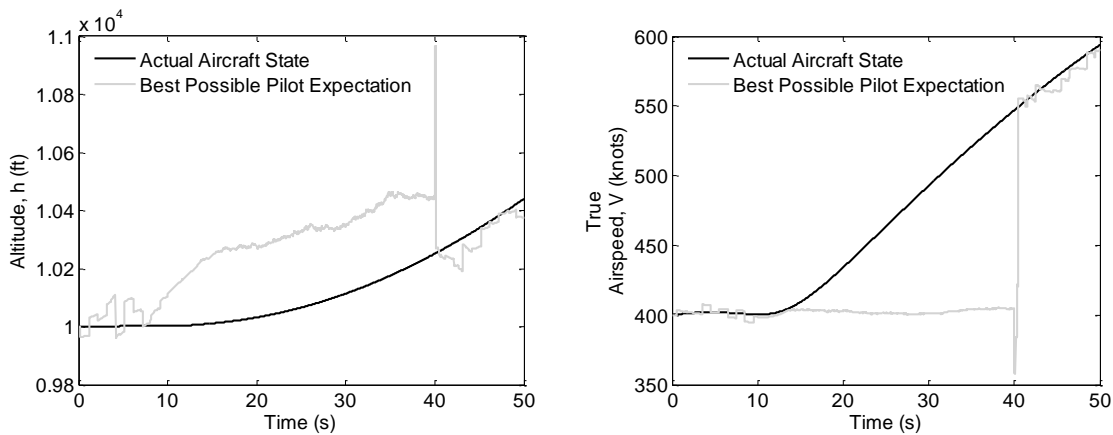
Figure 14. *Depiction of Altitude (left) and True Airspeed (right) During a No-pitch, Forward Acceleration Conducive to Somatogravic Illusions with a 30-second Distraction from 10 Seconds to 40 Seconds*

Finally, the relationship between the duration of distraction and the maximum 95% CI of error in RPE of pitch, altitude, and airspeed is provided in the right plots of

Figure 13a, b, and c. The relationships show the same trends as omission, though the rate of increase in error with duration is greater with distraction because there are no visual corrections from other flight displays portraying information about dynamics coupled with these states. The relationship between the maximum 95% CI of error in RPE of pitch and duration of distraction reveals the impact of the somatogravic illusion. The growth of error in RPE is similar to omission, but then there is a second growth period for the distraction case (for distractions lasting longer than 10 seconds). This growth arises from the sensation of pitch up that begins to take place about 10 seconds after the onset of the no-pitch, forward acceleration maneuver (as seen in Figure 15). It takes about 10 seconds for the illusion to set in because the acceleration reaches its peak around this time and sustains a fairly consistent value thereafter.
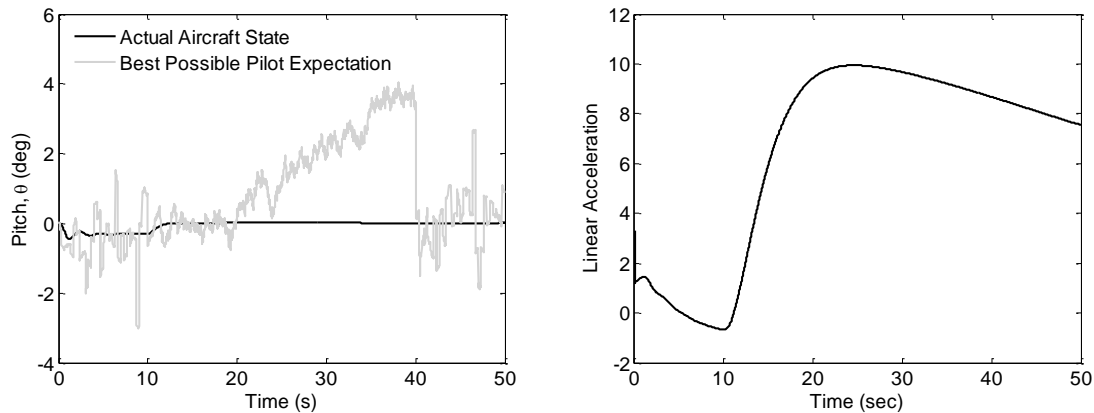
Figure 15. *Head-up Illusion from 20 to 40 seconds During a No-pitch, Forward Acceleration Maneuver Starting at 10 seconds with a 30-second Distraction from 10 Seconds to 40 Seconds*

To summarize, the impact of scan pattern on the maximum 95% CI of error in the RPE of roll and roll rate in a bank maneuver conducive to somatogyral illusions varies depending on scan performance and maneuver rotational rate (Figure 16 and Figure 17, respectively).

36

As seen in Figure 16 and Figure 17, the maximum 95% CI of error in RPE of roll and roll rate grow with larger scan periods or greater duration of omission or distraction. Also, the maximum 95% CI of error in RPE grows in a manner proportional to the maneuver. For example, the maximum 95% CI of error in RPE of roll grows linearly while the aircraft is banking to the target roll angle of 20 degrees, but plateaus once the target roll angle is achieved. Finally, these relationships quantify how scanning the instruments more frequently reduces the overall potential for error in expectation.
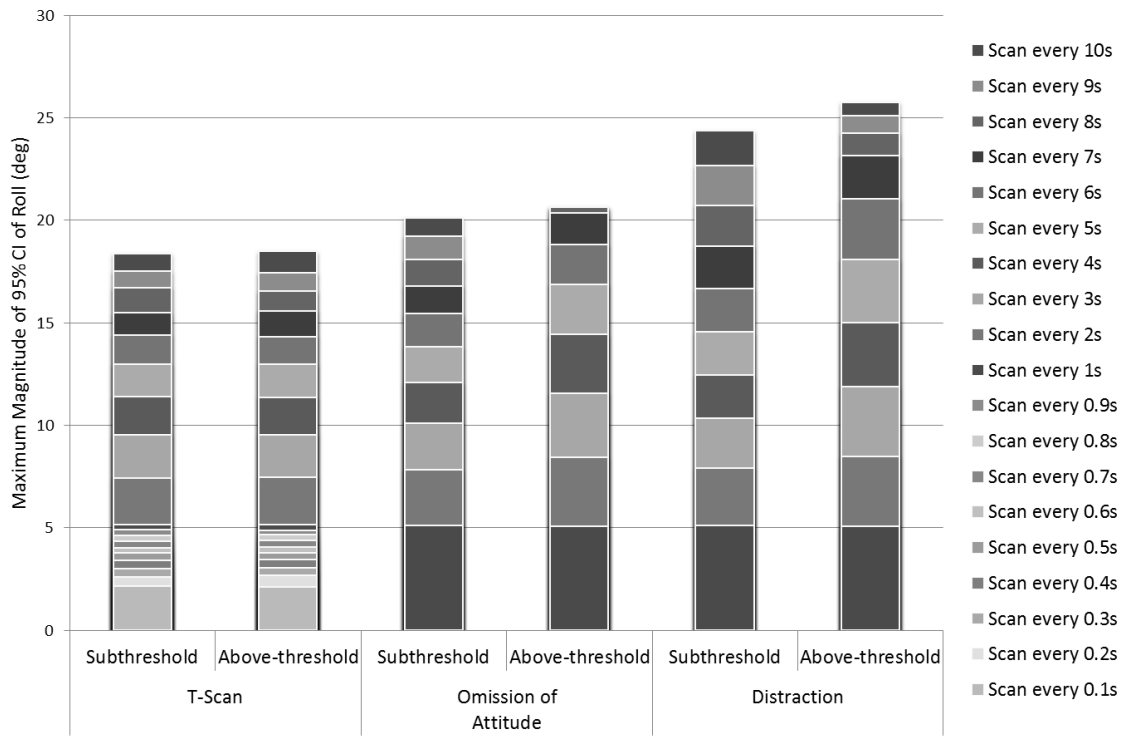
Figure 16. *Summary of the Impact of T scan, Omission, and Distraction on the Maximum 95% CI of Error in the Reference Pilot Expectation of Roll in a Banking Maneuver Conducive to Somatogyral Illusions*
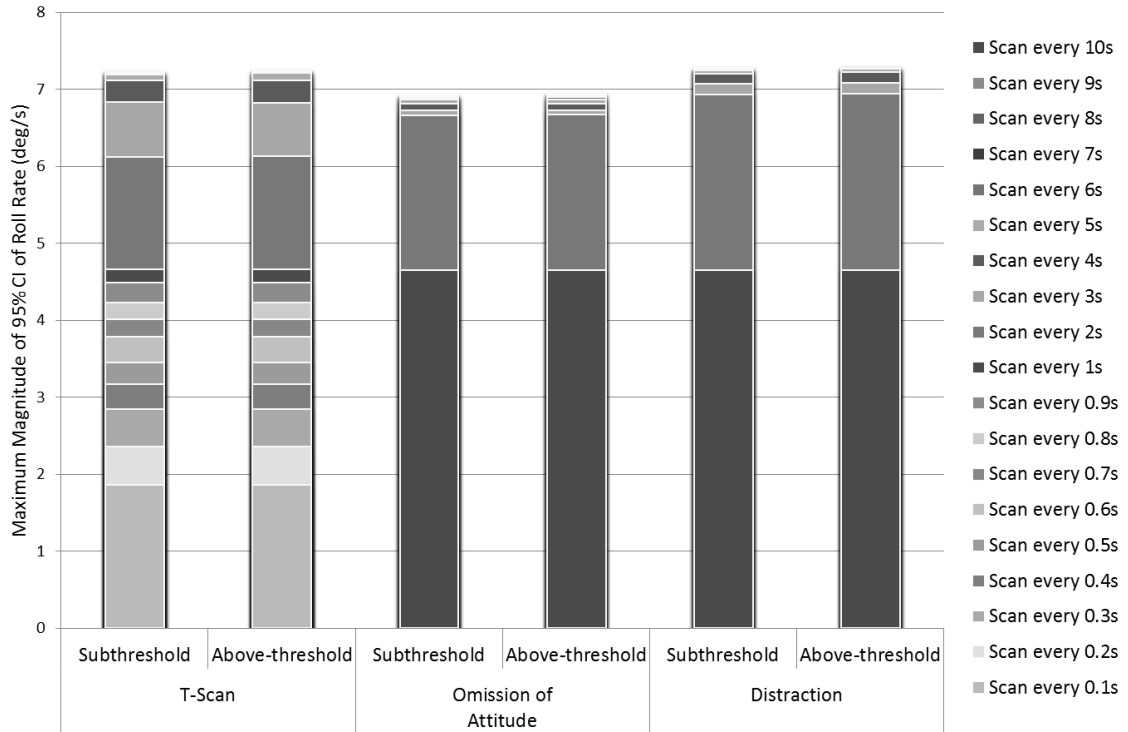
Figure 17. *Summary of the Impact of T scan, Omission, and Distraction on the Maximum 95% CI of Error in the Reference Pilot Expectation of Roll Rate in a Banking Maneuver Conducive to Somatogyral Illusions*

The impact of scan pattern on the maximum 95% of error in RPE of pitch in a no-pitch, forward acceleration maneuver conducive to somatogravic illusions is presented in Figure 18. A demonstrated here, performing a good scan, such as a T scan, can reduce the possible error in expectation. Degradation of a proper T scan, such as omitting a flight instrument or being distracted from all of the flight instruments, can increase the error in expectation. Not only should the pilot consider whether he or she is conducting a proper scan of all instruments, but also how frequently he or she scans the flight instruments. The more frequently the pilot scans the flight instruments, the lower the maximum 95% CI of error in RPE becomes.

38
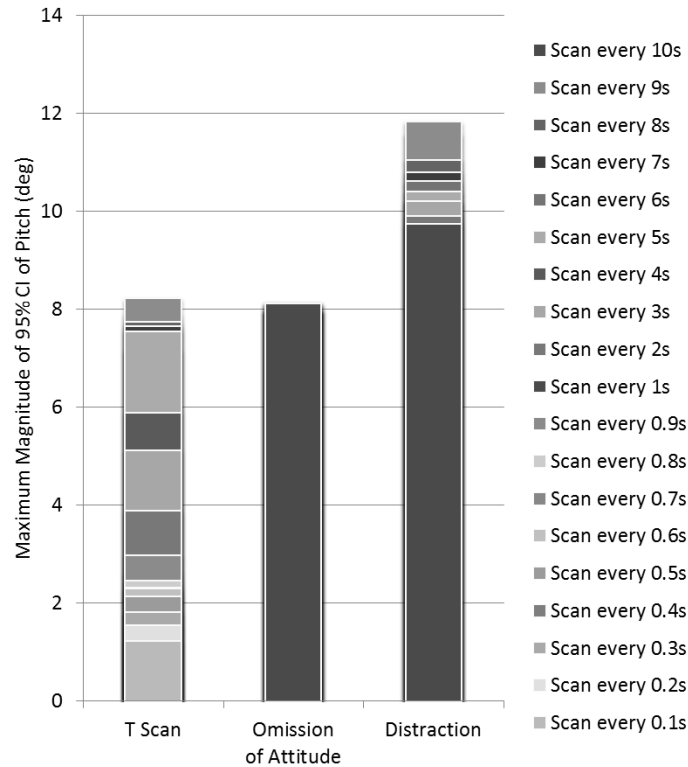
Figure 18. Summary of the Impact of T Scan, Omission, and Distraction on the Reference Pilot Expectation of Pitch in a No-Pitch, Forward Acceleration Maneuver Conducive to Somatogravic Illusions

Design Implications:

The results in this section quantify the impact of visual scans on the RPE during maneuvers conducive to vestibular illusions. First, relative to the selection of thresholds for alerting systems intended to re-direct the pilot's attention to the primary flight displays, the MBO provides the relationship between the maximum 95% CI of error in RPE of a state and the T scan period or duration of omission or distraction. These quantitative relationships can assist designers to design countermeasures or interventions based on the allowable error in expectation, which may itself vary in different phases of flight or maneuvers. It can also help designers to think about what aircraft states countermeasures should be based on. For example, the designer can assess whether an alert threshold should be based upon the roll angle or the roll rate, particularly in cases

where higher rates might lead to fast growth in error, yet slower rates may be below vestibular thershold

Second, the MBO also provides implications for required scan period for T scan. This information is useful for training and certification programs, which can be used to better train and certify pilots with scanning behavior to prevent susceptibility to vestibular illusions and decrease error in expectation.

Finally, the MBO provides the capability to examine diverse maneuvers and degradations in visual scans, preventions designers from solely focusing on one maneuver or one state of interest (e.g., the reference pilot expectation of pitch during a maneuver conducive to a head-up somatogravic illusion) and allow the designers to design with the whole picture in mind (i.e., the impact on the RPE for all states in a range of maneuvers).

The Impact of Accuracy of Pilot Perception

The impact of accuracy of pilot perception of the aircraft states through the flight displays also impacts the RPE. Accuracy can be improved by refining the resolution of the display or modifying the display features, such as photo-realistic presentations of attitude, making numeric values larger or smaller, tick marks more visible, changing color, etc. Display refinements and modifications can improve the pilot's perception of the information presented by flight displays if done correctly.

The MBO is able to capture the extent to which a pilot can accurately perceive aircraft state information from flight displays. In this computational experiment, a T scan is conducted every 1.0 second and the accuracy of pilot perception (σ_ε) is adjusted for each run. The study begins by analyzing the accuracy of pilot perception with an accuracy σ_ε of 0.01 deg. (that is, the pilot is able to accurately perceive the actual roll angle from the flight display with a standard deviation of 0.01 deg.) and continues up to

40

an σ_ε of 10 deg. Figure 19 shows the relationship between the maximum 95% CI of error in RPE of roll and the accuracy of pilot perception σ_ε during subthreshold and above-threshold bank maneuvers conducive to somatogyral illusions. This relationship quantifies how the error in RPE decreases with improved accuracy of pilot perception. Conversely, the relationship quantifies how, with greater inaccuracy of pilot perception σ_ε (e.g., poor display design), the error in RPE increases. Note, however, that even though the display can be refined to improve the accuracy of pilot perception there is always some error in expectation.
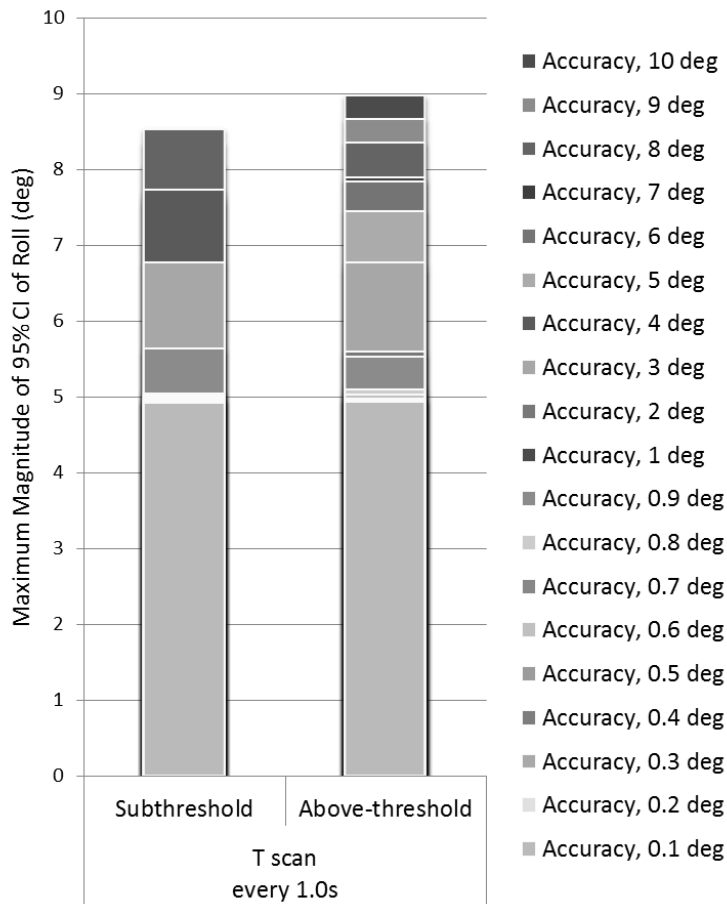
Figure 19. *Impact of Accuracy of Pilot Perception of Roll Angle during Subthreshold and Above-threshold Bank Maneuvers Conducive to Somatogyral Illusions*

41

Design implications:

As shown by the relationship between the maximum 95% CI of error in RPE of roll and accuracy of pilot perception σ_ε during subthreshold and above-threshold bank maneuvers conducive to somatogyral illusions, increasing the accuracy of pilot perception of the flight displays decreases the error in RPE of the aircraft states. Designers can use the MBO to identify what flight display improvements could have the greatest impact on decreasing the error in expectation. Also, the designer can use the MBO to identify which aircraft state expectations are most impacted by design improvements. For example, designers can investigate whether there is a greater return on investment to improve accuracy of pilot perception of attitude versus perception of other states.

Comparison of Effects

In the previous two sections, the impact of scan pattern and the impact accuracy of pilot perception were examined. Here, the two are effects are compared. Figure 20 quantifies the relationship between the maximum 95% CI of error in RPE of roll and the impact of accuracy of pilot perception σ_ε of roll angle as a function of T scan period during subthreshold and above-threshold bank maneuvers conducive to somatogyral illusions. As demonstrated in the previous section, improving the accuracy of pilot perception (i.e., reducing the value of σ_ε) reduces the error in RPE of roll, as the relationship in Figure 20 also demonstrates. The relationships shown in Figure 20 reveal that, as σ_ε increases, the error in RPE grows linearly with a shallow slope. There are also visible differences between the subthreshold and above-threshold cases, but both share the same overall growth characteristic.

42
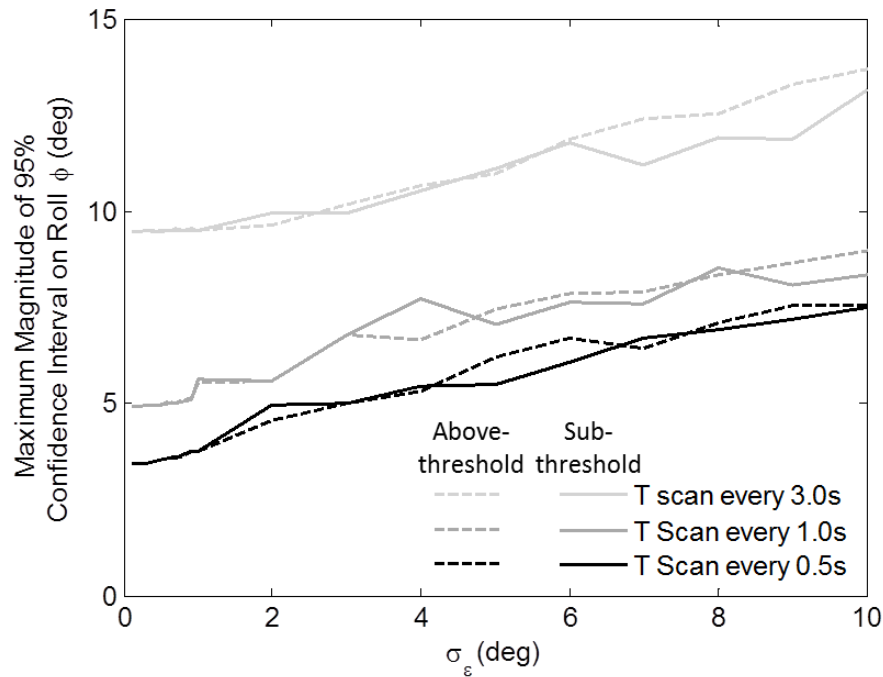
Figure 20. *Impact of Accuracy of Pilot Perception of Roll Angle as a Function of T Scan Period during Sub- and Above-threshold Bank Maneuvers Conducive to Somatogyral Illusions*

Figure 20 also indicates, however, that improving the scan pattern has a greater impact on reducing the error in RPE of roll. Scanning the flight instruments more frequently reduces the maximum 95% CI of error in RPE of roll more than improving the accuracy of pilot perception through improvements of flight displays. The relationship between the maximum 95% CI of error in RPE of roll and the accuracy of pilot perception as a function of a T scan performed every 3 seconds results in larger values of error in RPE of roll compared to when a T scan is performed every 1.0 second or 0.5 seconds. The same observation holds true for when a T scan is performed every 1.0 second to when T scans are performed every 0.5 seconds.

Another interesting effect on the RPE is whether the pilot is aware of the control surface deflections. Awareness of control surface deflections represents visual feedback from movement in yoke, active side stick, throttle, etc. Figure 21 and Figure 22 provide a

43

www.manaraa.com

comparison of the RPE propagated with and without awareness of control surface deflections due to distraction from the flight instruments during a sub-threshold roll. The plots on the right of Figure 21 and Figure 22 demonstrate that, without awareness of the control surface deflections, a subthreshold roll could go completely undetected. However, with awareness of control surface deflections (plots on the left), the pilot could at least acknowledge a change in aircraft state, even without detection by the vestibular system or visual confirmation from the flight displays. For a detailed look into the impact of control surface awareness, please refer to Whitcher et al (2015).
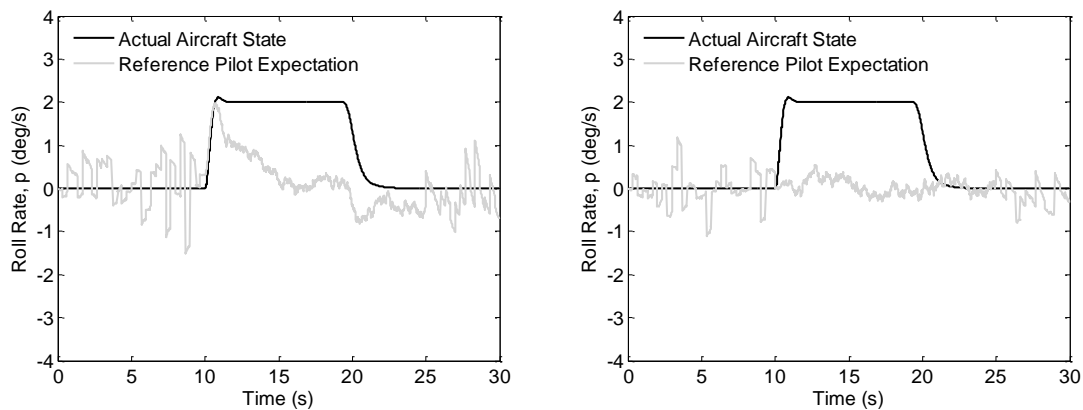
Figure 21. *Comparison of the Reference Pilot Expectation of Roll Rate with (left) and without (right) Awareness of Control Surface Deflections with a 15-second Distraction during a Sub-threshold Roll*
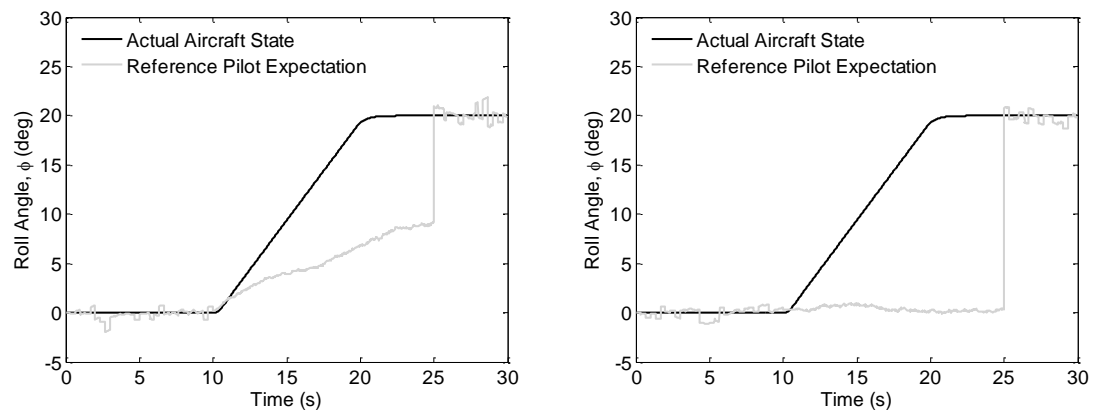
Figure 22. *Comparison of the Reference Pilot Expectation of Roll with (left) and without (right) Awareness of Control Surface Deflections with a 15-second Distraction during a Sub-threshold Roll*

44

Design Implications:

As demonstrated from the relationship between the maximum 95% CI of error in RPE of roll and the accuracy of pilot perception as a function of T scan period, improving the visual scan (e.g., performing a T scan more frequently) has a greater impact on reducing the error in RPE than improving the accuracy of pilot perception. Ensuring that pilots perform proper T scans at suitable scan periods can significant reduce the error in expectationin maneuvers conducive to vestibular illusions. The greatest impact for reducing the error in RPE occurs at the intersection between improving scan pattern and improving the extent to which the pilot can accurately perceive aircraft state information from the flight displays.

Also, having an awareness of control surface deflections (e.g., moving yoke, throttle, active side stick, etc.) can be helpful to reducing error in expectation. While this awareness alone does not provide a RPE with low error, it does indicate the correct trend, which may then cue the pilot to visually scan the instruments.

45

CHAPTER 5

QUANTITATIVE ASSESSMENT OF LOSS OF ENERGY STATE AWARENESS IN NEXTGEN OPEARATIONS

This chapter provides a quantitative assessment of loss of energy state awareness in Next Generation Air Transportation Systems (NextGen) operations. The purpose of NextGen is to increase airspace capacity and efficiency, which will shorten routes and save time and fuel. These operational changes will push aircraft closer to performance limits and increase pilot/crew reliance on automation (Bailey, 2010; Kaneshige, 2014). NextGen operations can involve multiple aircraft maneuvers within increasingly narrow tolerances for navigation precision, where these maneuvers may be executed automatically, such as when flown by the autoflight system via lateral and vertical navigation modes or potentially with future controller-pilot data link communications directed to the autoflight system.

Pilots are susceptible to loss of energy state awareness in current-day operations, and researchers are concerned that pilot susceptibility will increase in NextGen operations, particularly with increased use of automation (Bailey, 2010). Humans serve as poor passive monitors (such as monitoring flight instruments). Failure to monitor or understand energy state indicators (airspeed, altitude, or vertical speed) can result in loss of energy state awareness. There are also multiple potential distractors, such as checklists, managing aircraft systems, and air traffic control communications.

In the computational experiments in this chapter, altitude, airspeed, vertical speed, and specific energy are examined to assess the energy state awareness in NextGen arrivals. (The aircraft specific energy, also known as the energy height, is the total energy of the aircraft [kinetic plus potential] per unit weight.)

The impact of scan pattern will be analyzed at four points during the NextGen arrivals, as demonstrated by the markers labeled 1, 2, 3 and 4 in Figure 23. The first point

46

involves the initial descent, which calls for a reduction in altitude and airspeed. The second point of interest involves a clearance to speed up during the descent. The third point of interest involves noticeable differences in aircraft specific energy between the three NextGen arrival variants (40% into the descent). Finally, the fourth point involves a second speed up clearance, but much closer to landing.
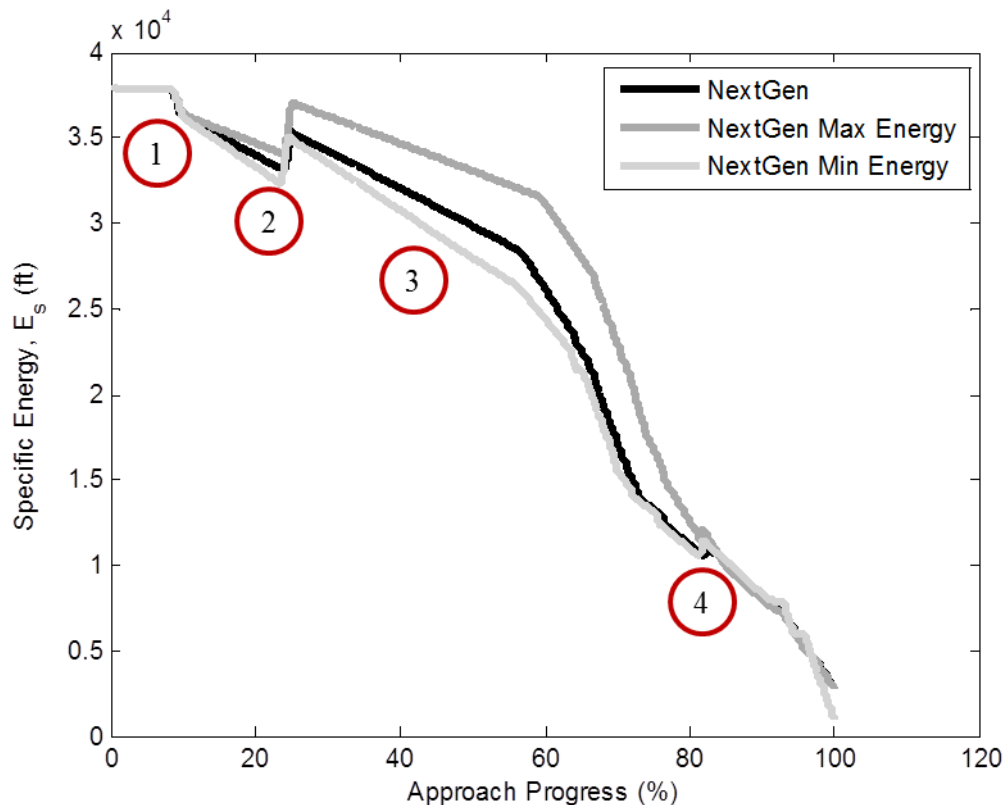
Figure 23. *The Four Points of Descent to be Examined in the Energy Profiles of the Three NextGen Arrival Variants*

The NextGen arrival used in these computational experiments are inspired by the work by Kaneshige et al. (2013) on NextGen human-in-the-loop studies. Three variants of a NextGen arrival are simulated (see Figure 23 for the total energy profile of each). Each arrival includes the initial descent and two airspeed clearances to increase the airspeed. The first variant of the NextGen arrival has air traffic clearances that maximize

47

energy levels. The second variant of the NextGen arrival has air traffic clearances that minimize energy levels. An overview of aircraft traffic clearances is provided in Table 3.

Table 3. An Overview of Clearances Given in the Three Variants of the NextGen Arrival

	NextGen Arrival	**Maximum Energy NextGen Arrival**	**Minimum Energy NextGen Arrival**
Clearance 1: Initial Descent Altitude	20,000 ft	22,000 ft	18,000 ft
Clearance 2: Speed Up (After Initial Descent)	320 knots	330 knots	330 knots
Clearance 3: Speed Up (Near Approach)	240 knots	240 knots	250 knots

The scan patterns that are examined are the T scan, omission (i.e., omitting one instrument from the T scan), and distraction (i.e., distraction from all instruments). The T scan will be analyzed with a range of scan periods from 0.1 to 10 seconds. The omission pattern will consist of a T scan with a scan period of one second. The omission is set to begin at the start of a maneuver and continue for a set duration of time that varies from 0 to 120 seconds. In these experiments, only omission of the altimeter and the attitude indicator are examined since these two instruments are critical for maintaining energy management. Finally, the distraction will have a T scan with scan period of 1 second before and after the distraction period. The distraction is set to begin at the start of a maneuver and continue for a set duration of time that ranges from 0 to 120 seconds.

Point 1: Initial Descent

This section analyzes the impact of scan pattern on the error in RPE of the aircraft state during the initial descent in a NextGen arrival (see Figure 24 for time histories of the altitude, airspeed, and vertical speed). The altitude clearances for the initial descent in each NextGen arrival are provided in Table 3. The airspeed decreases with the initial

48

descent, as is normal practice. Conversely, the magnitude of the vertical speed increases from zero.

The relationship between the T scan scanning period and the maximum 95% CI of error in RPE of altitude, airspeed, and vertical speed during the initial descent is presented in the left plots of Figure 25a, b, and c, respectively. The impact of the T scan is analyzed at the start of the descent in response to the altitude clearance given by the air traffic controller. These relationships quantify how, with larger scan periods, the error in RPE increases linearly. The error in RPE of altitude, airspeed, and vertical speed continues to grow because the altitude, airspeed, and vertical speed are still changing through the initial descent (see time histories in Figure 24). These relationships reveal that the growth in rate of error in RPE plateaus at longer scan periods, i.e. scan periods so long that the aircraft nears its target altitude, airspeed, and vertical speed between scans.

The relationships between the duration of omission of specific flight instruments and the maximum 95% CI of error in RPE of altitude, airspeed, and vertical speed, during initial descent are presented in the center plots of Figure 25a, b, and c, respectively. The error in RPE of altitude is only impacted by the omission of the altimeter, as expected. Here, the error in RPE grows with greater durations of omission and continues to grow since the aircraft is descending. The error in RPE of airspeed is only impacted by the omission of the airspeed indicator, with a slight disparity between the NextGen arrival variants due to slight differences in airspeed.

49
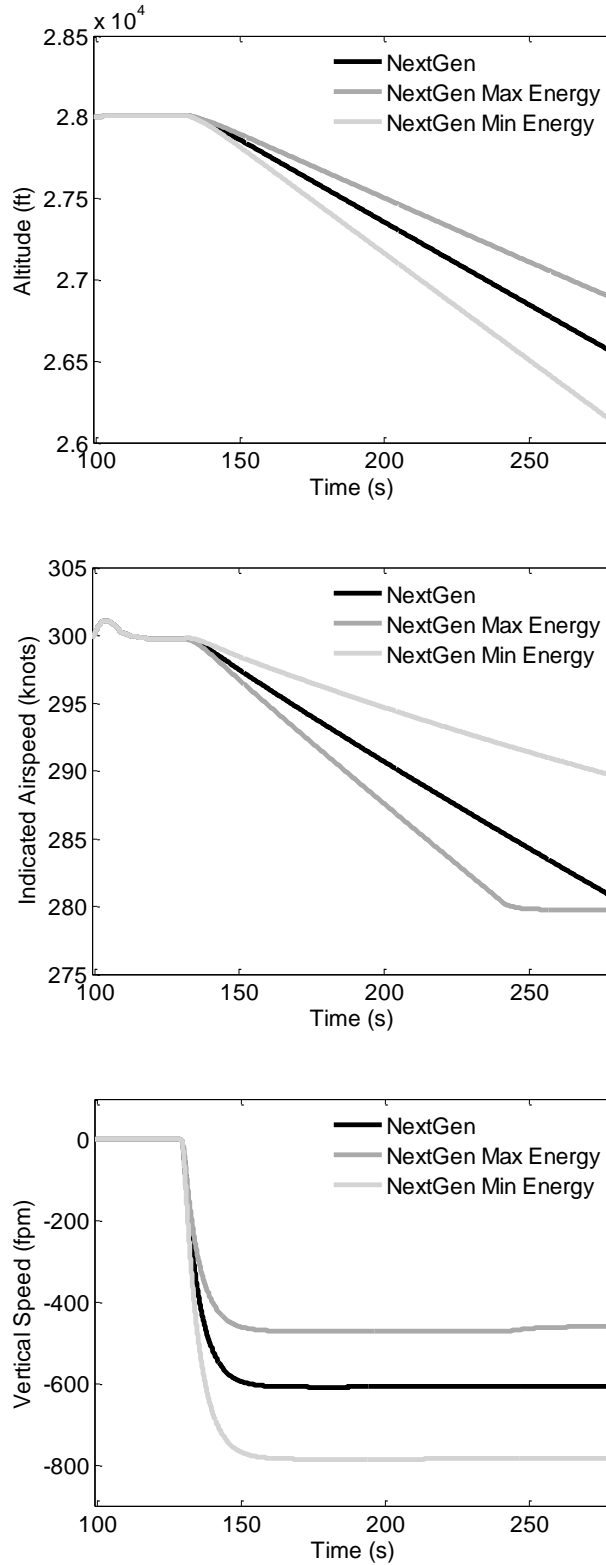
Figure 24. *Times Histories for Altitude, Airspeed, and Vertical Speed During the Initial Descent in the NextGen Arrivals*

50

(a) Maximum 95% CI of Altitude due to T Scan, Omission of Altitude and Airspeed, and Distraction
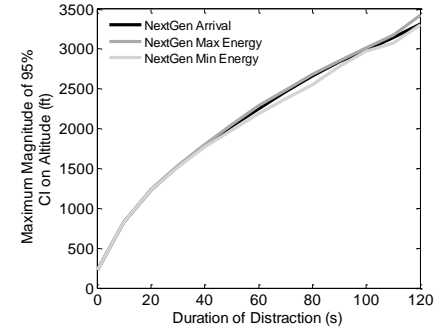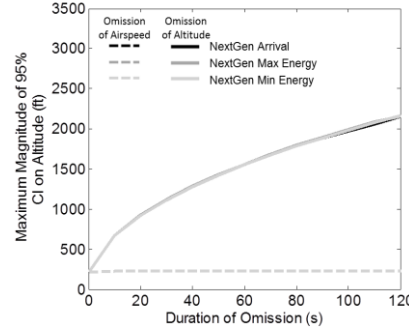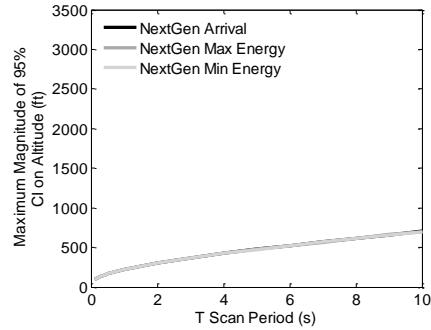
(b) Maximum 95% CI of Airspeed due to T Scan, Omission of Altitude and Airspeed, and Distraction
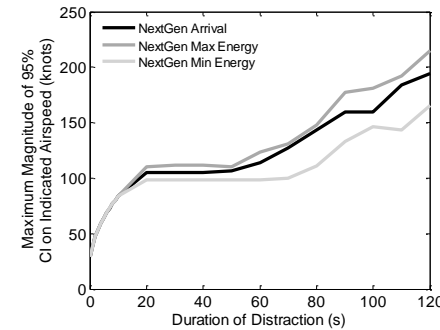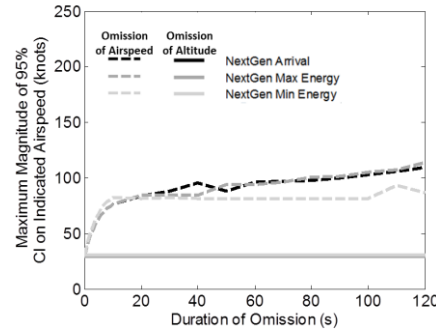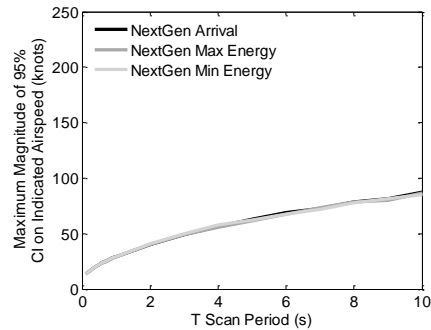
(c) Maximum 95% CI of Vertical Speed due to T Scan, Omission of Altitude and Airspeed, and Distraction
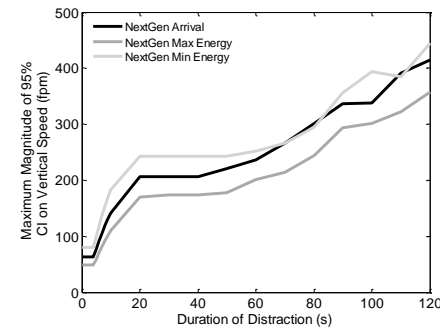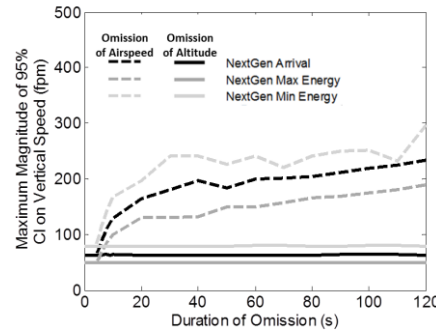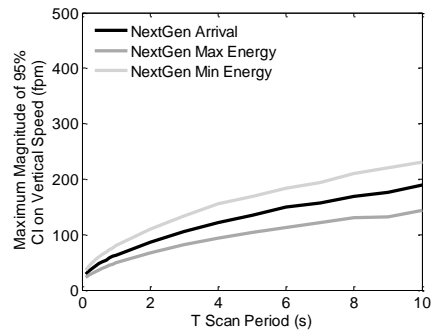
Figure 25. *Maximum 95% Confidence Interval of Error in RPE of Altitude, Indicated Airspeed, and Vertical Speed in the Initial Descent*

Finally, the error in RPE of vertical speed is impacted only by the omission of the airspeed indicator. Here, there are clear differences between the NextGen arrival variants: the minimum energy NextGen arrival has the greatest error in RPE of vertical speed because the minimum energy variant is given an altitude clearance to achieve a lower altitude by the same waypoint constraint than the other two variants. Hence, the aircraft must descend at a greater rate to achieve the altitude at the waypoint constraint. Overall, these relationships between duration of omission and the error in RPE demonstrate that susceptibility to loss of energy state awareness increases with greater duration of omission.

The relationship between the duration of distraction and the maximum 95% CI of error in RPE of altitude, airspeed, and vertical speed during initial descent is presented in the right plots of Figure 25a, b, and c, respectively. The error in RPE of altitude, airspeed, and vertical speed all increase with greater duration of distraction, which increases susceptibility to loss of energy state awareness. The error in RPE is greater with a distraction than an omission or T scan. The error in RPE of airspeed and vertical speed grow slightly differently: the error in RPE increases for approximately 20 seconds after the start of the distraction, and then plateaus for another 20 seconds. After this plateau, the error in RPE continues to grow again. The growth in the error in RPE of airspeed and vertical speed results from the aircraft's linear acceleration (Figure 26). The aircraft linear acceleration drops immediately in response to the initial descent clearance (here the airspeed is decreased from 300 knots to 280 knots). The acceleration then zeros out, which causes the error in RPE of airspeed and vertical speed to plateau. However, once the linear acceleration drops again to continue decreasing the speed, the error in RPE of airspeed and vertical speed continues to grow again.
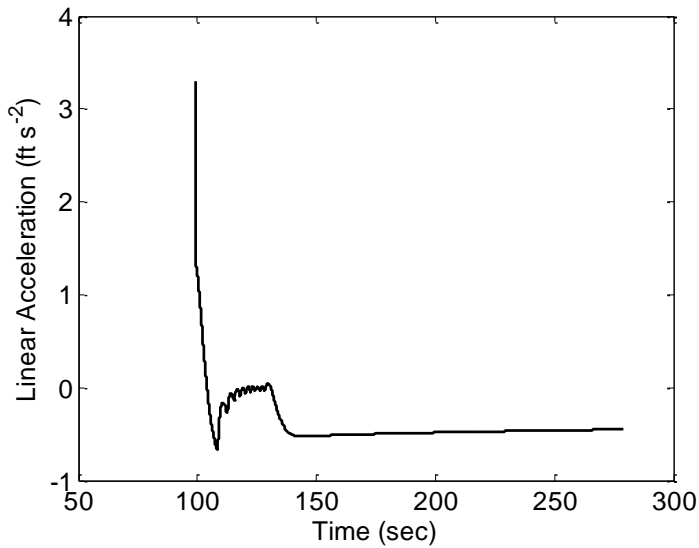
Figure 26. *Time History of Linear Acceleration During Initial Descent in the NextGen Arrival*

The relationships between the maximum 95% CI of error in RPE of specific energy and T scan scanning period, duration of omission and duration of distraction during initial descent are presented in the Figure 27. Here, the same overall trends in growth of error in RPE seen for altitude, airspeed, and vertical speed are seen here. The error in RPE of specific energy increases with longer T scan periods and greater durations of omission or distraction. The error in RPE of specific energy is not really impacted by different energy levels of the three NextGen arrival variants.
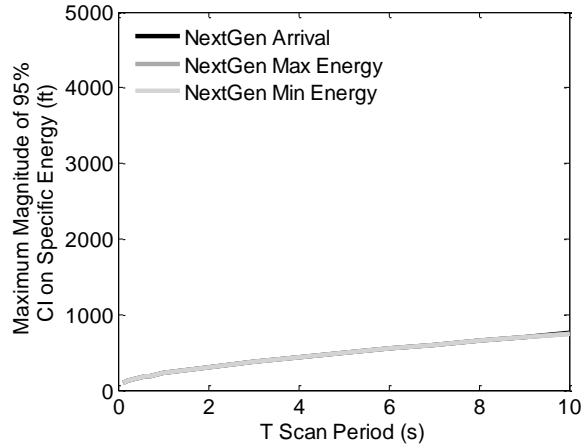
53

(a) Specific Energy due to T Scan
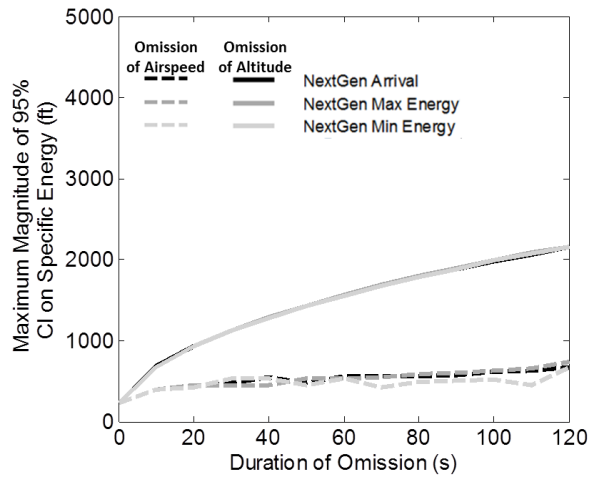
(b) Specific Energy due to Omission
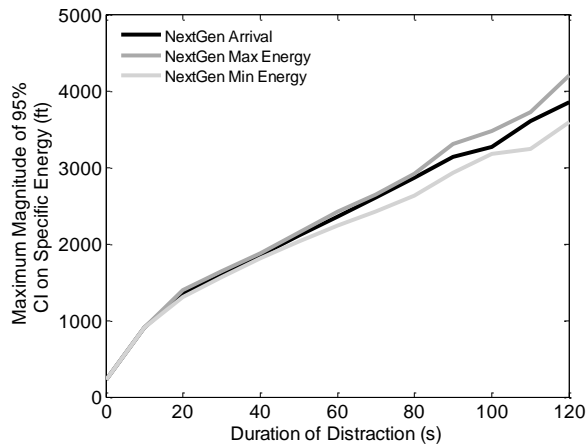
(c) Specific Energy due to Distraction

Figure 27. Maximum 95% Confidence Interval Error in RPE of Specific Energy During Initial Descent

54

To summarize, the impact of scan pattern on the maximum 95% CI of error in the RPE of altitude, airspeed, vertical speed, and specific energy during initial descent is described in Figures 28, 29, 30, and 31 for the four values of interest, respectively. As seen in Figure 28, a proper T scan of all primary flight instruments reduces the error in RPE of altitude during initial descent. Error in RPE is increased by degradations such as performing a T scan less frequently, omitting the altimeter from a T scan, or failing to perform the T scan at all (i.e., distraction).
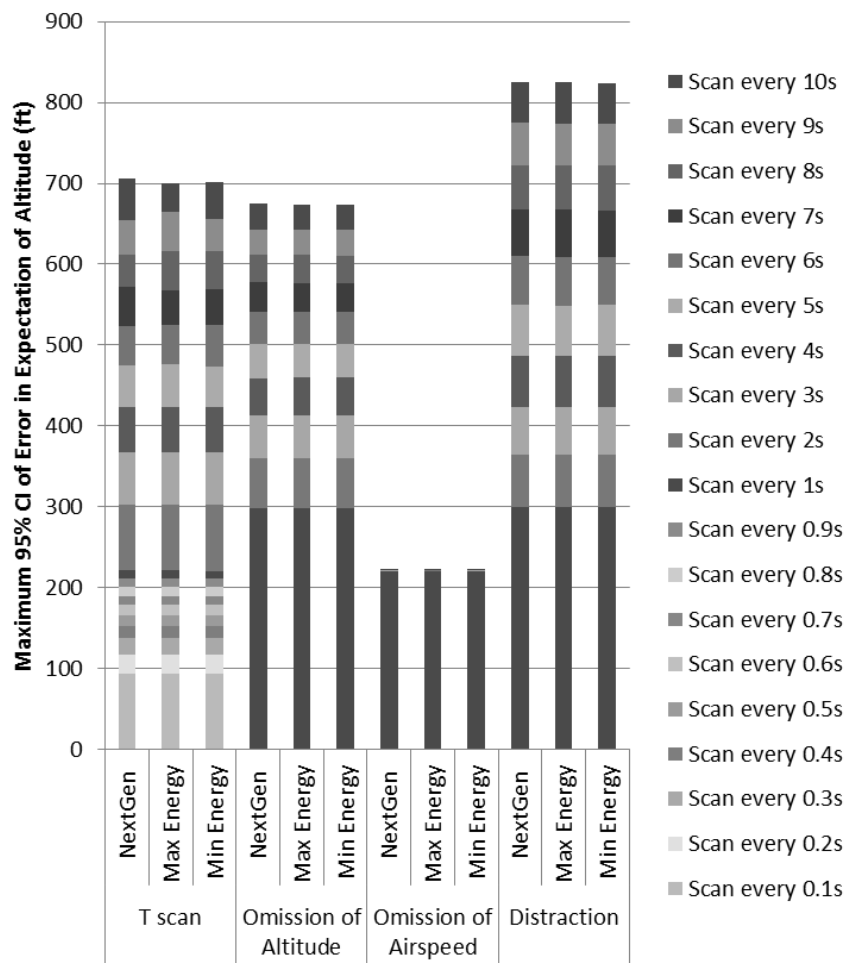
Figure 28. Summary of the Impact of T scan, Omission, and Distraction on the Maximum 95% CI of Error in the Reference Pilot Expectation of Altitude During Initial Descent
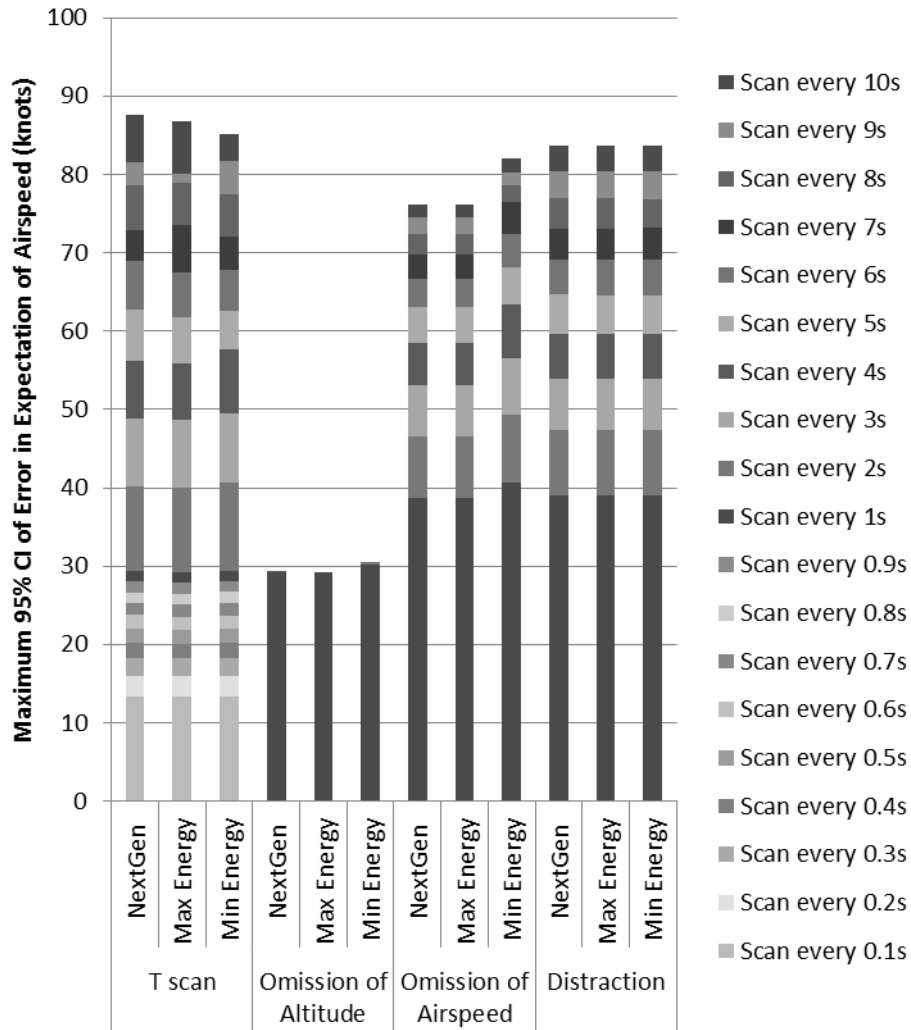
Figure 29. Summary of the Impact of T scan, Omission, and Distraction on the Maximum 95% CI of Error in the Reference Pilot Expectation of Airspeed During Initial Descent

Figure 29 quantifies how a proper T scan reduces the error in RPE of airspeed during the initial descent. Omission of the airspeed indicator increases the error in RPE of airspeed, while omission of the altimeter has no impact. With greater duration of omission of the airspeed indicator or distraction the error in RPE of airspeed increases. As seen, the error in RPE due to a distraction for 10 seconds and a T scan every 10 seconds is approximately the same. However, with greater durations of distraction beyond 10 seconds, the error in RPE of airspeed increases further, as seen in Figure 25.
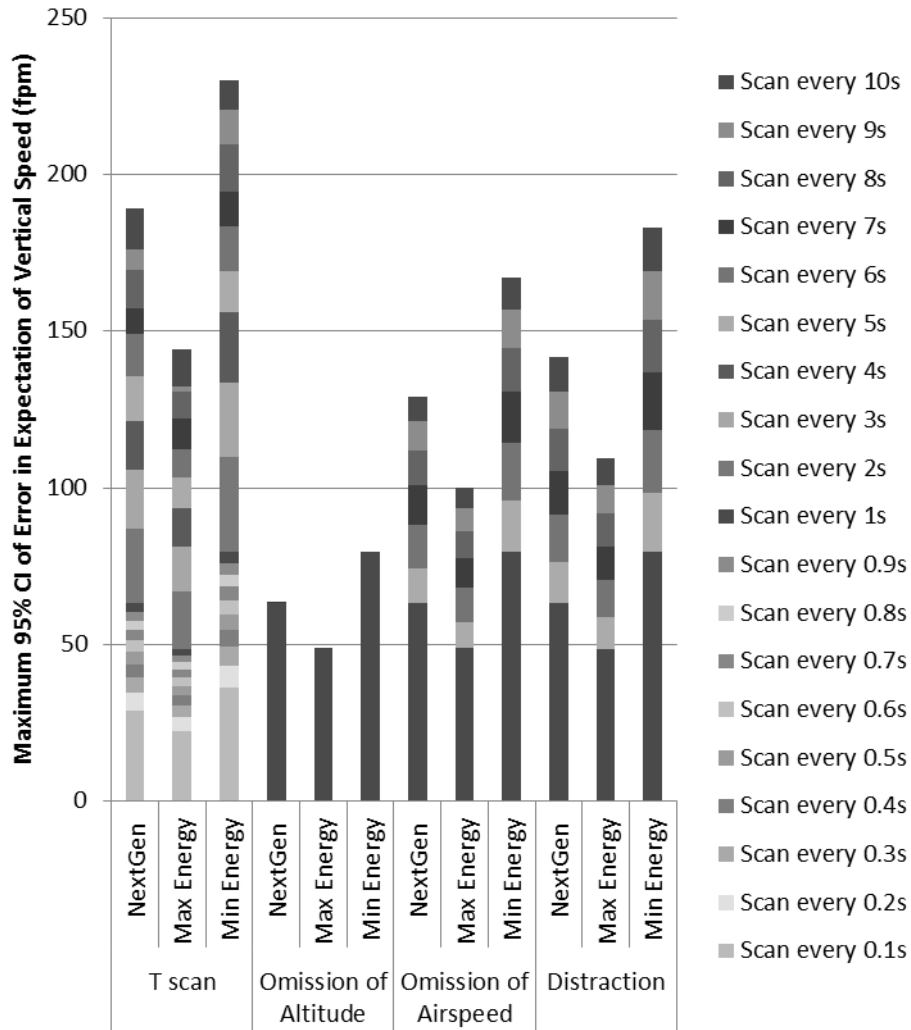
Figure 30. *Summary of the Impact of T scan, Omission, and Distraction on the Maximum 95% CI of Error in the Reference Pilot Expectation of Vertical Speed During Initial Descent*

Figure 30 quantifies how the error in RPE of vertical speed decreases with smaller scan periods during a T scan. Degradations to a proper T scan increase the error in expectation. The error in RPE increases with larger scan periods. The error in RPE also increases with greater duration of omission or distraction. Here, there are visible differences in error in RPE between the different NextGen arrival variants because each requires a different descent rate to meet its altitude clearance.
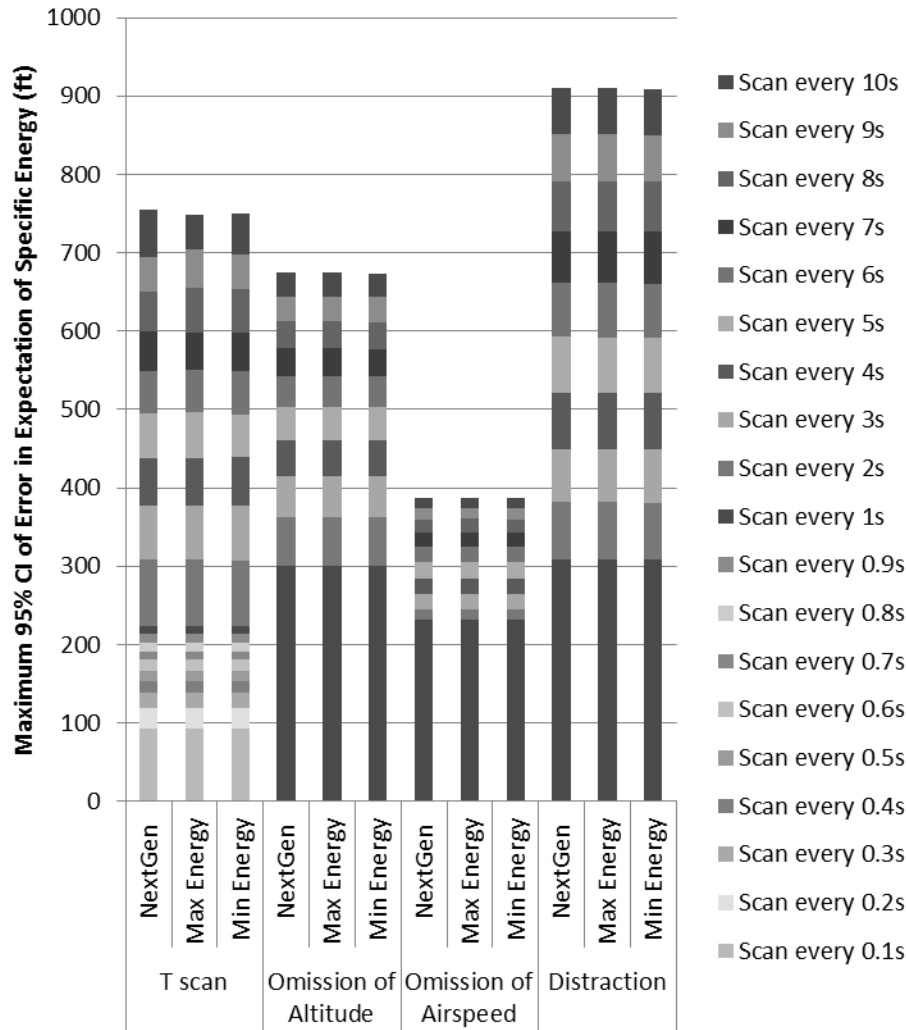
Figure 31. *Summary of the Impact of T scan, Omission, and Distraction on the Maximum 95% CI of Error in the Reference Pilot Expectation of Specific Energy During Initial Descent*

Similar overall trends are seen in the error in RPE of specific energy (Figure 31): the trends quantify how the error in RPE decreases with smaller scan periods. Also, degradation to a T scan increases error in expectation. Omission of both the altimeter and airspeed indicator increases the error in RPE in specific energy, although omission of the altitude has a greater impact on error in RPE during the initial descent. Finally, distraction results in the largest error in RPE of specific energy.

58

Point 2: Speed Up During Descent

This section analyzes the impact of scan pattern on the error in RPE of the aircraft state in a speed up during descent. Time histories of altitude, airspeed, and vertical speed are provided below in Figure 32.

The relationship between the T scan scanning period and the maximum 95% CI of error in RPE of altitude, airspeed, and vertical speed in a speed up during descent is presented in the left plots of Figure 33a, b, and c, respectively. The impact of the T scan is analyzed at the start of the speed up in response to the airspeed clearance. These relationships quantify how, with larger scan periods, the error in RPE increases linearly. The error in RPE of altitude, airspeed, and vertical speed continues to grow because the altitude, airspeed, and vertical speed are still changing at this point in the arrival. The relationships quantify how the growth rate of error in RPE abates with larger scan periods (i.e., the slope grows shallower), where the aircraft gets closer to its target altitude, airspeed, and vertical speed between visual scans.
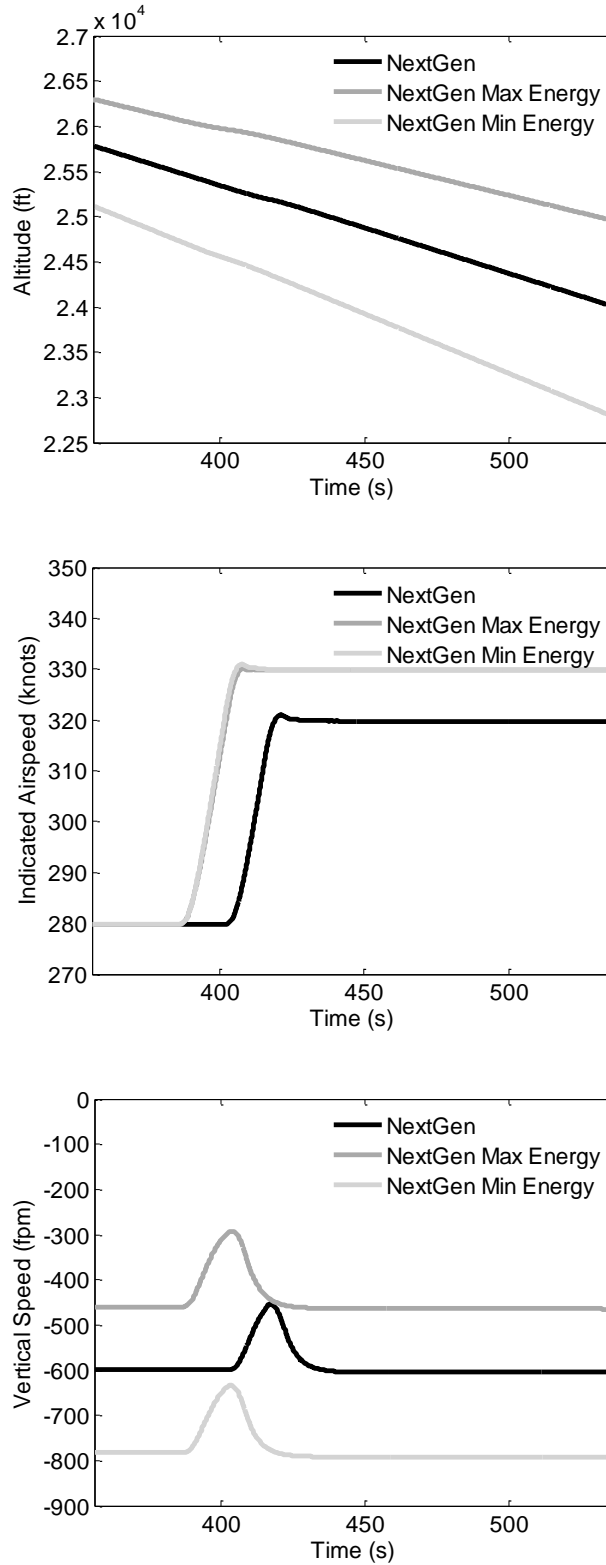
Figure 32. *Time Histories of Altitude, Airspeed, and Vertical Speed in a Speed Up During Descent in a NextGen Arrival*

(a) Maximum 95% CI of Altitude due to T Scan, Omission of Altitude and Airspeed, and Distraction
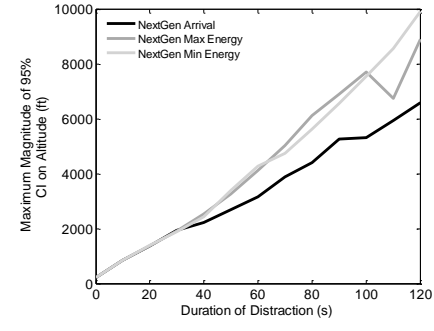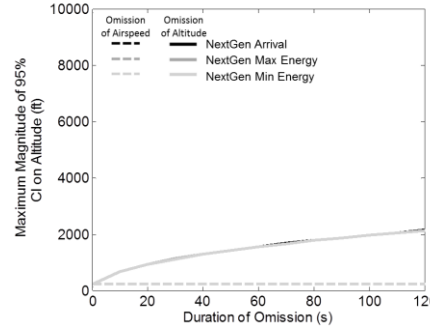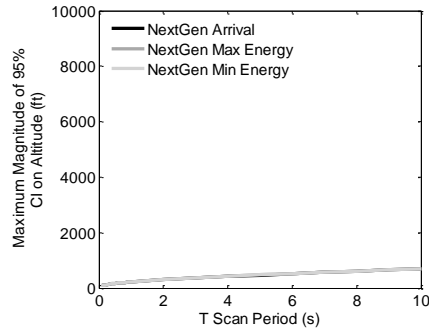
(b) Maximum 95% CI of Airspeed due to T Scan, Omission of Altitude and Airspeed, and Distraction
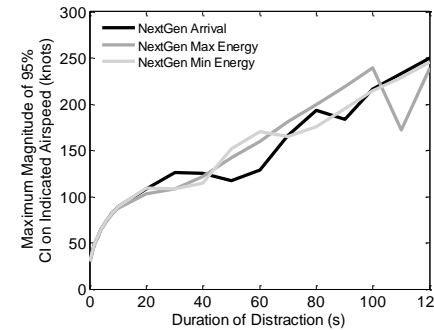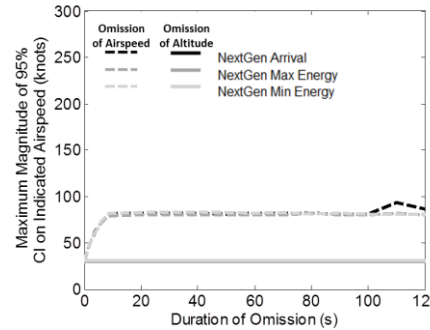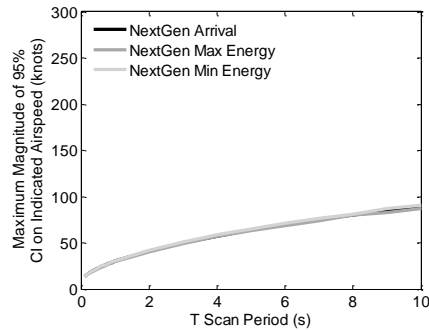
(c) Maximum 95% CI of Vertical Speed due to T Scan, Omission of Altitude and Airspeed, and Distraction
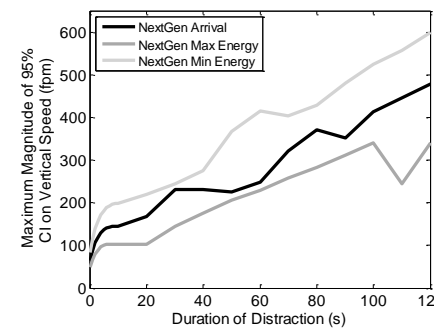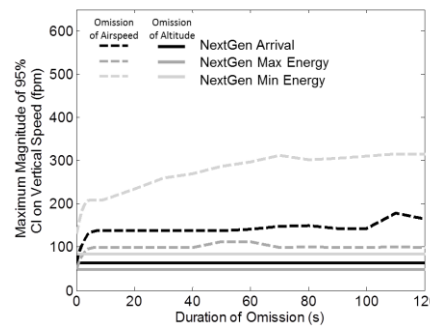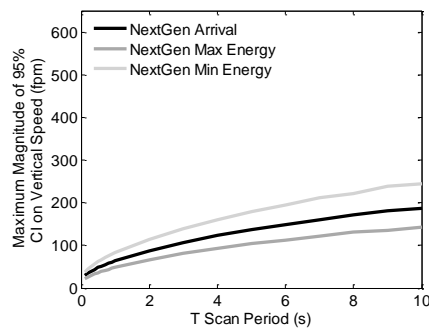
Figure 33. *Maximum 95% Confidence Interval of Error in RPE of Altitude, Indicated Airspeed, and Vertical Speed in a Speed Up During Descent*

61

The relationship between the duration of omission and the maximum 95% CI of error in RPE of altitude, airspeed, and vertical speed in a speed up during descent is presented in the center plots of Figure 33a, b, and c, respectively. The error in RPE of altitude is only impacted by the omission of the altimeter, as expected. Here, the error in RPE grows with larger scan periods and continues to grow since the aircraft is still in descent. The error in RPE of airspeed is only impacted by omission of the airspeed indicator. The error in RPE of vertical speed is impacted by omission of the airspeed indicator as well, with visible differences between the NextGen arrival variants: the minimum energy NextGen arrival variant has the greatest error in RPE because it requires a greater descent rate to achieve a lower altitude given the previous clearance (see Initial Descent). These results demonstrate that susceptibility to loss of energy state awareness increases with greater duration of omission in a speed up during descent.

The relationship between the duration of distraction and the maximum 95% CI of error in RPE of altitude, airspeed, and vertical speed in a speed up during descent is presented in the right plots of Figure 33a, b, and c, respectively. The error in RPE of altitude, airspeed, and vertical speed all increase linearly with greater duration of distraction. The error in RPE is greater with a distraction than omission or T scan. There is some disparity in error of expectation between the NextGen arrival variants, but all show the same overall trend. These results quantify how susceptibility to loss of energy state awareness increases with greater duration of distraction in a speed up during descent.

The relationships between the maximum 95% CI of error in RPE of specific energy and T scan scanning period, duration of omission, and duration of distraction in a speed up during descent are presented in the Figure 34. Here, the same overall trends are found in the growth of error in expectation: with greater duration of T scan period and duration of omission or distraction the error in RPE increases.
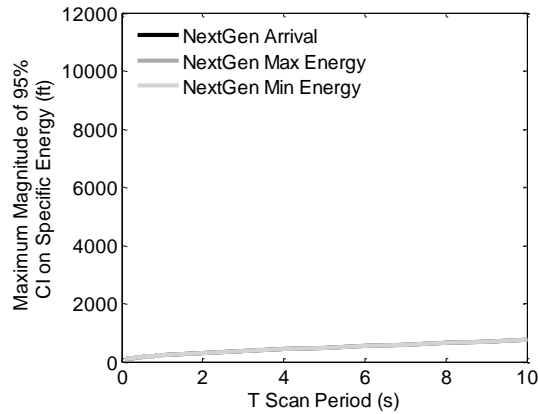
(a) Specific Energy due to T Scan
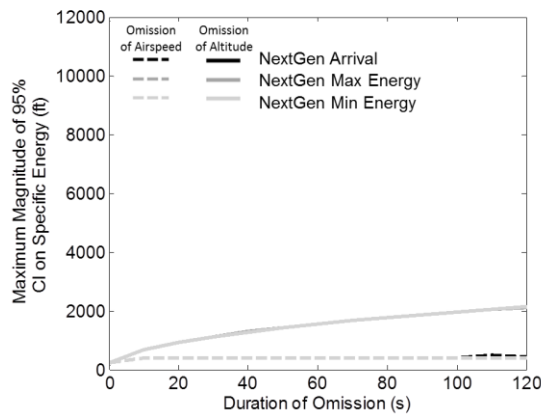
(b) Specific Energy due to Omission
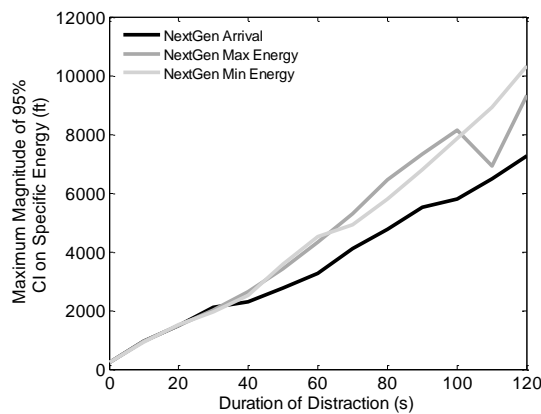
(c) Specific Energy due to Distraction

Figure 34. Maximum 95% Confidence Interval of Error in RPE of Aircraft Specific Energy with a Speed Up During Descent

63

These results quantify how performing a proper T scan can decrease the error in RPE and mitigate loss of energy state awareness. Also, increasing duration of omission of either the altimeter and airspeed indicator increases the error in RPE of specific energy, with omission of the altimeter having a greater impact. Finally, the error in RPE of specific energy grows with some disparity between the NextGen arrival variants with greater duration of distraction due to the different aircraft energy levels at this point in each arrival.

In summary, the impact of scan pattern on the maximum 95% CI of error in RPE of altitude, airspeed, vertical speed, and specific energy in a speed up during descent is presented in Figures 35, 36, 37, and 38, respectively. As seen in Figure 35, the results quantify how a proper T scan of all primary flight instruments reduces the error in RPE in a speed up during descent. Degrading a proper T scan increases the error in RPE as the scan period gets larger. Omitting the altimeter from a proper T scan increases the error in RPE of altitude. With greater duration of omission the error in RPE of altitude increases. Also, with greater duration of distraction of all instruments increases the error in RPE of altitude.

As seen in Figure 36, these results quantify how a proper T scan in a speed up during descent reduces the error in RPE of airspeed. An omission of the airspeed indicator impacts the error in RPE of airspeed, while omission of the altimeter has no visible impact. With greater duration of omission of the airspeed indicator the error in RPE of airspeed increases. Also, with greater duration of distraction the error in RPE of airspeed increases. As seen, the error in RPE with a 10-second distraction and a 10-second T scan is approximately equal. However, with greater duration of distraction, the error in RPE of airspeed far exceeds what is presented here.

64
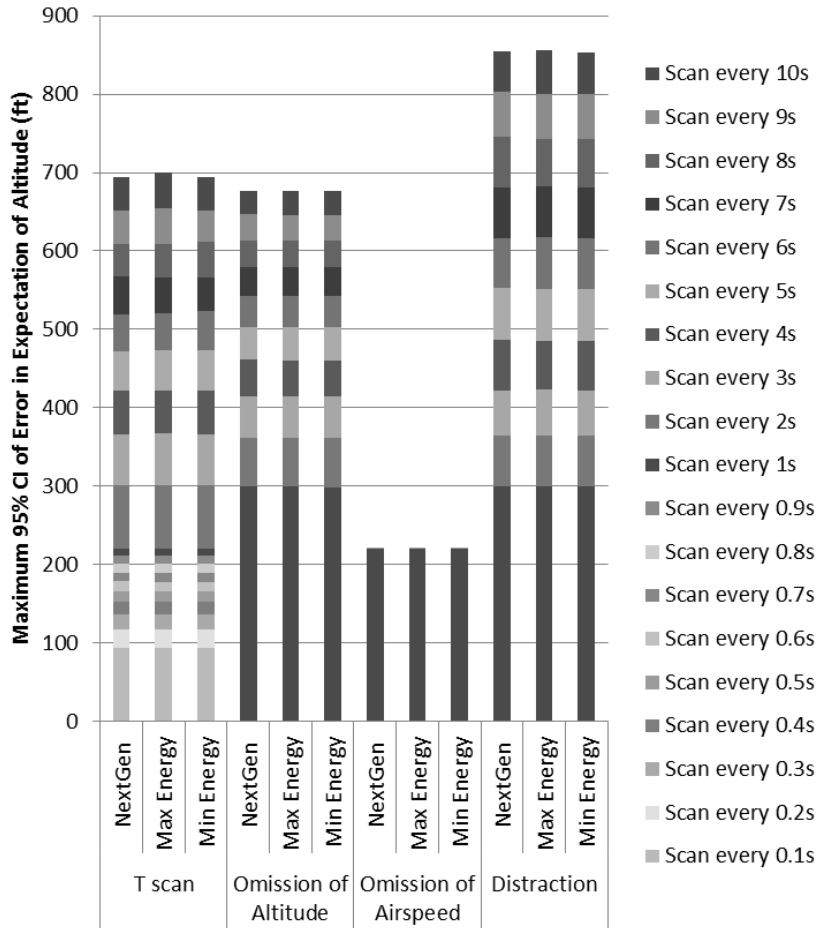
Figure 35. *Summary of the Impact of T scan, Omission, and Distraction on the Maximum 95% CI of Error in the Reference Pilot Expectation of Altitude in a Speed Up During Descent*
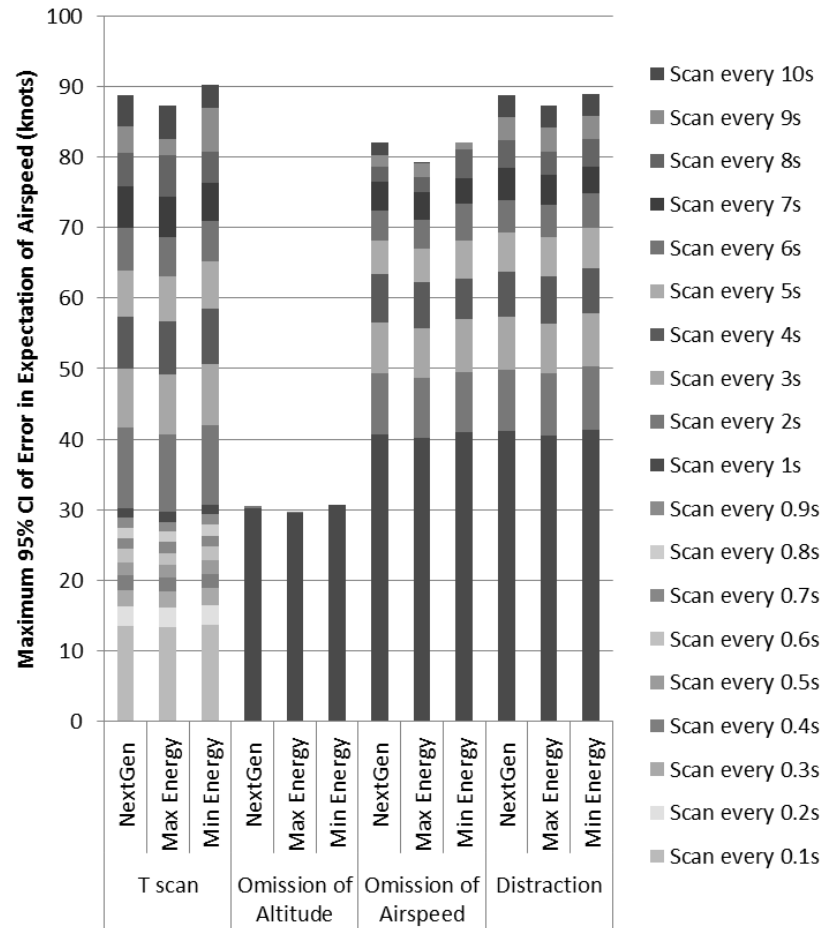
Figure 36. *Summary of the Impact of T scan, Omission, and Distraction on the Maximum 95% CI of Error in the Reference Pilot Expectation of Airspeed in a Speed Up During Descent*

65

Figure 37. *Summary of the Impact of T scan, Omission, and Distraction on the Maximum 95% CI of Error in the Reference Pilot Expectation of Vertical Speed in a Speed Up During Descent*

As seen in Figure 37, the relationships quantify how a proper T scan decreases the error in expectation. However, there is different growth behavior in the error in RPE of vertical speed between the different NextGen arrivals because the aircraft descent rate is different in each. Overall, the trends are similar to what has been seen before except that, in the short term, the error in RPE of vertical speed is greater with a 10-second T scan than a 10-second distraction.

66

Figure 38. *Summary of the Impact of T scan, Omission, and Distraction on the Maximum 95% CI of Error in the Reference Pilot Expectation of Specific Energy in a Speed Up During Descent*

As seen in Figure 38, the relationships quantify how a proper T scan reduces the error in RPE of specific energy, which can mitigate pilot susceptibility to loss of energy state awareness. Here, the same overall trends are seen: larger T scan periods or longer duration of omission or distraction increases the error in RPE of specific energy. Also, the omission of both the altimeter and the airspeed increase the error in RPE of specific energy, which is expected since specific energy is the summation of kinetic (airspeed) and potential (altitude) energy.

67

Point 3: Speed Up Near Landing

This section analyzes the impact of scan pattern on the error in RPE of the aircraft state during a speed up near landing as commanded in the NextGen arrivals. Time histories of altitude, airspeed, and vertical speed are provided in Figure 39.

The relationship between the T scan scanning period and the maximum 95% CI of error in RPE of altitude, airspeed, and vertical speed in a speed up near landing is presented in the left plots of Figure 40a, b, and c, respectively. Similar overall trends quantify how with larger scan periods the error in RPE increases linearly. Among the states, only the error in RPE of vertical speed shows any disparity between the NextGen arrival variants. The maximum energy NextGen arrival results in a greater error in RPE of vertical speed, which is attributable to higher vertical speed during this phase (as seen in Figure 39).

The relationship between the duration of omission and the maximum 95% CI of error in RPE of altitude, airspeed, and vertical speed in a speed up near landing is presented in the center plots of Figure 40a, b, and c, respectively. The error in RPE of altitude increases with duration of omission of the altimeter. Similarly, the error in RPE of airspeed and vertical speed both increase with duration of omission of the airspeed indicator. Again, the error in RPE of vertical speed in the maximum energy NextGen arrival variant is greater than the error in RPE of vertical speed in the other two NextGen arrival variants.
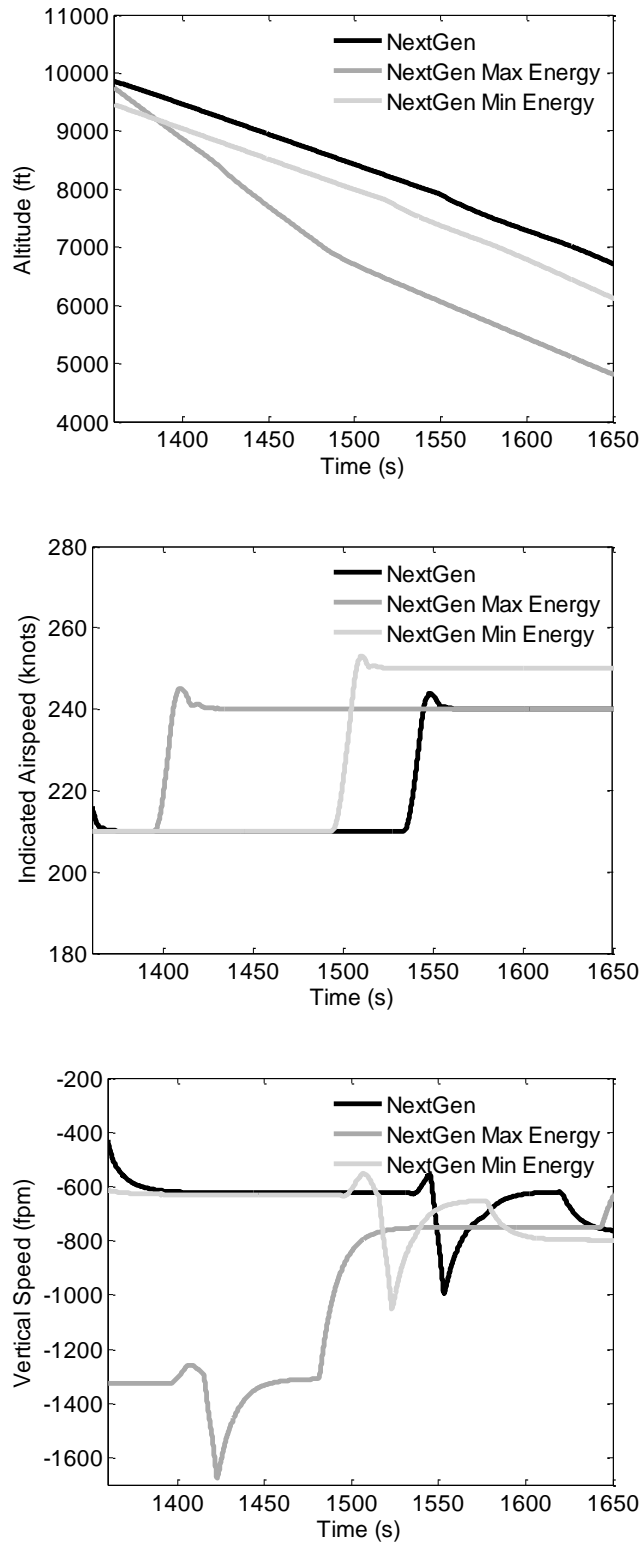
Figure 39. *Time Histories of Altitude, Airspeed, and Vertical Speed During a Speed Up*
Near Landing in the NextGen Arrivals

(a) Maximum 95% CI of Altitude due to T Scan, Omission of Altitude and Airspeed, and Distraction
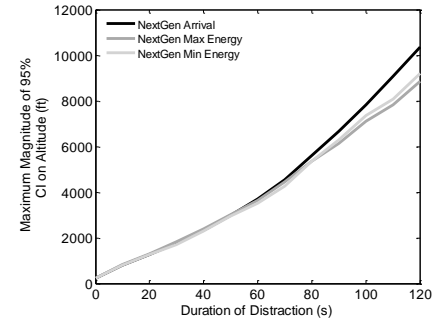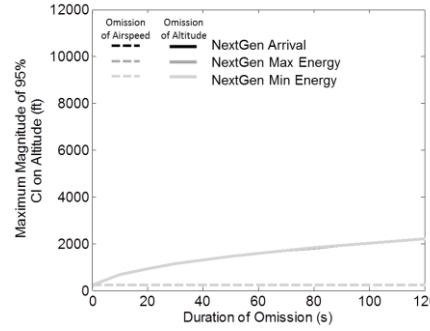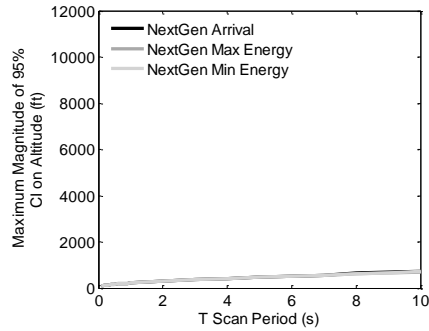
(b) Maximum 95% CI of Airspeed due to T Scan, Omission of Altitude and Airspeed, and Distraction
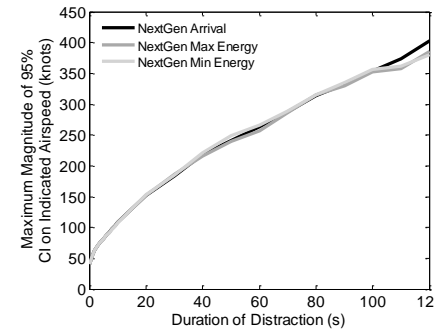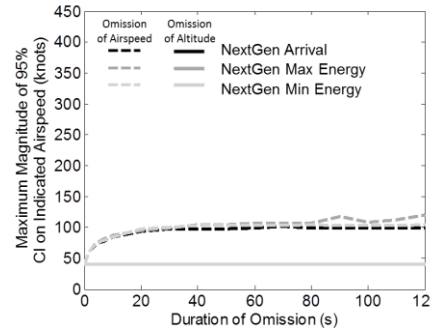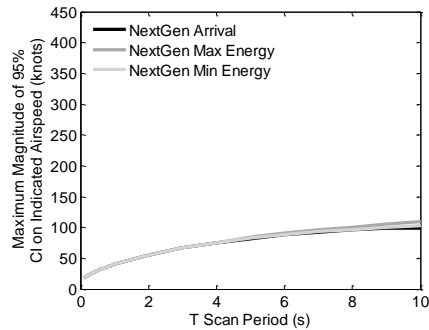
(c) Maximum 95% CI of Vertical Speed due to T Scan, Omission of Altitude and Airspeed, and Distraction

Figure 40. Maximum 95% Confidence Interval of Error in RPE of Altitude, Indicated Airspeed, and Vertical Speed in a Speed Up Near Landing

70

The relationship between the duration of distraction and the maximum 95% CI of error in RPE of altitude, airspeed, and vertical speed in a speed up near landing is presented in the right plots of Figure 40a, b, and c, respectively. The error in RPE of altitude, airspeed, and vertical speed all increase linearly with greater duration of distraction. The error in RPE of all states is greater with distraction than with an omission or a T scan. These results demonstrate that susceptibility to loss of energy state awareness increases with greater duration of distraction in a speed up near landing. Some disparity exists between NextGen arrival variants with a distraction, but each variant has the same overall trend – i.e., the error in RPE increases with greater duration of distraction.

The relationships between the maximum 95% CI of error in RPE of specific energy and T scan scanning period, duration of omission, and duration of distraction in a speed up near landing are presented in the Figure 41. The relationship reveals similar growth of error in RPE of specific energy: with larger T scan periods or greater duration of omission or distraction the error in RPE of specific energy increases.

71
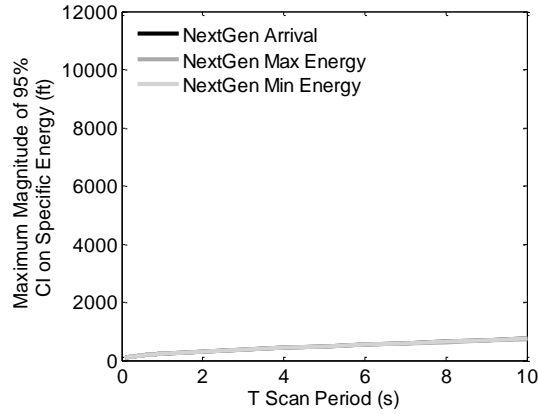
(a) Specific Energy with a T Scan
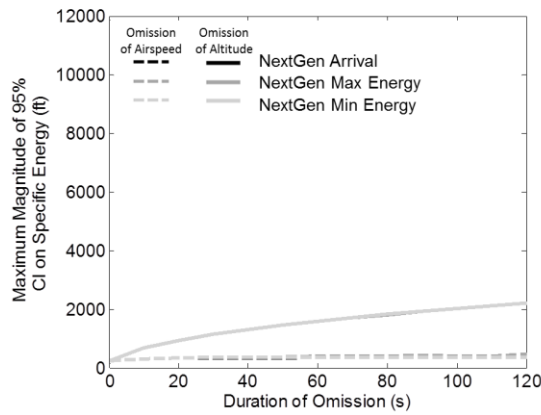
(b) Specific Energy with an Omission
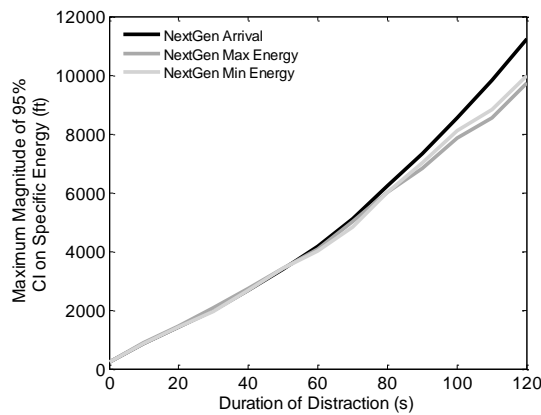
(c) Specific Energy with a Distraction

Figure 41. *Maximum 95% Confidence Interval Error in RPE of Aircraft Specific Energy Resulting During a Clearance to Speed Up Near Landing*

In summary, the impact of scan pattern on the maximum 95% CI of error in the RPE of altitude, airspeed, vertical speed, and specific energy in a speed up during descent is shown in Figures 42, 43, 44, and 45, respectively.

Figure 42. *Summary of the Impact of T scan, Omission, and Distraction on the Maximum 95% CI of Error in the Reference Pilot Expectation of Altitude in a Speed Up Near Approach*
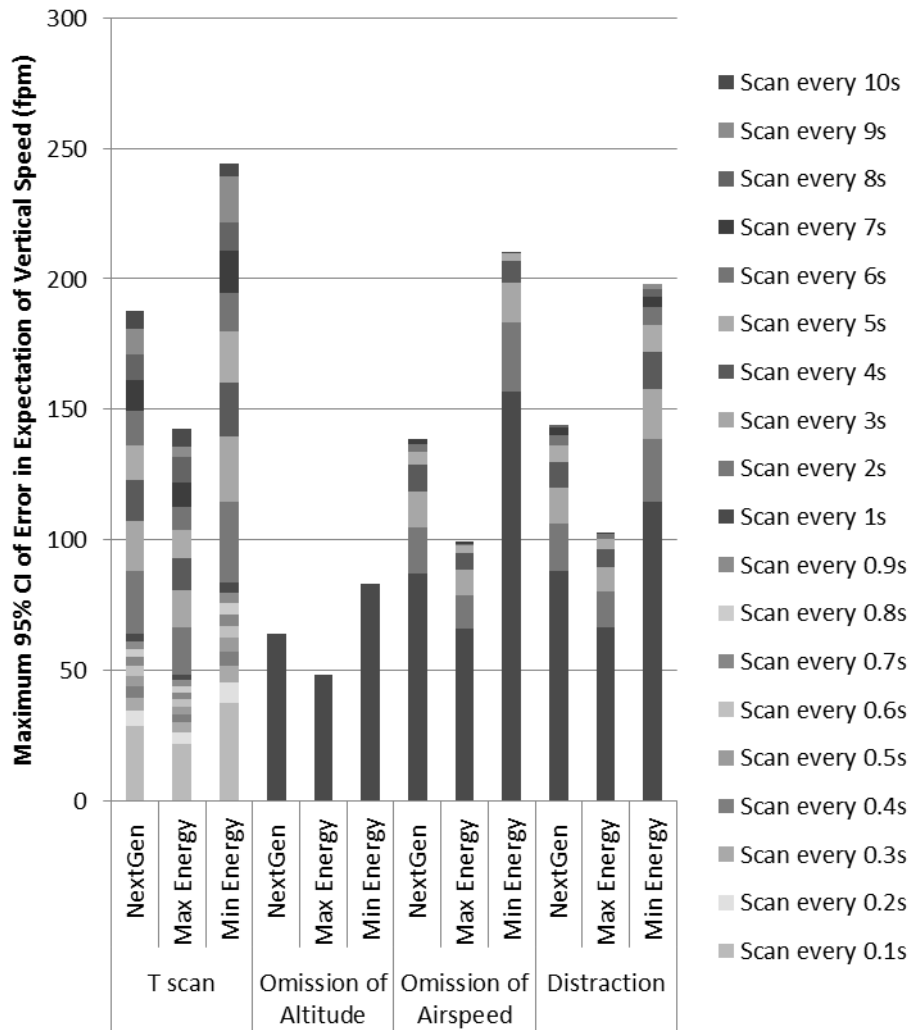
As seen in Figure 42, the results quantify how a proper T scan with smaller scan periods decreases the error in RPE of altitude. An omission of the altimeter from a T scan increases the error in RPE of altitude. An omission of the airspeed indicator has no impact on error in RPE of altitude. Finally, greater duration of distraction increases the

73

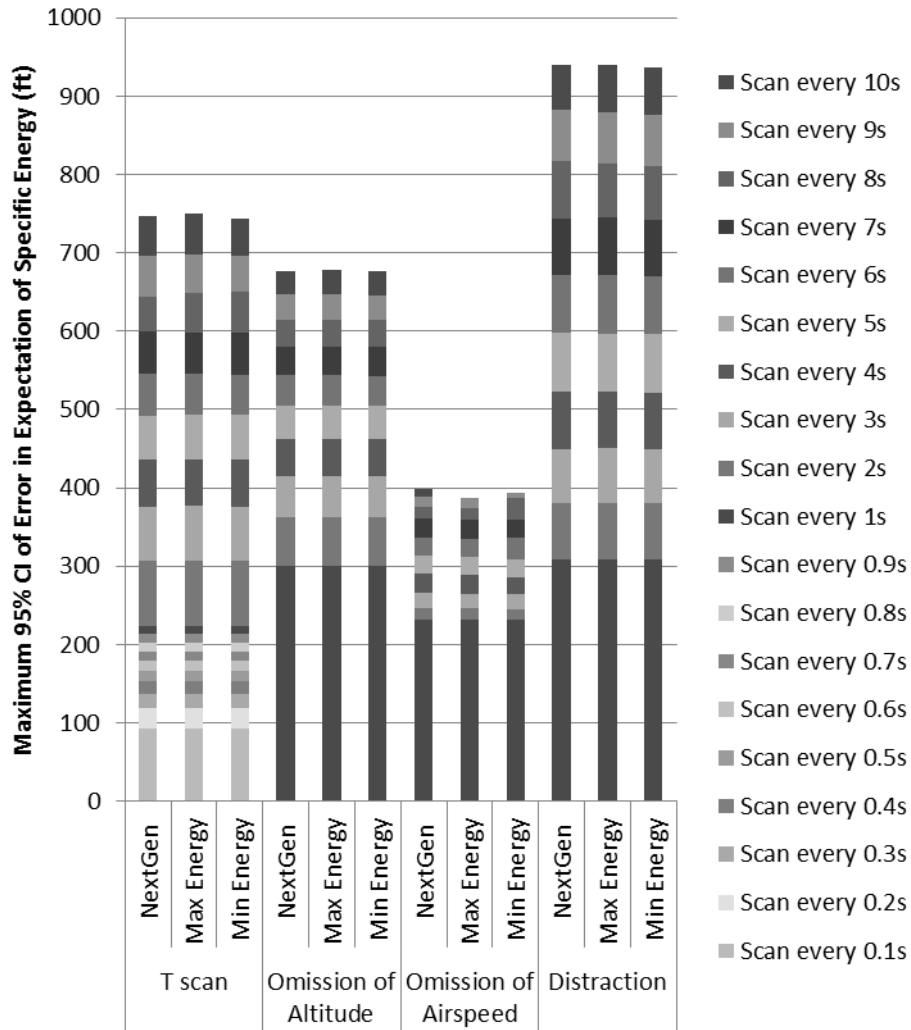error in RPE of altitude, which exceeds the error in RPE with a T scan or an omission of the altimeter.

Figure 43. *Summary of the Impact of T scan, Omission, and Distraction on the Maximum 95% CI of Error in the Reference Pilot Expectation of Airspeed in a Speed Up Near Approach*

In Figure 43 the results quantify how performing a proper T scan frequently decreases the error in RPE of airspeed. An omission of the airspeed indicator from a T scan increases the error in RPE of airspeed, while an omission of the altimeter has no impact. With greater duration of distraction the error in RPE of airspeed increases and exceeds error with a T scan or omission of the altimeter generally among the three NextGen arrival variants.

Figure 44. Summary of the Impact of T scan, Omission, and Distraction on the Maximum 95% CI of Error in the Reference Pilot Expectation of Vertical Speed in a Speed Up Near Approach

The relationships in Figure 44 quantify how performing a proper T scan frequently decreases the error in RPE of vertical speed. An omission of the airspeed indicator of T scan increases the error in RPE of vertical speed, while an omission of the altimeter has no impact. With greater duration of distraction the error in RPE of vertical speed increases.

Figure 45. Summary of the Impact of T scan, Omission, and Distraction on the Maximum 95% CI of Error in the Reference Pilot Expectation of Specific Energy in a Speed Up Near Approach

Figure 45 summarizes the relationships between maximum 95% CI of error in RPE of specific energy and scan pattern. These results quantify how performing a proper T scan with smaller scan periods decreases the error in RPE of specific energy. The error in RPE increases, however, with larger T scan periods or duration of omission or distraction. As seen, the error in RPE of specific energy increases with both an omission of the altimeter and the airspeed indicator. Finally, distraction has the greatest impact on the error in RPE of specific energy: the error in RPE with a distraction results in greater error than with a T scan or an omission.

76

Comparison Between Arrivals with Different Specific Energy

This final section analyzes the impact of scan pattern in a phase of flight where each NextGen arrival has a different specific energy level (Figure 46). Note: This phase of flight corresponds to when the aircraft has completed 40% of the arrival. The specific energy of the aircraft in the baseline NextGen arrival variant is lower than the specific energy of the aircraft in the maximum energy NextGen arrival variant, but greater than the specific energy of the aircraft in the minimum energy NextGen arrival variant.
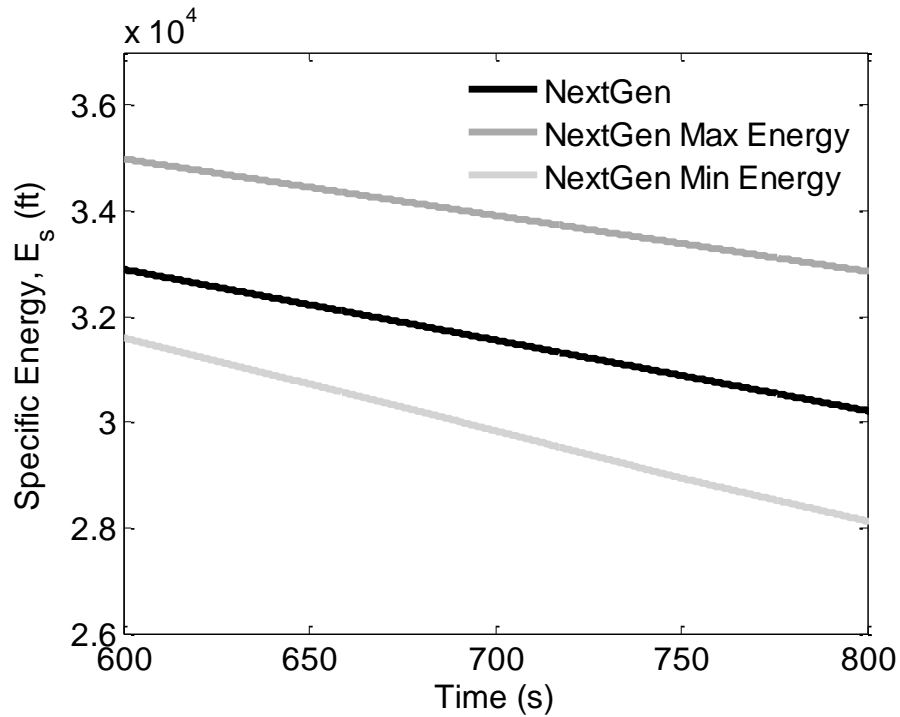
Figure 46. Time History of Specific Energy in an Aircraft Specific Energy Comparison for Each NextGen Arrival

The relationship between the T scan scanning period and the maximum 95% CI of error in RPE of altitude, airspeed, and vertical speed in each of the NextGen arrivals is presented in the left plots of Figure 47a, b, and c, respectively. These relationships quantify how there are no differences between error in RPE of altitude and airspeed in

77

each NextGen arrival. However, there are differences between the error in RPE of vertical speed in each NextGen arrival.

The relationship between the duration of omission and the maximum 95% CI of error in RPE of altitude, airspeed, and vertical speed in each of the NextGen arrivals is presented in the center plots of Figure 47a, b, and c, respectively. The error in RPE of altitude increases with duration of omission of the altimeter from the T scan, but there are no differences between the each of the NextGen arrivals in the three NextGen arrivals. The error in RPE of airspeed and vertical speed, however, both increase with duration of omission of the airspeed indicator and are different between each NextGen arrival.

The relationship between the duration of distraction and the maximum 95% CI of error in RPE of altitude, airspeed, and vertical speed in each of the NextGen arrivals is presented in the right plots of Figure 47a, b, and c, respectively. The error in RPE of altitude, airspeed, and vertical speed increases with greater duration of distraction and have differences between the each of the NextGen arrivals between the three NextGen variants. These differences arise from differences in altitude, airspeed, and vertical speed among each NextGen arrival variant.

The relationships between the maximum 95% CI of error in RPE of specific energy and T scan scanning period, duration of omission, and duration of distraction in a comparison of aircraft energy levels are presented in the Figure 48. The relationships show there is little to no difference between the each of the NextGen arrivals of specific energy resulting from the three NextGen arrivals with a T scan or

(a) Maximum 95% CI of Altitude due to T Scan, Omission of Altitude and Airspeed, and Distraction
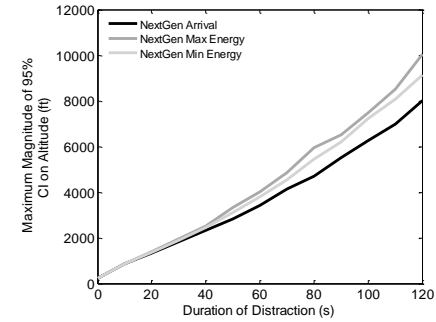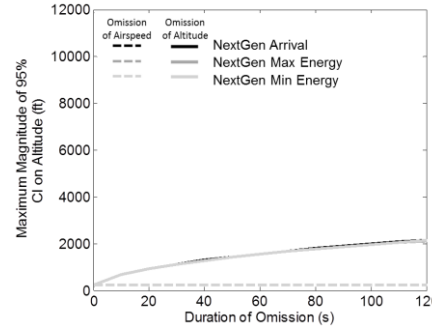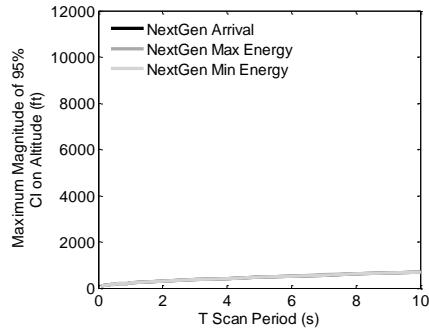
(b) Maximum 95% CI of Airspeed due to T Scan, Omission of Altitude and Airspeed, and Distraction
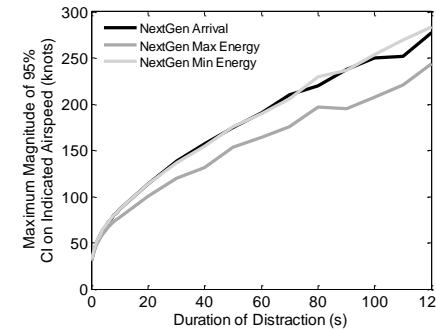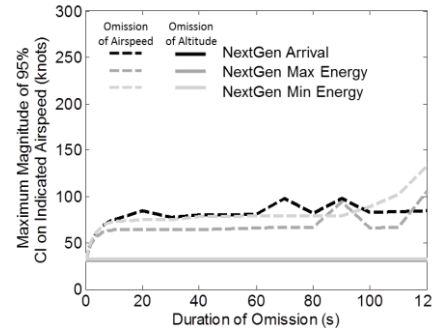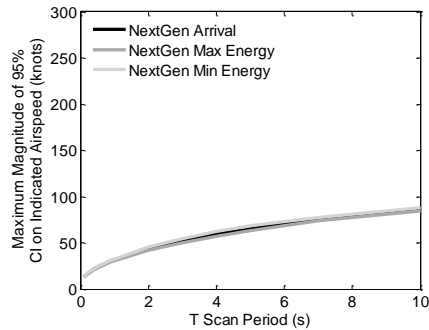
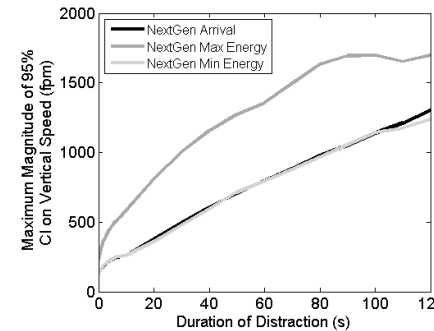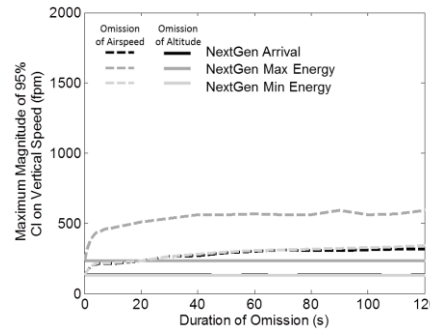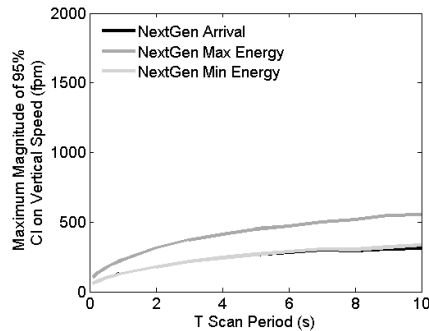(c) Maximum 95% CI of Vertical Speed due to T Scan, Omission of Altitude and Airspeed, and Distraction
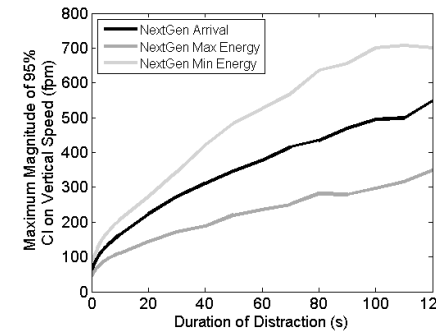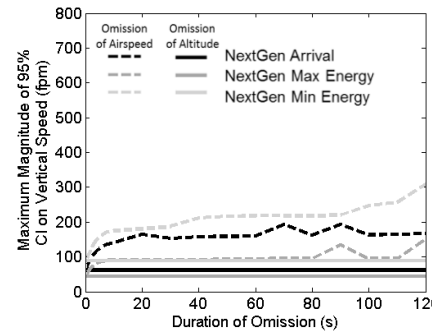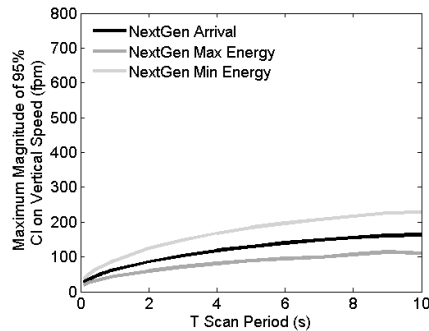
Figure 47. *Maximum 95% Confidence Interval of Altitude, Indicated Airspeed, and Vertical Speed as a Function of the NextGen Arrival Variants*

79
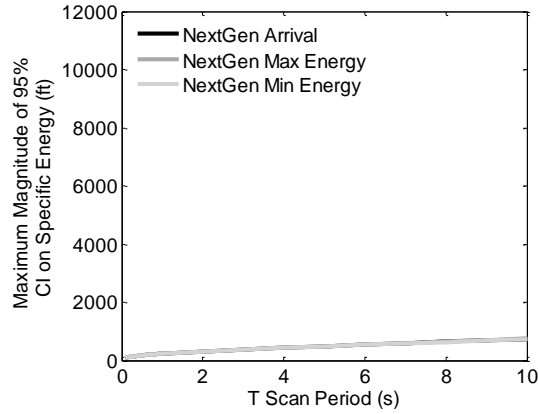
(a) Specific Energy due to Omission
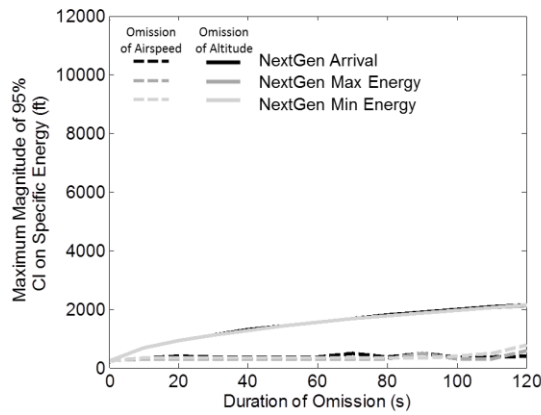
(b) Specific Energy due to Omission
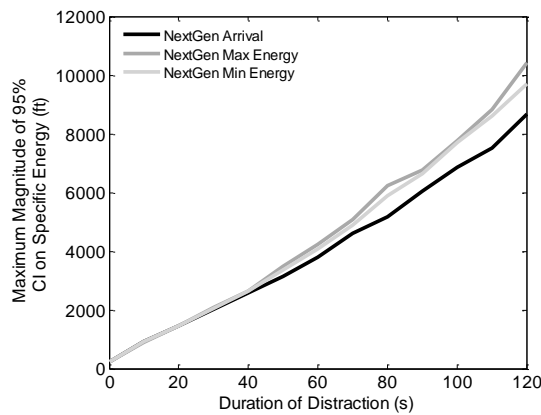
(c) Specific Energy due to Distraction

Figure 48. Maximum 95% Confidence Interval of Aircraft Specific Energy as a Function of the NextGen Arrival Variants

omission of altitude or airspeed. There are differences, however, between each NextGen arrival in the errors in RPE of specific energy resulting with distraction. Finally, the relationships quantify how the error in RPE of specific energy increases with larger T scan periods and greater duration of omission and distraction.

In summary, the impact of scan pattern on the maximum 95% CI of error in the RPE of altitude, airspeed, vertical speed, and specific energy for each of the NextGen arrivals is shown in Figures 49, 50, 51, and 52, respectively.
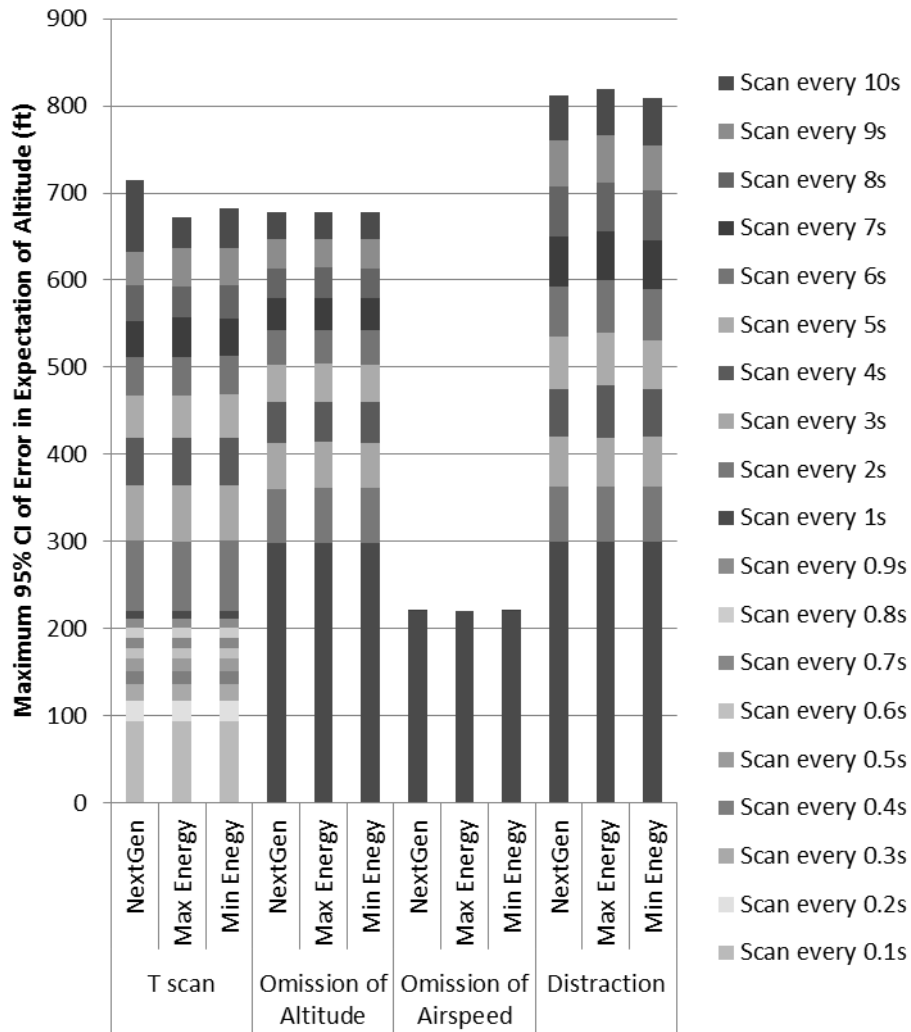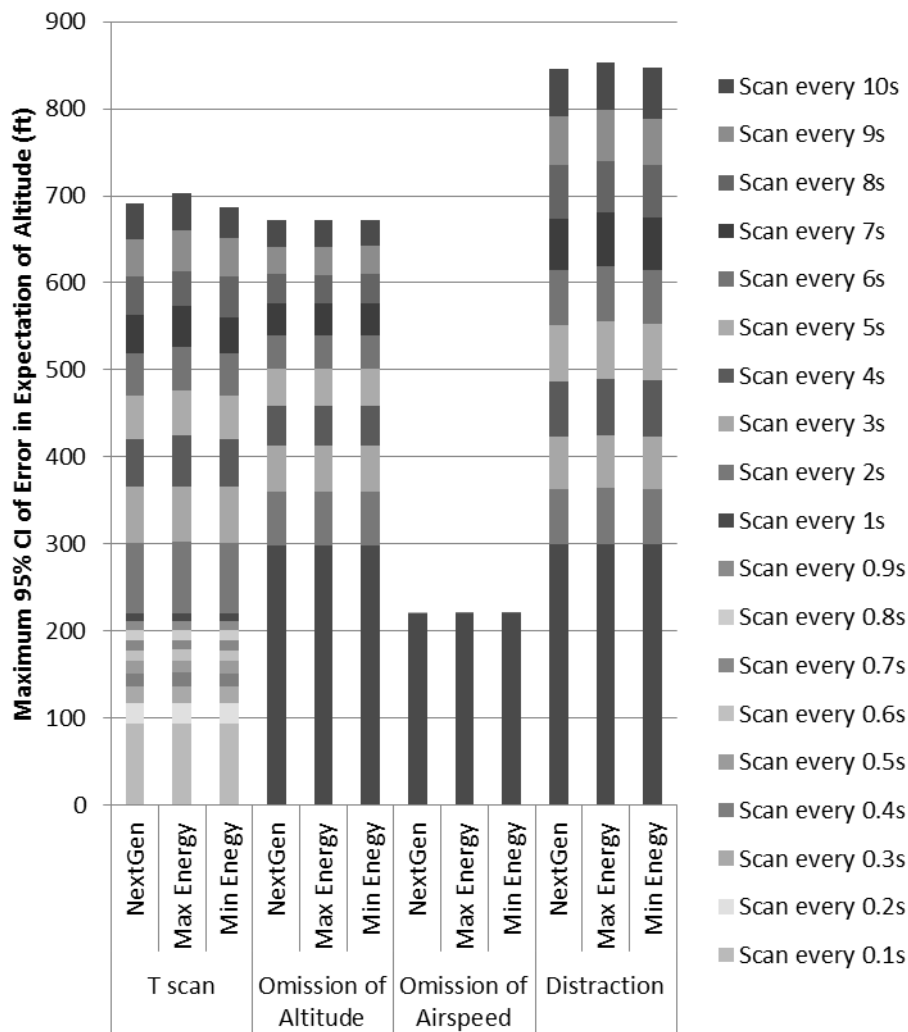

Figure 49. *A Summary of the Impact of T scan, Omission, and Distraction on the Maximum 95% CI of Error in the Reference Pilot Expectation of Altitude as a Function of the NextGen Arrival Variants*

81

Figure 49 quantifies how performing a proper T scan frequently decreases the error in RPE of altitude. An omission of the altimeter from a T scan increases the error in RPE of altitude, while an omission of the airspeed indicator has no impact. Finally, greater duration of distraction increases the error in RPE of altitude and exceeds error due to T scan or omission of the altimeter.
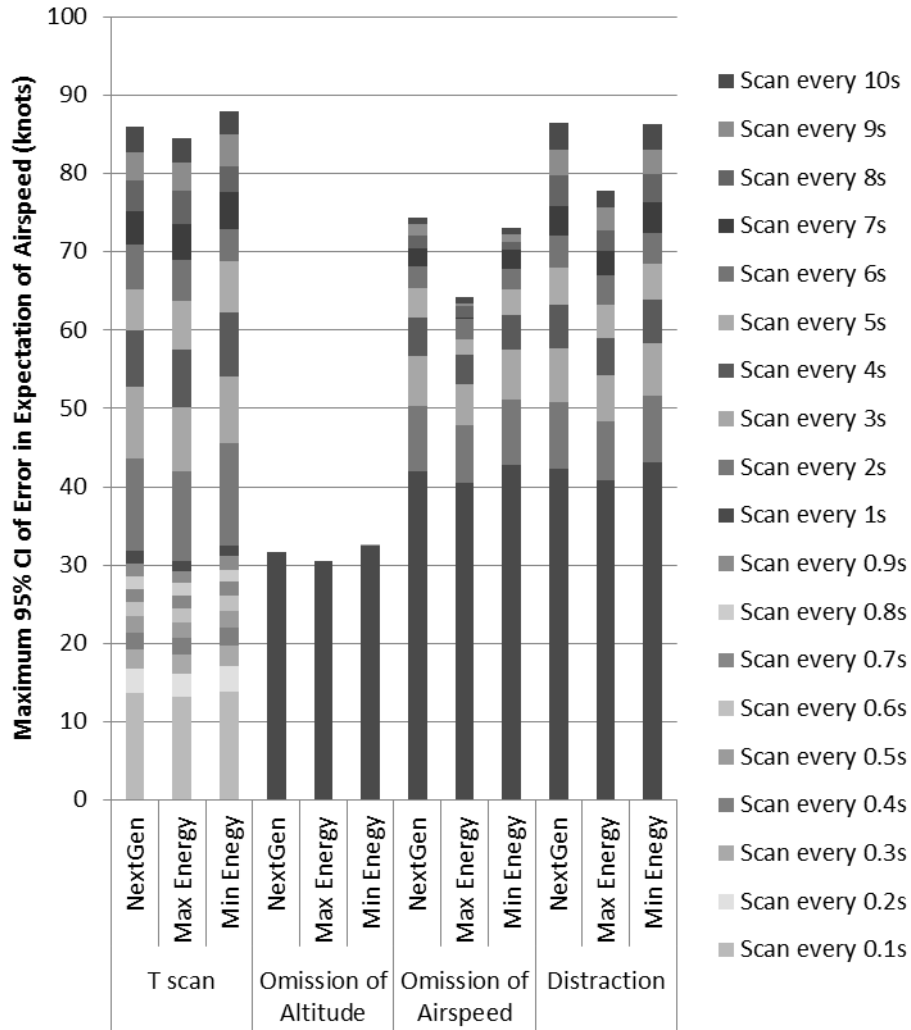
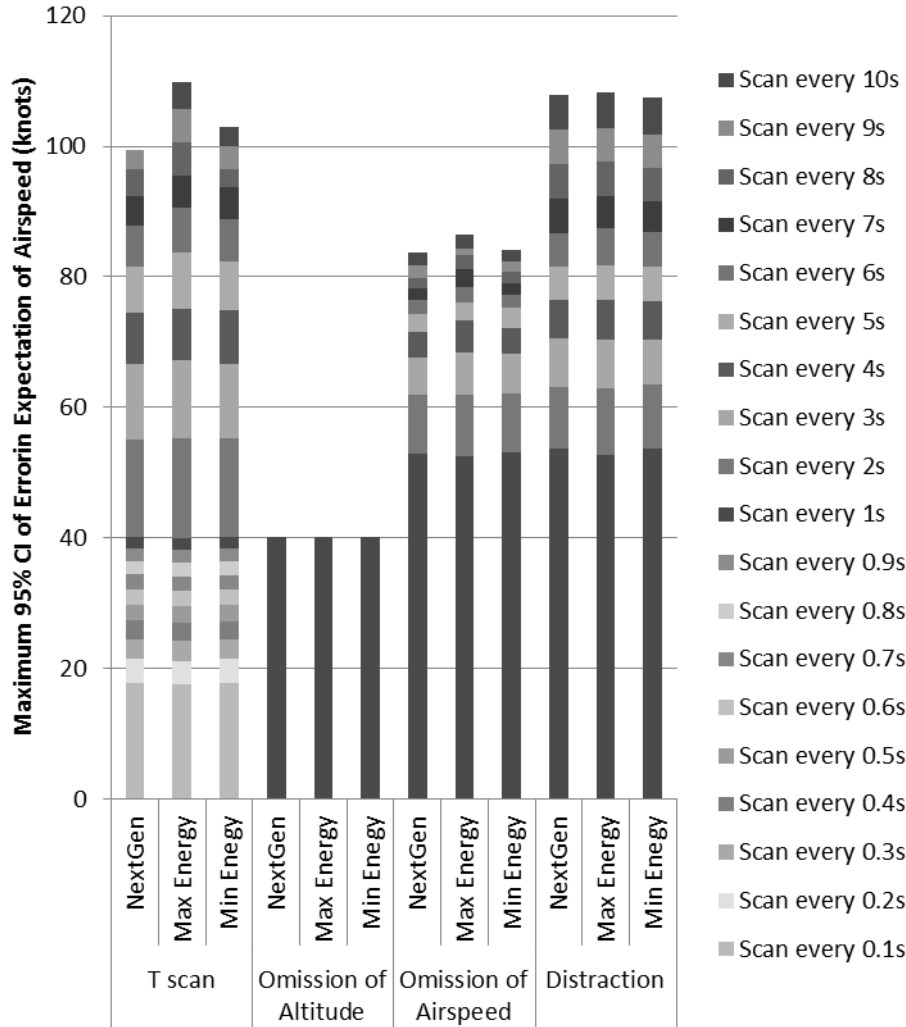***Figure 50.*** *A Summary of the Impact of T scan, Omission, and Distraction on the Maximum 95% CI of Error in the Reference Pilot Expectation of Airspeed as a Function of the NextGen Arrival Variants*

Figure 50 quantifies how performing a proper T scan frequently decreases the error in RPE of airspeed. An omission of the airspeed indicator of T scan increases the error in RPE of airspeed, while an omission of altitude has no impact. Also, greater

82

duration of distraction increases the error in RPE of airspeed. The error in RPE of airspeed with an omission or distraction differs depending on the energy level of the aircraft. The figure shows these disparities in the bars corresponding to omission of airspeed and distraction.
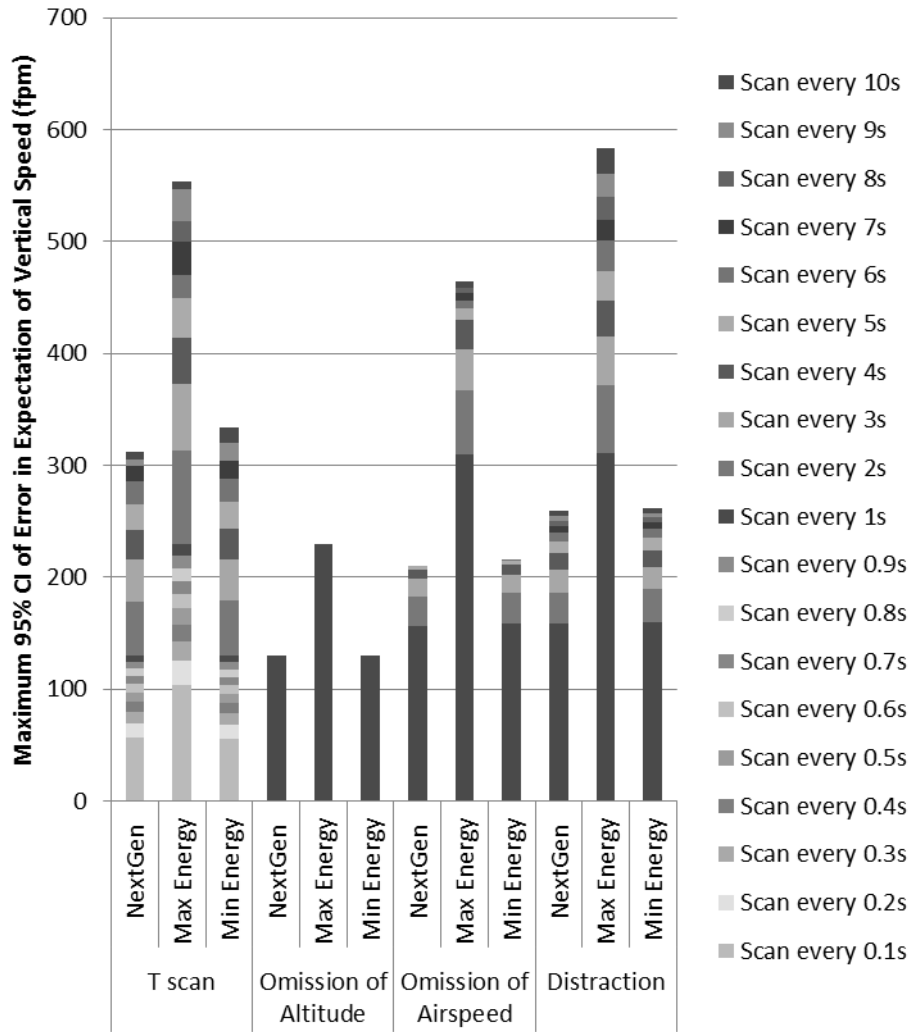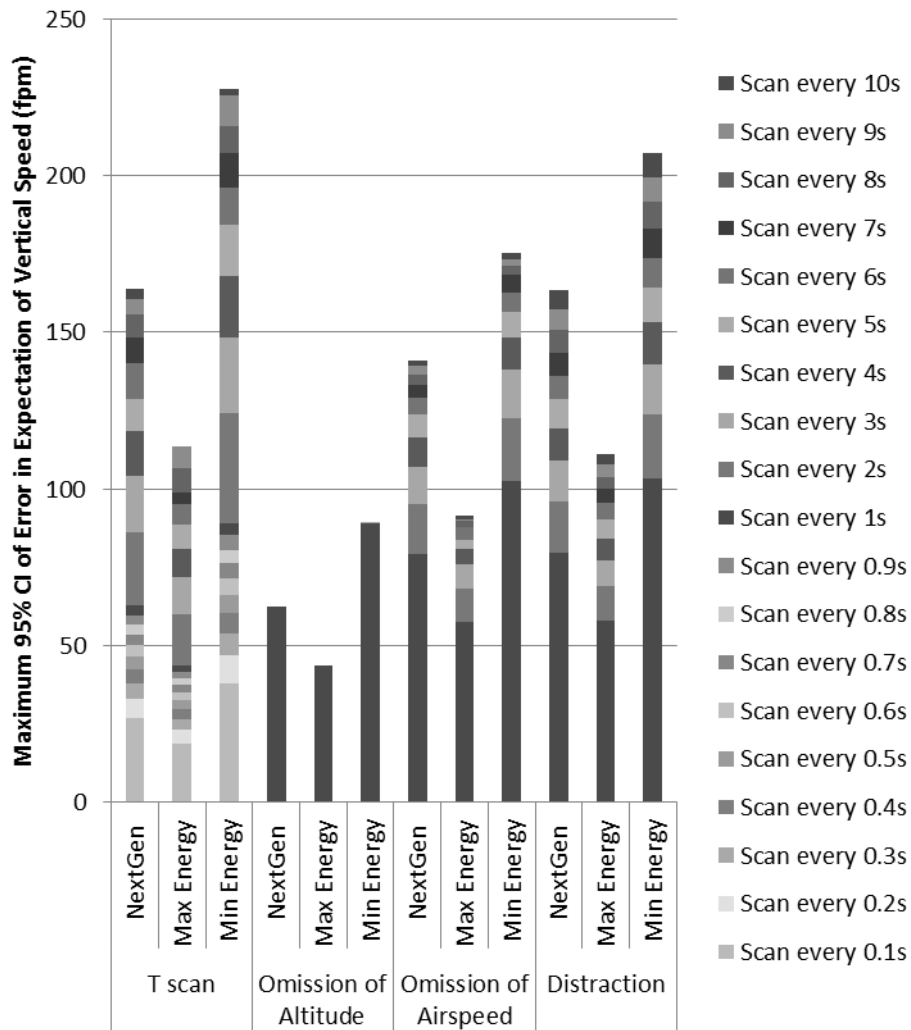

***Figure 51.** A Summary of the Impact of T scan, Omission, and Distraction on the Maximum 95% CI of Error in the Reference Pilot Expectation of Vertical Speed as a Function of the NextGen Arrival Variants*

Figure 51 quantifies how the error in RPE of vertical speed differs depending on the aircraft specific energy level. As seen, the error in RPE varies for T scan in different NextGen arrival variants. Error in RPE of vertical speed with omission and distraction also show differences depending on the aircraft specific energy level. The relationships

shown in Figure 51 also show how performing a proper T scan decreases the error in RPE of vertical speed. An omission of the airspeed indicator from the T scan increases the error in RPE of vertical speed. Finally, greater duration of distraction increases the error in RPE of vertical speed.
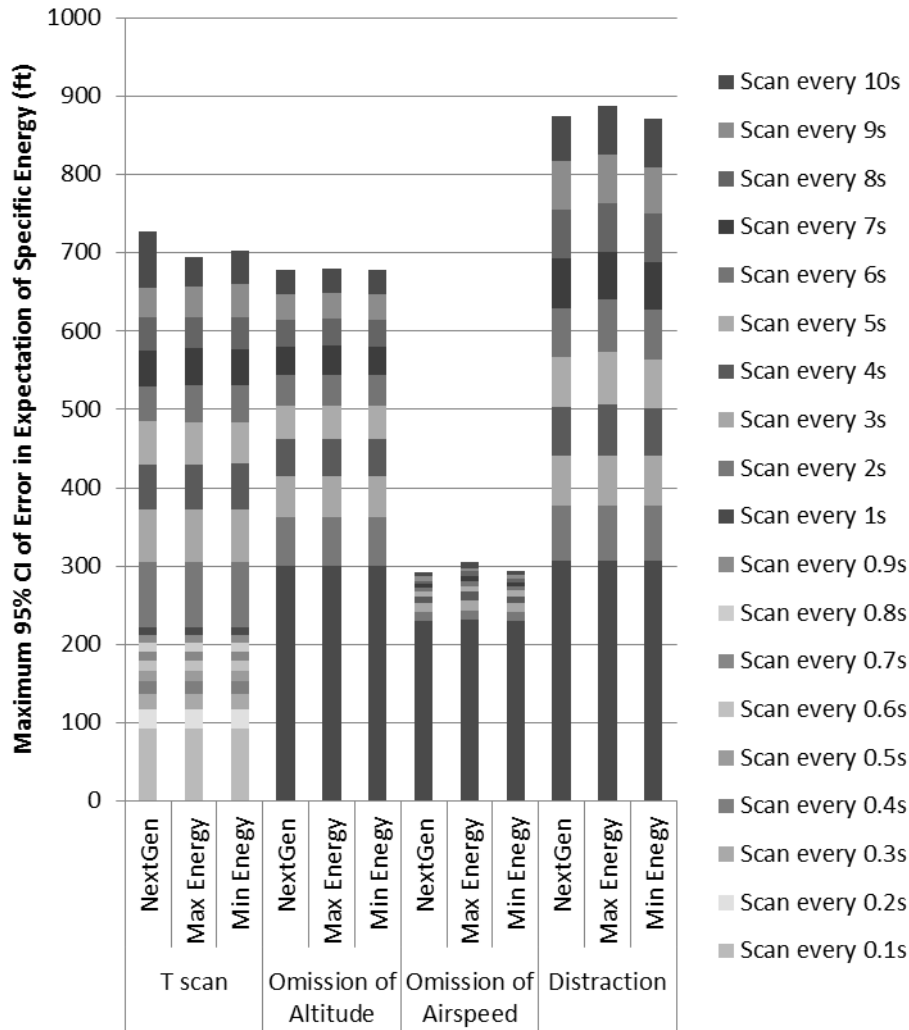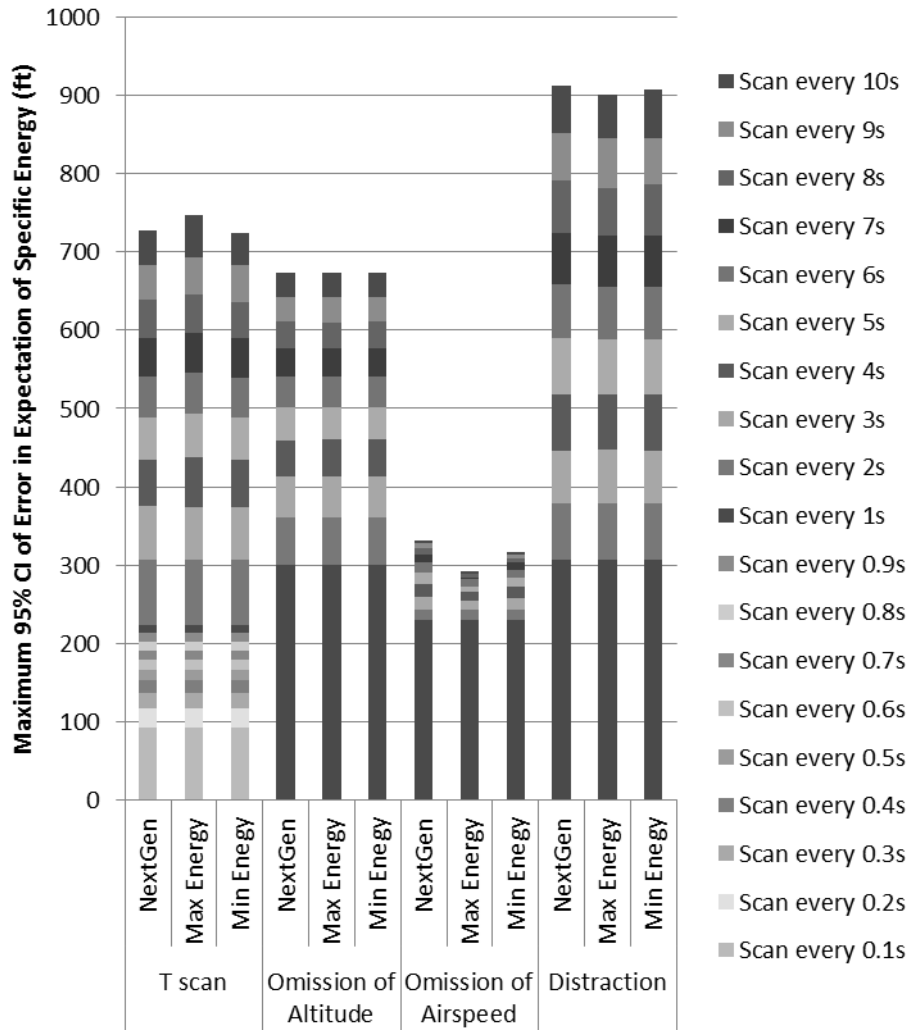

Figure 52. *A Summary of the Impact of T scan, Omission, and Distraction on the Maximum 95% CI of Error in the Reference Pilot Expectation of Specific Energy as a Function of the NextGen Arrival Variants*

A summary of the impact of T scan scanning period and duration omission and distraction on the maximum 95% CI of error in RPE of specific energy in each of the NextGen arrivalsis provided in Figure 52. Here, the error in RPE of specific energy does not change dramatically, but some differences are visible. Greater disparity between each

of the NextGen arrivals resulting from the three NextGen arrival variants is visible with greater duration of omission and distraction (as seen in Figure 48).

Design Implications:

The results in this chapter demonstrate how the MBO can be used to investigate the RPE in NextGen operations. The relationship between the maximum 95% CI of error in RPE of the aircraft states and the scan pattern can be used to quantitatively assess susceptibility to loss of energy state awareness in NextGen operations as well as current-day operations. Designers can use these relationships to assess error in RPE of altitude, airspeed, and vertical speed, which are critical for maintaining energy state awareness. Designers can also use these relationships to determine what amount levels of error are acceptable or not acceptable, and develop from that baseline.

Secondly, the MBO can be used to examine scan performance in NextGen operations. This ability can benefit training and certification programs by helping to identify ideal scanning behavior for preventing or mitigating loss of energy state awareness. Particularly, this ability can help trainers and certification programs identify how often a pilot should scan the flight instruments. It can also identify how pilots can best recover from omission or distraction.

These results in this chapter also demonstrate that the MBO can be used to identify better display design. For example, this chapter examined the impact of error in RPE of specific energy. Designers could use the MBO to test new display designs that provide specific energy information and the rate of change of specific energy. Designers could then determine if using this information has a greater impact than other display information, such as vertical speed. The MBO provides the capability to examine new display designs and help designers determine whether it is a new design is feasible or makes a greater impact on reducing the error in RPE.

Finally, the results from the NextGen experiments can help to determine whether the error in RPE surpasses energy levels corresponding to stall speed or over speed particularly near landing. For example, the specific energy of the aircraft might be too high, making it difficult for the aircraft to lose energy fast enough for landing. It would be beneficial to examine the error in RPE during this scenario and identify what could potentially happen.

CHAPTER 6

CONCLUSIONS

Summary

This thesis applied a model-based observer (MBO) to predict the reference pilot expectation and quantitatively assess spatial disorientation and loss of energy state awareness. This work demonstrated that the MBO is able to capture vestibular illusions associated with spatial disorientation. The results also demonstrated how the error in RPE is impacted by atmospheric turbulence (Ch. 3). The quantitative assessment of spatial disorientation examined the error in RPE of aircraft state (see Ch. 4) in subthreshold and above-threshold roll maneuvers and in no-pitch, forward acceleration maneuvers conducive to somatogyral illusions and somatogravic illusions, respectively. The results quantified how performing a T scan decreases pilot susceptibility to these illusions, while a visual scan that omits one instrument or is completely distracted from all instruments increases it. Also, the results quantitatively describe the relationship between the accuracy of pilot perception and the error in RPE. A comparison between the impact of scan pattern and accuracy of pilot perception showed, however, that improving the scan pattern has a greater impact on reducing the error in RPE than improving the accuracy of pilot perception. Similarly, the quantitative assessment of loss of energy state awareness examined the error in RPE of aircraft state in NextGen operations (see Ch. 5). The results also quantified how performing a T scan decreases pilot susceptibility to loss of energy state awareness.

This thesis work demonstrated how the MBO can be used to provide design implications for countermeasures and interventions to combat spatial disorientation and loss of energy state awareness. The design implications from both Ch. 4 and Ch. 5 are summarized below:

87

- The MBO can be used to investigate the RPE during maneuvers conducive to vestibular illusions or operations conducive to loss of energy state awareness;

- The MBO can assist designers to design countermeasures or interventions based on error in RPE;

- The MBO can guide designers to identify what aircraft states (or other variables such as energy) that countermeasures should focus on;

- The MBO can assess the required scan period for T scan;

- The MBO allows countermeasure design to be based on analysis of a range of maneuvers, including entire flights or phases of flight;

- Designers can use the MBO to identify whether improving scan pattern or accuracy of pilot perception have the greatest impact on RPE;

- The designer can use the MBO to identify which aircraft state expectations are most impacted by design improvements; and

- The designer can use the MBO to examine the extent that pilot awareness of control surface deflections impacts RPE.

Contributions

This thesis work applied a MBO to predict the RPE that can be achieved with any given instrument scan and established models of vestibular sensing, and the statistical properties of this error such as its 95% confidence interval. The MBO developed in the Georgia Tech Cognitive Engineering Center was applied in several computational experiments examining how the maximum 95% confidence interval of the error in RPE increased with degraded scan, particularly in spatial disorientation and loss of energy state awareness related scenarios. First, the results from the quantitative assessments of spatial disorientation and loss of energy state awareness quantified how performing a T

88

scan with smaller scan periods decreases the error in RPE of the aircraft state. Performing a T scan frequently can prevent susceptibility to spatial disorientation and loss of energy state awareness. The results also quantified how omission of one instrument and distraction from visually scanning all instruments increase error in RPE of the aircraft state, but a T scan can reduce this error.

Second, the computational experiments conducted for this thesis have also demonstrated that the MBO can compare multiple aspects of design. For example, Chapter 4 presented a comparison between the impact of a T scan and accuracy of pilot perception. The comparison demonstrates the MBO's ability to quantify which effects have a greater impact than others. Finally, a quick analysis of awareness of control surface deflections was conducted. This analysis quantitatively demonstrated how awareness of control surface deflections decreased the error in RPE.

Also, this work demonstrates how the MBO can be used to develop countermeasure designs to keep error levels below adequate error levels. With the MBO, the aviation community can now determine what could be adequate, safe, or maximum allowable levels of error for each aircraft state. The MBO can then be used to assess whether the error in RPE exceeds the allowable error.

Finally, this thesis relates the results of the computational experiments into design implications for intervention or countermeasure design to combat spatial disorientation and loss of energy state awareness. The computational experiments in this thesis specifically analyzed error in RPE in maneuvers and operations associated with spatial disorientation and loss of energy state awareness. The relationships between the maximum 95% CI of error in RPE and different effects (e.g., scan pattern) reveal some implications for designing effective countermeasures or interventions, as listed earlier in the *Summary* section of this chapter.

Future Work

This thesis examined the relationship between the error in RPE of the aircraft state scan pattern in spatial disorientation and loss of energy state awareness scenarios. There are still many computational experiments that can further examine maneuvers conducive to spatial disorientation and concepts of operation potentially susceptible to loss of energy state awareness. For example, there are more vestibular illusions associated with spatial disorientation. This thesis provides a template for conducting such experiments and analyzing the results. Also, further experimentation can improve or strengthen design implications for countermeasures or interventions.

As demonstrated in Chapter 3, the error in RPE is impacted by atmospheric turbulence. It might be interesting to investigate this finding even further, such as examining the impact of turbulence intensity on the error in RPE in different maneuvers. It was also shown that the error in RPE does not necessarily grow in a general manner to the maneuver. Hence, it is important to ensure that all maneuvers of interest are examined and that no assumptions are made about the growth of error during one maneuver based on the findings of another.

The model of visual scanning can be modified to include additional flight instruments, such as the sideslip indicator or vertical speed indicator. Also, the scan patterns can be modified to be more dynamic. In this thesis, a T scan was conducted at every scan period or an omission or distraction for a fixed duration. The scan patterns, however, can be modified to conduct a T scan with different scan periods or several incidents of omission or distraction or both in a given experiment.

Designers and researchers can use this approach to foster the development process of countermeasure design or intervention. The MBO can be used to identify how countermeasures can prevent or mitigate spatial disorientation or loss of energy state awareness. It can also be used in the testing process, training, or real operations,

www.manaraa.com

particularly with an eye tracker. First, for testing processes, designers can use the MBO for an overview analysis to help drive key countermeasure design. As the process continues, the MBO can be used in a later stage, such as when countermeasures are in testing phases, where the MBO can be used to determine whether the pilot behavior with the countermeasure mirrors the behavior required for the intended benefits of the countermeasure. For example, if designing an alerting system correct scan behavior, are the pilots found to actually respond to the alert as anticipated? As another example, if a display is designed to provide adequate awareness of the aircraft state and energy levels with a T scan performed every 0.8 seconds, the MBO can be used to determine whether the pilot actually performs a T scan every 0.8 seconds as intended by the display design.

Second, for training purposes, the MBO can be used to identify scan patterns that decrease the error in expectation. Specifically, training programs can quantitatively identify what scan patterns reduce the error in RPE to adequate levels. The MBO can also provide feedback on the error in RPE given the pilot's scan behavior and the aircraft's current state. The MBO can further be used to identify how to best monitor the flight instruments while training pilots to monitor the autoflight system. For example, are there specific states the pilot should monitor during particular autopilot maneuvers? These types of questions can be addressed by the MBO when designing training procedures.

Finally, the MBO has potential use in real-time flight simulators or in flight decks. For example, the MBO can be used to determine the error in RPE in real time, and provide feedback to the pilot. Pilot feedback can take the form of an alerting system, for example, and alert the pilot of potential error in RPE of certain states, especially in cases of omission or distraction. Using the MBO in a real-time system can mitigate potential error in RPE and help the pilot to maintain attitude and energy state awareness.

APPENDIX A: SCRIPTS FOR MANUEVERS

Subthreshold Bank Maneuver

```cpp
//      Initialize an aircraft model
        ManeuverPrimitives* Aircraft = ManeuverPrimitives::GetReadyWM(scenario, "Aircraft");

//      Set maneuverPrimitive to 'true' to run maneuver primitives experiments,
//      'false' for optimal profile descents experiments
        maneuverPrimitive       = true;

//      Set variables below to 'true' for type of maneuver desired.
//      Set 'false' otherwise.
        bank                    = true;
        pitch                   = false;
        acceleration            = false;

//      Set desired state targets for maneuver primitives
        phiStart                = 20.0;
        thetaStart              = 15;
        thrustStart             = 248000.0;

        phiEnd                  = 0.0;
        thetaEnd                = 0.0;

//      Set the rotation rate limiter (deg/s) for the start and end of maneuver
//      limitStart must be >= 0 deg/s
//      limitEnd must be <= 0 deg/s
        limitStart              = 2.0;
        limitEnd                = -2.0;

//      Set the time to start and end the maneuver
//      Set to desired start time when running maneuver primitives
//      Set to ALONGTIMEAWAY when OPD experiments
        maneuverStartTime       = 10.0;
        maneuverEndTime         = 30.0;

//      If running OPDs, select desired OPD:
//              1 = RIIVR (current-day)
//              2 = RIIVR (NextGen, fast-to-slow scheme)
//              3 = SADDE (current-day)
//              4 = SADDE (NextGen, slow-to-fast scheme)
//              5 = SADDE (NextGen, early descent)
//              6 = SADDE (NextGen, early descent, max energy)
//              7 = SADDE (NextGen, early descent, min energy)
        selectOPD = 7;

//      Set start time for OPD experiments
//      Set to 1.0 for OPD
//      Set to ALONGTIMEAWAY when running maneuver primitives
        nextGenStart = ALONGTIMEAWAY;

        if(maneuverPrimitive){
                /*
                *@brief The following initialization for the aircraft model is used for
                *               maneuver primitive experiments.
                */
        Aircraft->acModel->set_initial_values(34.606, -116.035, 28000.0, 0.0, 400, 0.0, 0.0);

        }
```

Above-threshold Bank Maneuver

```
//      Initialize an aircraft model
        ManeuverPrimitives* Aircraft = ManeuverPrimitives::GetReadyWM(scenario, "Aircraft");


//      Set maneuverPrimitive to 'true' to run maneuver primitives experiments,
//      'false' for optimal profile descents experiments
        maneuverPrimitive       = true;


//      Set variables below to 'true' for type of maneuver desired.
//      Set 'false' otherwise.
        bank                    = true;
        pitch                   = false;
        acceleration            = false;


//      Set desired state targets for maneuver primitives
        phiStart                = 20.0;
        thetaStart              = 15;
        thrustStart             = 248000.0;

        phiEnd                  = 0.0;
        thetaEnd                = 0.0;


//      Set the rotation rate limiter (deg/s) for the start and end of maneuver
//      limitStart must be >= 0 deg/s
//      limitEnd must be <= 0 deg/s
        limitStart              = 3.0;
        limitEnd                = -3.0;


//      Set the time to start and end the maneuver
//      Set to desired start time when running maneuver primitives
//      Set to ALONGTIMEAWAY when OPD experiments
        maneuverStartTime       = 10.0;
        maneuverEndTime         = 30.0;


//      If running OPDs, select desired OPD:
//              1 = RIIVR (current-day)
//              2 = RIIVR (NextGen, fast-to-slow scheme)
//              3 = SADDE (current-day)
//              4 = SADDE (NextGen, slow-to-fast scheme)
//              5 = SADDE (NextGen, early descent)
//              6 = SADDE (NextGen, early descent, max energy)
//              7 = SADDE (NextGen, early descent, min energy)
        selectOPD = 7;


//      Set start time for OPD experiments
//      Set to 1.0 for OPD
//      Set to ALONGTIMEAWAY when running maneuver primitives
        nextGenStart = ALONGTIMEAWAY;

        if(maneuverPrimitive){
                /*
                *@brief The following initialization for the aircraft model is used for
                *               maneuver primitive experiments.
                */
        Aircraft->acModel->set_initial_values(34.606, -116.035, 28000.0, 0.0, 400, 0.0, 0.0);

        }
```

Acceleration Maneuver

```
//      Initialize an aircraft model
        ManeuverPrimitives* Aircraft = ManeuverPrimitives::GetReadyWM(scenario, "Aircraft");


//      Set maneuverPrimitive to 'true' to run maneuver primitives experiments,
//      'false' for optimal profile descents experiments
        maneuverPrimitive       = true;


//      Set variables below to 'true' for type of maneuver desired.
//      Set 'false' otherwise.
        bank                    = false;
        pitch                   = false;
        acceleration            = true;


//      Set desired state targets for maneuver primitives
        phiStart                = 20.0;
        thetaStart              = 15;
        thrustStart             = 248000.0;

        phiEnd                  = 0.0;
        thetaEnd                = 0.0;


//      Set the rotation rate limiter (deg/s) for the start and end of maneuver
//      limitStart must be >= 0 deg/s
//      limitEnd must be <= 0 deg/s
        limitStart              = 2.0;
        limitEnd                = -2.0;


//      Set the time to start and end the maneuver
//      Set to desired start time when running maneuver primitives
//      Set to ALONGTIMEAWAY when OPD experiments
        maneuverStartTime       = 10.0;
        maneuverEndTime         = 30.0;


//      If running OPDs, select desired OPD:
//              1 = RIIVR (current-day)
//              2 = RIIVR (NextGen, fast-to-slow scheme)
//              3 = SADDE (current-day)
//              4 = SADDE (NextGen, slow-to-fast scheme)
//              5 = SADDE (NextGen, early descent)
//              6 = SADDE (NextGen, early descent, max energy)
//              7 = SADDE (NextGen, early descent, min energy)
        selectOPD = 7;


//      Set start time for OPD experiments
//      Set to 1.0 for OPD
//      Set to ALONGTIMEAWAY when running maneuver primitives
        nextGenStart = ALONGTIMEAWAY;

        if(maneuverPrimitive){
                /*
                *@brief The following initialization for the aircraft model is used for
                *               maneuver primitive experiments.
                */
        Aircraft->acModel->set_initial_values(34.606, -116.035, 10000.0, 0.0, 400, 0.0, 0.0);

        }
```

Temporal Actions for Maneuvers

```cpp
//        Temporal Action to start maneuver of choice
          TemporalAction& startManeuver = this>create_script_event<TemporalAction>("startManeuver");
          startManeuver.set_next_update_time(this->maneuverStartTime);
          startManeuver.next_update = [&](){
                    startManeuver.timestep_update_time(ALONGTIMEAWAY);

          };

          startManeuver.resource_update = [&,Aircraft](){
                    cout<<"Script Event startManeuver!"<<endl;

                    string name = Aircraft->acModel->name;
                    if (this->bank) {
                              startManeuver.set_resource_value<bool>(name+"headingLoopEnabled", false);
                              startManeuver.set_resource_value<bool>(name+"phiLoopEnabled", true);

                              startManeuver.set_resource_value<double>(name+"phiLoopTarget_deg", this>phiStart);
                              Aircraft->acModel->ac.engageRateLimit(Autopilot::PHI, this->limitStart) ;

                    }else if (this->pitch) {
                              startManeuver.set_resource_value<bool>(name+"altitudeLoopEnabled", false);
                              startManeuver.set_resource_value<bool>(name+"airspeedLoopEnabled", false);
                              startManeuver.set_resource_value<bool>(name+"thetaLoopEnabled", true);

                              startManeuver.set_resource_value<double>(name+"thetaLoopTarget_deg", this->thetaStart);
                              Aircraft->acModel->ac.engageRateLimit(Autopilot::THETA, this->limitStart) ;

                    }else if(this->acceleration) {
                              startManeuver.set_resource_value<bool>(name+"airspeedLoopEnabled", false);
                              startManeuver.set_resource_value<bool>(name+"thrustLoopEnabled", true);

                              startManeuver.set_resource_value<bool>(name+"altitudeLoopEnabled", false);
                              startManeuver.set_resource_value<bool>(name+"thetaLoopEnabled", true);

                              startManeuver.set_resource_value<double>(name+"thrustLoopTarget_lbf", this->thrustStart);
                              startManeuver.set_resource_value<double>(name+"thetaLoopTarget_deg", 0.0);
                    }
          };

          scenario.link_action2setresource(startManeuver,name+"altitudeLoopEnabled",0,0,0);
          scenario.link_action2setresource(startManeuver,name+"airspeedLoopEnabled",0,0,0);
          scenario.link_action2setresource(startManeuver,name+"headingLoopEnabled",0,0,0);
          scenario.link_action2setresource(startManeuver,name+"phiLoopEnabled",0,0,0);
```

```cpp
        scenario.link_action2setresource(startManeuver,name+"phiLoopTarget_deg",0,0,0);
        scenario.link_action2setresource(startManeuver,name+"thetaLoopEnabled",0,0,0);
        scenario.link_action2setresource(startManeuver,name+"thetaLoopTarget_deg",0,0,0);
        scenario.link_action2setresource(startManeuver,name+"thrustLoopEnabled",0,0,0);
        scenario.link_action2setresource(startManeuver,name+"thrustLoopTarget_lbf",0,0,0);

//      Temporal Action to end maneuver of choice
        TemporalAction& endManeuver = this->create_script_event<TemporalAction>("endManeuver");
        endManeuver.set_next_update_time(this->maneuverEndTime);
        endManeuver.next_update = [&](){
                endManeuver.timestep_update_time(ALONGTIMEAWAY);
        };

        endManeuver.resource_update = [&,Aircraft](){
                cout<<"Script Event endManeuver!"<<endl;

                string name = Aircraft->acModel->name;
                if (this->bank) {
                        endManeuver.set_resource_value<double>(name+"phiLoopTarget_deg", this->phiEnd);
                        Aircraft->acModel->ac.engageRateLimit(Autopilot::PHI, this->limitEnd) ;
                }else if (this->pitch) {
                        endManeuver.set_resource_value<double>(name+"thetaLoopTarget_deg", this->thetaEnd);
                        Aircraft->acModel->ac.engageRateLimit(Autopilot::THETA, this->limitEnd) ;
                }

        };

        scenario.link_action2setresource(endManeuver,name+"phiLoopTarget_deg",0,0,0);
        scenario.link_action2setresource(endManeuver,name+"thetaLoopTarget_deg",0,0,0);
```

APPENDIX B: DATA STORAGE FOR ALL EXPERIMENTS

The data for the computational experiments are stored in the 'Velcro' database via the School of Industrial and Systems Engineering (ISYE). The tables below provide the Run ID numbers for each experiment. To view the data, use the Matlab scripts provided on the CEC RDrive while on the ISYE network. The scripts can be found, specifically, in the individual folders listed at Experiment Data and Proj Docs \ Bozan – MS Thesis – Spring 2015 \ Thesis Results. The scripts in each folder correspond with the type of maneuver of interest (e.g., bank, no-pitch forward acceleration, or NextGen).

Maneuvers Conducive to Vestibular Illusions

Sub-threshold Bank	
Scan Behavior	**Run IDs**
T-Scan	20709:20727
Omission of Altitude	20728:20758
Omission of Airspeed	20759:20789
Omission of Attitude	20790:20820
Omission of Heading	20821:20851
Distraction	20852:20882

Above Threshold Bank	
Scan Behavior	**Run IDs**
T-Scan	20535:20553
Omission of Altitude	20554:20584
Omission of Airspeed	20585:20615
Omission of Attitude	20616:20646
Omission of Heading	20647:20677
Distraction	20678:20708

Acceleration (No-pitch)	
Scan Behavior	**Run IDs**
T-Scan	20883:20901
Omission of Altitude	20902:20932
Omission of Airspeed	20933:20963
Omission of Attitude	20964:20994
Omission of Heading	20995:21025
Distraction	21026:21056

97

Changing R (0.1 to 10) during sub bank	
Scan Behavior	**Run IDs**
T-Scan (0.5s)	20416:20434
T-Scan (1s)	20435:20453 RunID(2) = 20455
T-Scan (3s)	20456:20474

Changing R (0.1 to 10) during abv bank	
Scan Behavior	**Run IDs**
T-Scan (0.5s)	20475:20493
T-Scan (1s)	20494:20512 RunID(9)=20513 RunID(11)=20514
T-Scan (3s)	20516:20534

NextGen Operations

Clearance 1: Altitude (early descent)

NextGen Arrival Baseline

Simulation start time 99s
Omission/Distraction window: 129s -249s
Simulation End Time: 279s

Aircraft->acModel->set_initial_values(lat, lon, alt, hdg, spd, vspd, time);
(Retrieved using InitNextGen.m)

```
Aircraft->acModel->set_initial_values(34.5127, -115.798, 28000.0, 115.773, 472.398,
0.0, 99.0);
```

NextGen Arrival	
Scan Behavior	**Run IDs**
T scan	29607:29625
Omission of Altitude	25016:25136
Omission of Airspeed	25137:25257
Distraction	24895:25015

98

Maximum Energy NextGen Arrival

Simulation start time 99s
Omission/Distraction window: 129s -249s
Simulation End Time: 279s

```
Aircraft->acModel->set_initial_values(34.5127, -115.798, 28000.0, 115.773, 472.398,
0.0, 99.0);
```

Max Energy Variant	
Scan Behavior	**Run IDs**
T scan	29626:29644
Omission of Altitude	25258:25378
Omission of Airspeed	25379:25499
Distraction	25500:25620

```
Aircraft->acModel->set_initial_values(34.5127, -115.798, 28000.0, 115.773, 472.398,
0.0, 99.0);
```

Min Energy Variant	
Scan Behavior	**Run IDs**
T scan	29645:29663
Omission of Altitude	25621:25741
Omission of Airspeed	25742:25862
Distraction	25863:25983

Clearance 2: Speed up

NextGen Arrival Baseline

Simulation Start Time: 372s
Omission/Distraction window: 402s – 522s
Simulation End Time: 552s

```
Aircraft->acModel->set_initial_values(34.3061, -115.176, 25625.1, 110.8, 422.626, -
9.9941, 372.0);
```

NextGen Arrival	
Scan Behavior	**Run IDs**
T scan	29664:29682
Omission of Altitude	26226:26346
Omission of Airspeed	26347:26467
Distraction	26105:26225

99

Maximum Energy NextGen Arrival

Simulation Start Time: 356s
Omission/Distraction Window: 386s – 506s
Simulation End Time: 536s

```
Aircraft->acModel->set_initial_values(34.3166, -115.21, 26299.1, 110.8, 427.679, -
7.6639, 356.0);
```

Max Energy Variant	
Scan Behavior	**Run IDs**
T scan	29683:29701
Omission of Altitude	26468:26588
Omission of Airspeed	26589:26709
Distraction	26710:26830

Minimum Energy NextGen Arrival

Simulation Start Time: 356s
Omission/Distraction Window: 386s – 506s
Simulation End Time: 536s

```
Aircraft->acModel->set_initial_values(34.3181, -115.215, 25120.1, 110.801, 418.914, -
13.0107, 356.0);
```

Min Energy Variant	
Scan Behavior	**Run IDs**
T scan	29702:29720
Omission of Altitude	26831:26951
Omission of Airspeed	26952:27072
Distraction	27073:27193

Clearance 3: Speed up Near Approach

NextGen Arrival Baseline

Simulation Start Time: 1503s
Omission/Distraction Window: 1533s – 1653s
Simulation End Time: 1683s

```
Aircraft->acModel->set_initial_values(33.6165, -112.879, 8397.87, 93.2001, 238.307, -
10.389, 1503.0);
```

NextGen Arrival	
Scan Behavior	**Run IDs**
T scan	29493:29511
Omission of Altitude	27194:27314
Omission of Airspeed	27315:27435
Distraction	27436:27556

Maximum Energy NextGen Arrival

Simulation Start Time: 1364s
Omission/Distraction Window: 1394s – 1514s
Simulation End Time: 1544s

```
Aircraft->acModel->set_initial_values(33.6469, -113.001, 9668.39, 86.9023, 243.154, -
22.1378, 1364.0);
```

Max Energy Variant	
Scan Behavior	**Run IDs**
T scan	29512:29530
Omission of Altitude	27557:27677
Omission of Airspeed	27678:27798
Distraction	27799:27919

<u>Minimum Energy NextGen Arrival</u>

Simulation Start Time = 1463s
Omission/Distraction Window: 1493s – 1613s
Simulation End Time = 1643s

```
Aircraft->acModel->set_initial_values(33.6277, -112.967, 8382.86, 92.6002, 238.256, -
10.5025, 1463.0);
```

Min Energy Variant	
Scan Behavior	**Run IDs**
T scan	29531:29549
Omission of Altitude	28041:28161
Omission of Airspeed	28162:28282
Distraction	28283:28403

Energy Comparison

<u>NextGen Arrival Baseline</u>

Simulation Start Time: 629s
Omission/Distraction Window: 659s – 779s
Simulation End Time: 809s

```
Aircraft->acModel->set_initial_values(34.1121, -114.554, 23072.6, 110.6, 461.835, -
10.0823, 629.0);
```

NextGen Arrival	
Scan Behavior	**Run IDs**
T scan	29550:29568
Omission of Altitude	28404:28524
Omission of Airspeed	28525:28645
Distraction	28646:28766

102

Maximum Energy NextGen Arrival

Simulation Start Time: 596s
Omission/Distraction: 626s – 746s
Simulation End Time: 776s

```
Aircraft->acModel->set_initial_values(34.11265, -114.604, 24487.7, 110.9650, 488.139, -
7.8413, 596.0);
```

Max Energy Variant	
Scan Behavior	**Run IDs**
T scan	29569:29587
Omission of Altitude	28767:28887
Omission of Airspeed	28888:29008
Distraction	29009:29129

Minimum Energy NextGen Arrival

Simulation Start Time: 614s
Omission/Distraction: 644s – 764s
Simulation End Time: 794

```
Aircraft->acModel->set_initial_values(34.1206, -114.583, 21763.8, 110.7, 465.678, -
13.1932, 614.0);
```

Min Energy Variant	
Scan Behavior	**Run IDs**
T scan	29588:29606,
Omission of Altitude	29130:29250
Omission of Airspeed	29251:29371
Distraction	29372:29492

REFERENCES

Angelaki, D. E., & Cullen, K. E. (2008). Vestibular system: the many facets of a multimodal sense. *Annu. Rev. Neurosci.*, *31*, 125-150.

Baron, S., & Kleinman, D. L. (1969). The human as an optimal controller and information processor. *Man-Machine Systems, IEEE Transactions on*, *10*(1), 9-17.

Baron, S., Kleinman, D. L., & Levison, W. H. (1970). An optimal control model of human response part II: prediction of human performance in a complex task. *Automatica*, *6*(3), 371-383.

Bailey, R. E., Ellis, K. K., & Stephens, C. L. (2013). Test and Evaluation Metrics of Crew Decision-Making And Aircraft Attitude and Energy State Awareness. *AIAA*.

Bateman, D. (2010). Some Thoughts on Reducing the Risk of Aircraft Loss of Control. *AIAA Aircraft Loss of Control. Session III: Potential System Solutions. Toronto, Canada*.

Belcastro, C. M., & Foster, J. V. (2010, August). Aircraft loss-of-control accident analysis. In *AIAA Guidance, Navigation and Control Conference, Toronto, Canada*.

Boeing. (2013). Statistical Summary of Commercial Jet Airplane Accidents: Worldwide Operations 1959-2013. *Aviation Safety, Boeing Commercial Airlines, Seattle, Washington*.

Borah, J., Young, L. R., & Curry, R. E. (1988). Optimal estimator model for human spatial orientationa. *Annals of the New York Academy of Sciences*, *545*(1), 51-73.

Bryan, L. A. (1954). *180-degree turn experiment* (No. 11). University of Illinois.

Cheung, B. (2004). Nonvisual Spatial Orientation Mechanisms. Chapter 2 in *Spatial Disorientation in Aviation*, 2004, (Vol. 203). AIAA, 37-94.

CAST. (2013). CAST Safety Enhancement Plan – Technical Report. Available at: www.skybrary.aero/index.php/Portal:CAST_SE_Plan

Crider, D. A. (2010). Upset recovery training: Lessons from accidents and incidents. Aeronautical Journal, 114(1160), 629-636

Devouassoux, Y., & Pritchett, A. (2001, October). Application of Kalman filtering to pilot detection of failures. In *Digital Avionics Systems, 2001. DASC. 20th Conference* (Vol. 1, pp. 3D3-1). IEEE.

Gibb, R., Ercoline, B., & Scharff, L. (2011). Spatial disorientation: decades of pilot fatalities. Aviation, space, and environmental medicine, 82(7), 717-724.

Gillingham, K. & Wolfe, J. (1986). Spatial orientation in flight. USAF School of Aerospace Medicine. USAFSAM-TR-85-31.

Gresty, M. A., Golding, J. F., Le, H., & Nightingale, K. (2008). Cognitive impairment by spatial disorientation. Aviation, space, and environmental medicine, 79(2), 105-111.

Hess, R. (1996). Feedback control models – manual control and tracking. Chapter 38 in *Handbook of Human Factors and Ergonomics*. G. Salvendy (ed). New York: John Wiley and Sons.

Howard, J. D., & Johnston, A. (1986). AFTI/F-16 gravity-induced loss-of-consciousness and spatial disorientation auto-recovery system. NAECON 1986, 752-758.

Jacobson, S. R. (2010). Aircraft Loss of Control Causal Factors and Mitigation Challenges. *& Proceedings*

Jaslow, H. (2002). Spatial disorientation during a coordinated turn. *Journal of aircraft*, *39*(4), 572-576.

Jones, D. G., & Endsley, M. R. (1996). Sources of situation awareness errors in aviation. *Aviation, Space, and Environmental Medicine*.

Kaneshige, J., Sharma, S., Martin, L., Lozito, S., & Dulchinos, V. (2013). Flight-Deck Strategies and Outcomes When Flying Schedule-Matching Descents. *AIAA*, *4537*, 19-22.

Kleinman, D. L., Baron, S., & Levison, W. H. (1970). An optimal control model of human response part I: Theory and validation. *Automatica*, *6*(3), 357-369.

Krueger, W. W. (2011). Controlling motion sickness and spatial disorientation and enhancing vestibular rehabilitation with a user-worn see-through display. *The Laryngoscope*, *121*(S2), S17-S35

Kuo, A. D. (1995). An optimal control model for analyzing human postural balance. *Biomedical Engineering, IEEE Transactions on*, *42*(1), 87-101.

Lessard, C. S. (2000). Spatial disorientation: dealing with aeronautical illusions [Guest Editorial]. Engineering in Medicine and Biology Magazine, IEEE, 19(2), 25-27.

Lone, M. M., & Cooke, A. K. (2010, January). Review of pilot modelling techniques. In *48th AIAA Aerospace Sciences Meeting Including the New Horizons Forum and Aerospace Exposition, number AIAA-2010-297, Orlando, Florida*.

MacNeilage, P. R., Ganesan, N., & Angelaki, D. E. (2008). Computational approaches to spatial orientation: from transfer functions to dynamic Bayesian inference. *Journal of neurophysiology*, *100*(6), 2981-2996.

McGrath, B. J., Rupert, A. H., & Guedry, F. E. (2003). Analysis of Spatial Disorientation Mishaps in the US Navy. *Spatial Disorientation in Military Vehicles: Causes, Consequences and Cures*.

Merfeld, D. M., Young, L. R., Oman, C. M., & Shelhamer, M. J. (1993). A multidimensional model of the effect of gravity on the spatial orientation of the monkey. *Journal of vestibular research: equilibrium & orientation*.

Merfeld, D.M. (1990). *Spatial orientation of the squirrel monkey: An experimental and theoretical investigation*. (Doctoral dissertation). Retrieved from DSpace@MIT. (13983)

Nashner, L. M. (1970). *Sensory feedback in human posture control*. (Doctoral dissertation) Retrieved from DSpace@MIT. (13805)

Navathe, P. D., & Singh, B. (1994). An operational definition for spatial disorientation. *Aviation Space and Environmental Medicine*, *65*, 1153-1153.

Newman, M. C. (2009). *A multisensory observer model for human spatial orientation perception* (Doctoral dissertation, Massachusetts Institute of Technology).

Newman, M. C., Lawson, B. D., Rupert, A. H., & McGrath, B. J. (2012) The Role of Perceptual Modeling in the Understanding of Spatial Disorientation During Flight and Ground-based Simulator Training. *& Proceedings*

Onur, C. (2014). *Developing a computational model of the pilot's reference expectation of aircraft state given vestibular and visual cues* (Master's Thesis). Retrieved from SMARTech. (53110)

Ormsby, C. C. (1974). *Model of human dynamic orientation* (Doctoral dissertation) Retrieved from DSpact@MIT. (9857)

Pommellet, P.E. (1990). *Suboptimal estimator of spatial orientation of a pilot*. (Master's Thesis). Retrieved from DSpace@MIT. (46462)

Previc, F. H., & Ercoline, W. R. (Eds.). (2004). *Spatial disorientation in aviation* (Vol. 203). AIAA.

Rupert, A. H. (2000). An instrumentation solution for reducing spatial disorientation mishaps. *Engineering in Medicine and Biology Magazine, IEEE*, *19*(2), 71-80.

Sadovnichy, V. A., Alexandrov, V. V., Soto, E., Alexandrova, T. B., Astakhova, T. G., Vega, R., ... & Shulenina, N. E. (2007). A mathematical model of the response of the semicircular canal and otolith to vestibular system rotation under gravity. *Journal of Mathematical Sciences*, *146*(3), 5938-5947.

Salvendy, G. (2012). *Handbook of human factors and ergonomics*. Wiley. com.

Small, R. L., Keller, J. W., Wickens, C. D., Socash, C. M., Ronan, A. M., & Fisher, A. M. (2006). *Multisensory integration for pilot spatial orientation*. Micro Analysis and Design Boulder Co.

Whitcher, L. & Pritchett, A. (2015). *A Quantitative Analysis of the Effects of Diminished Pilot Control State Awareness Using Computational Work Models*. TBD.